
# Rainfall-Runoff Modeling in a Small Catchment in Austria

**By:**

**Majid Galoie**

**Institute of Hydraulic Engineering and Water Resources Management**

**Graz University of Technology (TU Graz)**

**Austria**

**September 2013**

**Academic PhD Dissertation in:**
**Hydraulic Engineering and Water Resources Management**

**Supervisor:**
**Univ.-Prof. Dipl.-Ing. Dr.techn. Gerald Zenz**
**(TU Graz)**

**Reviewer:**
**Univ.-Prof. Dr.-Ing. Dirk Muschalla**
**(TU Graz)**

## Table of Contents

# List of Tables

# List of Figures

**Appendix A**

## Abstract

The aim of this thesis is to simulate the process of rainfall-runoff modeling for a small catchment area, which is situated at northern Graz in Austria, using ArcGIS, Hec-GeoHMS and Hec-HMS. Since a rainfall-runoff modeling is depend on a lot of parameters such as meteorologic conditions, geospatial parameters, loss parameters, hydraulic conditions and so on, for this reason, the process of rainfall-runoff modeling is dissected into four major section as 1. Rainfall Analysis, 2. Terrain Analysis, 3. Loss Analysis and, 4. Runoff Modeling.

In rainfall analysis section and in order to determine the probability of occurrence of any rainfall event, the frequency distribution, which can fit the past characteristics on the magnitude and the probability of occurrence of such rainfalls, should be known. In this thesis, in order to find the best-fit probability distribution model, some parameter estimation techniques such as L-moments and maximum likelihood models are used and for goodness of fit test, three methods are used as Chi-Square, Kolmogorov-Smirnov and the root mean square error (RMSE). In this thesis, a comparison between four commonly used rainfall frequency distributions are carried out such as Generalized Extreme Value (GEV), Gumbel, Log-Pearson type III (LP III) and 3-parameter Log-normal (LN III). The analysis will show that the best-fit probability distribution for the rainfall data which has been recorded at northern Graz, is the Gumbel distribution.

In terrain analysis section, to derive the spatial and geomorphologic variations of the model, Hec-GeoHMS is used. Digital Elevation Model (DEM), which consists elevation and location information for all points of the area, is an input for Hec-GeoHMS. In this thesis, a very high resolution DEM (Micro-scale: 1m × 1m) is used in order to obtain the basin characteristics more precisely. Also for river routing, the Muskingum-Cunge method (8-point cross section) is used.

In loss analysis section, since the SCS curve number (CN) procedure is a widely used method for estimating direct runoff from rainfall on small to medium-sized basins, in this thesis, SCS-CN method is used for estimation of rainfall losses.

Finally, the rainfall-runoff modeling will be completed for a small catchment area in Austria (the Shoeckelbach basin) using Hec-HMS software and for calibrating the model, some observed data will be used.

After the calibration process, it is possible to do some investigations on the high flood risk regions in the basin, the impact of land use change on peak discharges and the impact of climate change on the runoff modeling. The high flood risk map can be then extracted by investigation of discharges, the river cross sections (the stage-discharge relation) and tributaries in the basin.

In order to show the accuracy of the modeling, the high flood risk map is compared with HORA[1] which shows a very good agreement and a successful modeling. Also, for flood control in high flood risk regions, levee and a retention dam are investigated.

This model then will be used as an input file for Hec-RAS in order to determine the high flood risk regions in the Schoeckelbach basin.

1- http://hora.gv.at/

## Acknowledgement

I would like to express my sincere gratitude to all those who gave me the possibility to complete this thesis. At first and foremost, I would like to express my deepest appreciation to my supervisor Prof. Gerald Zenz and the reviewer of my thesis Prof. Dirk Muschalla from Graz University of Technology (TUGraz). Also I would like to give my special thanks to my family, especially my brother Dr. Vahid Galavi from Plaxis BV (Netherlands) who kindly support me financially during my study in TUGraz. Also, I appreciate Afro Asian Institute (AAI) Graz for their financial support in 2010-2012.

My sincere thanks also go to Dr. Artemis Motamedi from Isfahan University of Technology (Iran) who kindly helped me during preparing and reviewing this thesis.

I deeply indebted to Prof. Saeid Eslamian from Isfahan University of Technology (Iran) who kindly gave me valuable information and guidance which helped me in completing this thesis especially in chapter two.

I also thank Dr. Helmut Knoblauch for his kind helps during my study in TUGraz.

# Chapter 1

# Introduction

## 1.1 Introduction

Flooding induced by storm events is a major concern in many regions of the world; more than one third of the total economic loss from natural catastrophes is caused by flooding and it is responsible for two thirds of people affected by natural disasters (Kafle, et al. 2010). In order to assess the consequences of floods caused by storm events, a catchment modeling is required. Basin models are in general designed to prepare synthetic hydrologic data for designing hydraulic structures or for forecasting. Basin models also can help us to study the potential impacts of changes in land use or climate. In basin modeling, when we need flood hydrograph and water availability, the relation between precipitation and discharge at the river's outlet should be modeled. This process is called "Rainfall - runoff modeling".

## 1.2 Procedure of rainfall-runoff modeling

The rainfall runoff model is one of the most frequently used models in hydrology (TR-55). It determines the hydrograph of runoff which leaves the watershed from the rainfall received by the watershed.

In general, the procedure of a hydrologic model can be summarized as following:

1. Problem definition and setting objectives
2. Model selection
3. Methodology

As rainfall-runoff modeling is a large hydrological modeling scale and the choice of this model is vary based on the purpose the modeling is being done for, these three steps should be appropriately considered first because they can lead the process to the reliable results.

### 1.2.1 Problem definition and setting objectives

The main purpose of this thesis is to model the high flood risk regions in a small catchment area in Austria (the Schoeckelbach basin). In order to find the inundation areas and make a flood risk map, the flood hydrographs in all reaches and junctions are

needed because they are the main data for every hydraulic project. To estimate these flood hydrographs, a rainfall-runoff modeling should be carried out.

In general, a rainfall-runoff modeling is a mathematical model which may be empirical, statistical or founded on known physical laws. The process of rainfall-runoff modeling is based on the law of the conservative of mass which is simply defined as follow:

$$I - \Delta S = O \tag{1-1}$$

Where:

I: Inflow,

O: Outflow,

$\Delta S$: change in storage.

This is the basic equation of hydrology which explains that for a rainfall-runoff modeling (outflow), the amount of inflow (precipitation) and change in storage (losses) should be modeled. Based on these brief statements, the main objectives of this thesis can be summarized as follows:

1. Rainfall analysis and determining an Intensity-Duration-Frequency (IDF) relation which can be incorporated in the model.
2. Loss analysis in order to evaluate changes in storage and determine the excess rainfall in the basin.
3. Develop a comprehensive analysis of rainfall – runoff in the catchment area and use of the computed hydrograph for flood map generation.
4. Calibrate the model with observed data.
5. Determine the high flood risk areas in the basin and evaluate the ability of the current hydraulic structures in the basin for floods protection.

This thesis also investigates the impacts of land use and climate change on flood hydrographs in order to estimate runoff variations in the future.

### 1.2.2 Model selection

The model is selected based on an understanding of the objectives and model difficulties. This process often depends on the type of system to be modeled, the hydrological elements to be modeled, data availability and its quality, data requirements for model calibration and model simplicity.

For rainfall-runoff modeling some models are available as follows:

1. **Empirical methods**: which use simple equations in order to estimate runoff flow at the outlet of the basin as a response to the rainfall. These equations are often derived from regression relationships. Empirical regression equations for most catchments are produced a very poor estimation of runoff.
2. **Large scale energy-water balance methods**: which are based on available energy and water balance hypothesis. These methods often use large scale observed data (such as rational equation) and their results may not be reliable for the local regions.
3. **Conceptual rainfall-runoff models**: which are widely used in Australia for water resources planning. These models convert rainfall to runoff considering evapotranspiration, movement of water and storage using a series of mathematical equations. In these models, it is assumed that the climatic conditions (time series) and model parameters are consistent across the catchment. They are calibrated easily and provide good results in gauged and un-gauged catchments.
4. **Landscape daily hydrological models**: which model the typical landscape process. These models often use for when additional variables such as soil moisture, recharge, salinity and etc. are needed. These models have greater complicity in compare to models which produce only stream flows.
5. **Fully distributed physically based hydrological models**: which make a spatial and temporal coordinates at a very fine scale for the entire catchment and equations are solved for each cell in the computational domain in order to find the solution.

Rainfall-runoff models are nonlinear processes which depend on the spatial and temporal distribution of the rainfall, catchment characteristics, land cover, soil type and etc., so it is difficult to explain the response of catchments with the simple equations or models. Based on the above statements, the specifications of good models for rainfall-runoff modeling should be as ability in simulation of short time events, simplicity in using, using of common equations and methods in modeling and capability of calibration as automatically and manually.

The Hydrologic Modeling System (HEC-HMS) was designed by the U.S. Army Corps of Engineers to simulate the rainfall - runoff processes. This is a semi-distributed, physically based hydrologic model which can simulate individual storm events as well as continuous rainfall input. This software has a variety of model options and it considers basin characteristics, land use, soil type, climatic conditions and time intervals in simulations.

Since rainfall – runoff models include both spatial and geomorphologic variations, Geographic Information Systems (GISs) have been widely used to simplify the estimation of runoff from watershed in recent years (USACE-HEC, 2010). Also, the HEC-GeoHMS computer program is an extension package used in ArcGIS software. This software can model and derive basin characteristics from Digital Elevation Model (DEM) and prepare this information as an input file for Hec-HMS which is used for runoff modeling in this thesis. Also, using Hec-GeoHMS, it is possible to create SCS CN map which is necessary for loss analysis during the process of rainfall-runoff modeling in Hec-HMS.

### 1.2.3 Methodology

Prior to explain the methodology, the available data for rainfall-runoff modeling in a basin should be investigated. These available data for the Schoeckelbach basin are collected as follows:

1. A digital elevation model (DEM) in very high resolution (1m by 1m).
2. Soil type map file which is based on FAO classification (250m by 250m).
3. Land cover map (30m by 30m).

4. Rainfall data for the nearest gauge to the basin (there is no any installed rainfall station in the Schoeckelbach basin).
5. Observed peak discharge data which were modeled statistically for various frequencies for a reach in the basin.

Based on these available data, the procedure for rainfall-runoff modeling can be summarized as follows:

**a. Rainfall analysis**

The observed data for calibration in this thesis are based on peak discharges for various frequencies. For this reason, the most important part of rainfall analysis is Intensity-Duration-Frequency (IDF) analysis. Because of existence of a rainfall data for limited duration, a best-fit probability distribution should be modeled. In this thesis L-moments and maximum likelihood methods are used in order to find the best-fit probability distribution and using a graphical method, IDF relation (Sherman equation) is modeled. The input data for this step is rainfall data.

**b. Terrain analysis**

In order to derive the basin characteristics such as basin border, sub-basins, reaches, slope and etc. a terrain analysis should be carried out. In this thesis this process is done using Hec-GeoHMS toolkit which is an extension for ArcGIS. The input data for this step is DEM.

Also the Muskingum-Cunge method for channel flood routing is used because it can increase accuracy, consistency and range of physical conditions when compared to other flood routing methods (the Natural Resources Conservation Service NRCS, 1965 and 1983).

**c. Loss analysis**

There are several methods to model rainfall losses. In this thesis SCS CN method is used because of soil data and land use conditions and also its simplicity. SCS CN method gives good results for basins covered by relatively homogenous land use and soil data and these data for the Schoeckelbach basin are almost homogenous. The input data for this step are soil data, land cover data and basin boundary. This process can be done in Hec-GeoHMS.

**d. Runoff modeling and calibration**

In this thesis, runoff modeling is done using Hec-HMS. All data which were prepared in the previous steps are used to simulate the hydrographs for various storm frequencies. After that, the model is calibrated using automatically and manually methods. Peak-weighted root mean square error (PWRMSE) method is used for automatic calibration. The modification of CN and time of concentration for steep sub-basins are used for manual calibration.

**e. Determining the high flood risk regions and validation**

In this thesis, Hec-RAS is used in order to determine the high flood risk regions. The hydrograph of floods which were simulated in the previous step is used as input for Hec-RAS in this step. For validation, the output results are compared with Natural Hazard Overview and Risk Assessment Austria (HORA[1]).

All these steps will be explained in the next chapters.

Basically, five softwares will be used in this thesis. Figure 1.1 briefly explains the model process for each of them.

## 1.3 Overview of the study area

The Schoeckelbach basin is located at northern Graz (the second largest city in Austria). The basin has a drainage area of 33.79 $km^2$. Skøien et al. (2003) divided catchments in Austria into three groups based on their area:

(a) small (3-70 $km^2$)
(b) medium (70-250 $km^2$)
(c) large (250-130,000 $km^2$)

Based on this classification, the Schoeckelbach basin is classified as small catchment.

The Schoeckelbach basin is a north to south oriented basin; streams originate from the northern parts of the basin and join together in the main river in the south part of the basin. Also, the main river is connected to the Mur River at the outlet of the basin.

1- http://hora.gv.at/

Figure (1.2) illustrates the study area location in Austria-Graz and figure (1.3) illustrates its coordinates.

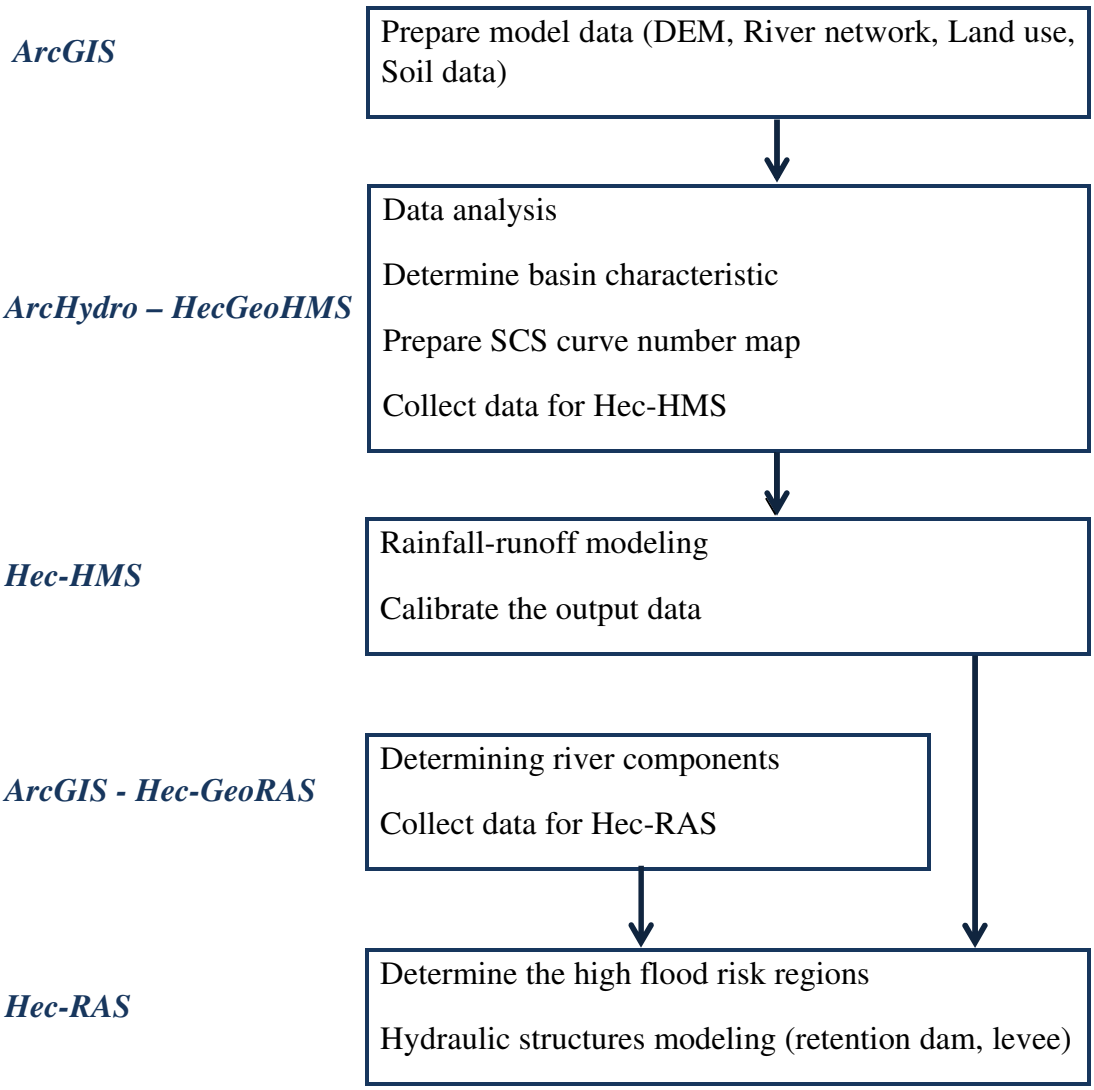


Figure 1.1: Thesis framework and methodology

### 1.3.1 Summary climate information for Graz[2]

The Schoeckelbach climate is strongly influenced by the Graz location (347 meters above sea level) standing on the south-eastern side of the Alps. Graz is quite protected from prevailing winds from the Atlantic and the center of Europe. As a result of this situation, the climate in Graz can feel distinctly Mediterranean[2]. The driest and most

2- http://www.graz.climatemaps.info

reliable weather in Graz falls between June and October, with daytime averages of around 25°C / 77°F in July and August.

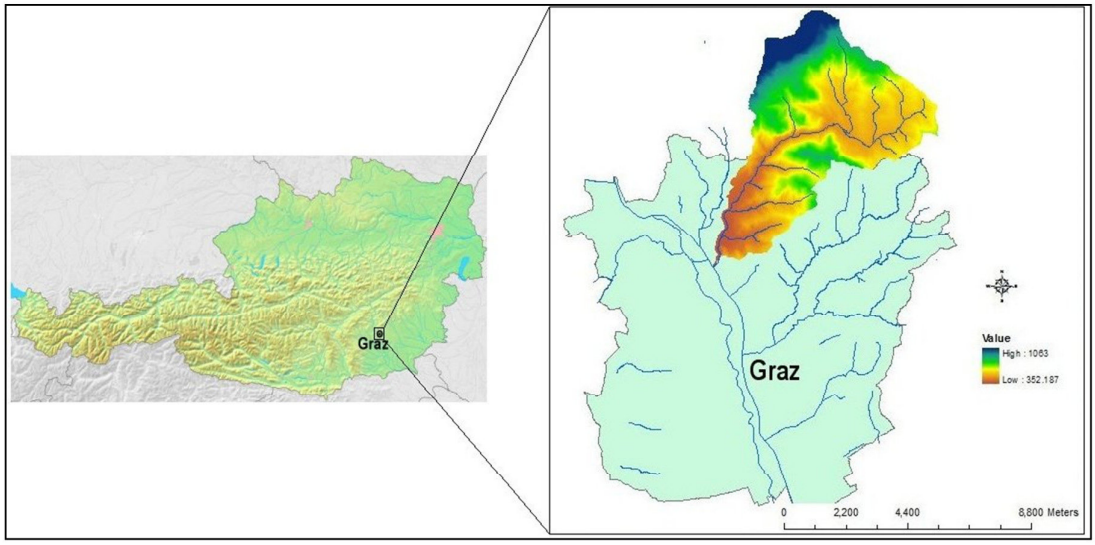


Figure 1.2: The Schoeckelbach basin location in Austria-Graz.

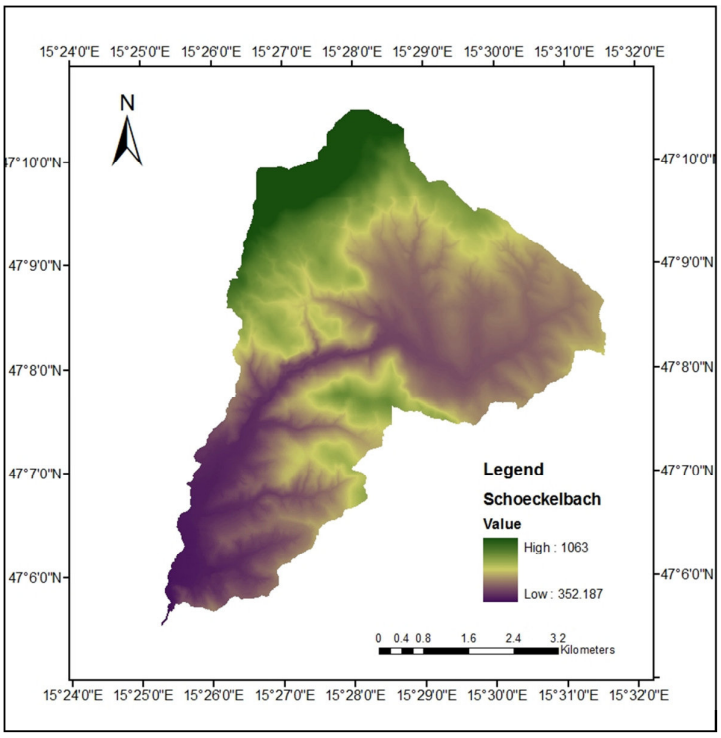


Figure 1.3: The Schoeckelbach basin coordinates and elevations.

Autumns in Graz and fairly short lived, since the summers can be long. When the winter climate arrives, heavy overnight frosts add a noticeable crispness to the air,

followed soon by spells of snowy weather. Spring is usually quite early with daytime temperatures staying above 10°C / 50°F.

Figures (1.4) to (1.8) display average monthly climate indicators in Graz based on 15 years of historical weather readings[3].

In Graz, on balance, there are 142 days annually on which greater than 0.1 mm (0.004 in) of precipitation (rain, sleet, snow or hail) occurs or 11.8 days on an average month. Also, the month with the wettest weather is July when on balance 127 mm (5.0 in) of rain, sleet, hail or snow falls across 15 days.

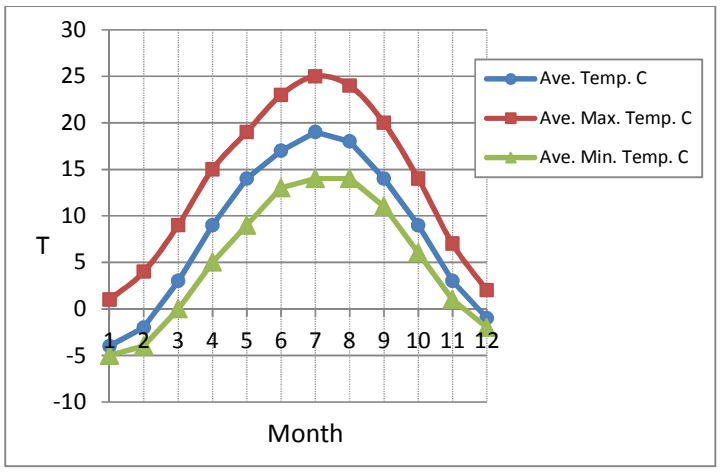


Figure 1.4: Summary of temperature information for Graz (Schoeckelbach)

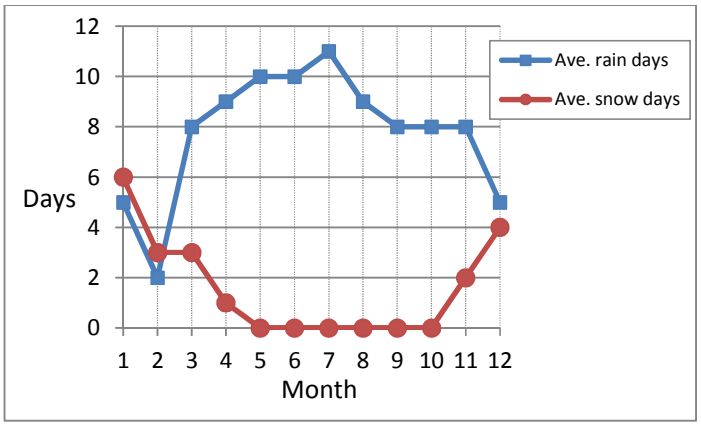


Figure 1.5: Summary of rainfall information for Graz (Schoeckelbach)

3-http://www.graz.climatetemp.info

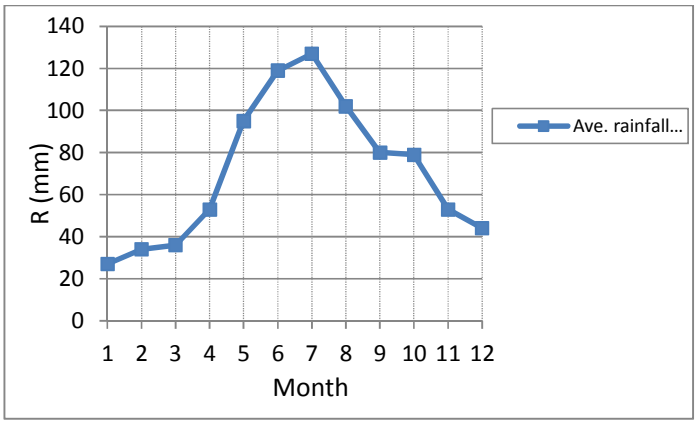


Figure 1.6: Summary of mean rainfall information for Graz (Schoeckelbach)

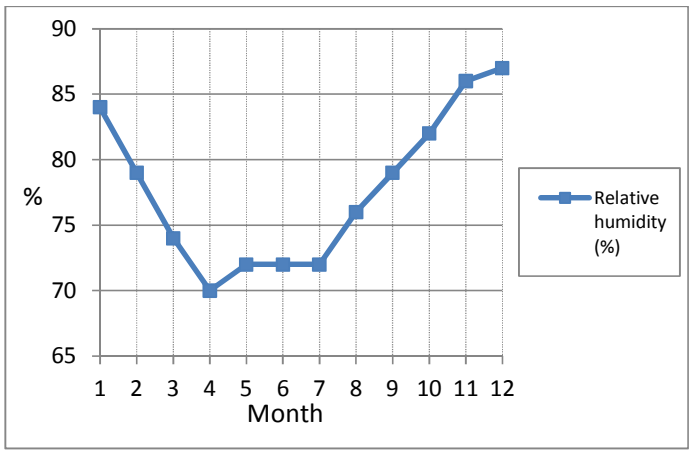


Figure 1.7: Relative humidity information for Graz (Schoeckelbach)

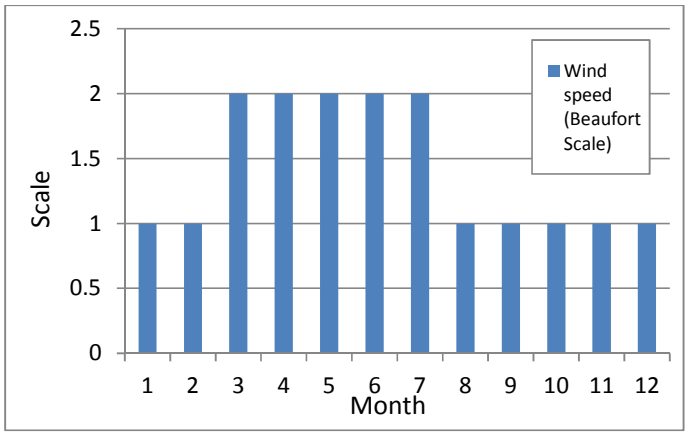


Figure 1.8: Wind speed information for Graz (Schoeckelbach)

## 1.4 Structure of the thesis

This thesis is subdivided into 6 chapters including introduction. These sex chapters can be summarized as follows:

1. Introduction: which gives a very briefly introduction about entire thesis including the location of the Schoeckelbach basin.
2. Rainfall analysis: This provides IDF relation for the Schoeckelbach basin. The best-fit probability distribution which fitted the observed rainfall data is determined in this chapter in order to estimate IDF parameters. The IDF relationship will be used for rainfall-runoff modeling in chapter 5.
3. Terrain analysis: The Hec-GeoHMS process will be discussed in this chapter. Derivation of the catchment characteristics, specification of the river network parameters, the channel routing method and its parameters will be presented in chapter 3.
4. Loss analysis: This presents the estimation of the loss method parameters and preparing SCS CN grid for the model.
5. Runoff modeling using Hec-HMS: The process of rainfall-runoff modeling and calibration are discussed in this chapter. Also, this chapter includes the impact of land use change and climate change on peak discharges in the future.
6. Flood management using Hec-RAS: The process of determining the high flood risk regions in the Schoeckelbach basin will be presented in this chapter. This process will be done in Hec-RAS.
7. Appendix A: In this appendix, some additional Figures are provided for more information. All of these Figures were discussed in chapters 5 and 6.
8. Appendix B: In this Appendix, some methods which were used in this thesis are presented. These methods can be found in more details in many hydrology textbooks and for this reason they are explained briefly in this appendix.

The structure of the thesis and the major input data are illustrated in Figure 1.9.

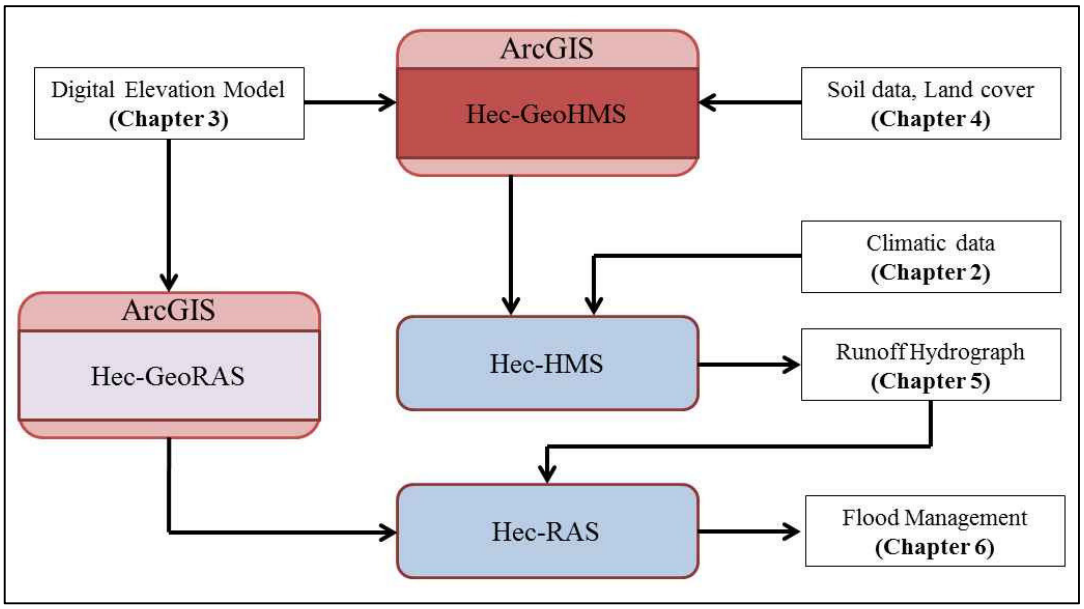


Figure 1.9: Structure of the thesis

# Chapter 2

# Rainfall Analysis

## 2.1 Introduction

Rainfall analysis is the first step to determine the rainfall event in many hydrologic design projects because rainfall is the driving force behind all storm water studies and designs. In fact, in order to prepare satisfactory storm water management projects, it is necessary to understand and model the rainfall data.

One of the most important parts of a rainfall analysis is Intensity-Duration-Frequency (IDF) analysis which is used to derive the necessary characteristics of point rainfall for shorter durations. In order to evaluate an approximately precise IDF relation, the recorded rainfall data series should be studied for identifying data gaps and also outlier data. After that, annual extremes are extracted from the recorded time series data for each duration and then, the annual extreme data is fitted to a proper probability distribution model in order to estimate rainfall quantities.

In order to obtain the best-fit probability distribution model, the parameters for a few commonly used rainfall analysis distributions should be estimated and then the best-fit probability distribution could be selected among these probability distributions. In this thesis L-moments and maximum likelihood methods are used. L-moments method was introduced by Hosking (1990) and it is a recent development in mathematical statistics, which simplifies the parameter estimation process in frequency analysis.

Also for goodness fit analysis, three methods are used as Chi-Square, Kolmogorov-Smirnov and the root mean square error (RMSE) method. After these analyses, it is possible to choose the best fit probability distribution. This probability distribution model is necessary because the fitted distribution can not only be used to interpolate, but also to extrapolate to find return periods of extreme values that were not apparent during the relatively short period of observation.

In this chapter, a rainfall Intensity-Duration-Frequency (IDF) relation will be generated for northern Graz from the historic rainfall data which has been recorded for several years. The analyses involve the following steps:

1. Data series identification
2. Distribution identification
3. Statistical confidence analysis

4. Estimation of IDF relation parameters
5. Sources of errors in rainfall estimation

All these steps will be explained in this chapter.

## 2.2 Data series identification

For the Schoeckelbach basin there is not any installed rainfall station in the area and, therefore, there is not any recorded rainfall data for this specific area. The municipality of Graz is running some additional rainfall stations in Graz and also a gauge on the Schoeckelbach which may be useful in the future.

However, for this research, the nearest neighbor rainfall station which is situated in the Andritz basin should be used. Figure 2.1 illustrates the position of the Andritz rainfall station which is very close (500 m) to the Schoeckelbach basin.

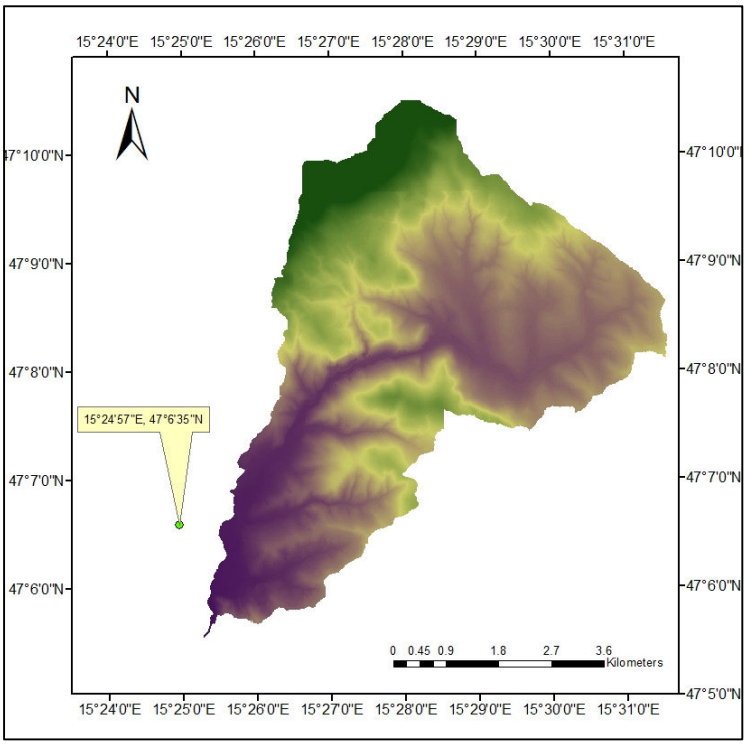


Figure 2.1: The position of the Andritz rainfall station

Although this station is placed outside the Schoeckelbach basin, but it is possible to use its rainfall data for the Schoeckelbach basin because according to Table 2.1 which gives a guideline as to the number of rain-gauges to be erected in a given area, and also considering the area of the Schoeckelbach basin (33.79 $km^2$), this rainfall gauge is

enough for both the Andritz and the Schoeckelbach basin (the area of both the Andritz and the Schoeckelbach basin is less than 80 $km^2$) (see also section 2.6 for the sources of errors in rainfall estimation).

Table 2.1: Rain-gauge density (Chow, 1964)

| **Area status** | **Rain-gauge density** |
|---|---|
| Plains | 1 in 520 $km^2$ |
| Elevated regions | 1 in 260-390 $km^2$ |
| Hilly and very heavy rainfall areas | 1 in 130 $km^2$ preferably with 10% of the rain-gauge stations equipped with the self-recording type |

For this rain gauge, there are 2 kinds of rainfall data are available:

1. Daily rainfall data which have been recorded every day at 7 A.M. for about 66 years (from 01.01.1946 to 30.09.2012).
2. 15-minute rainfall data which have been recorded every 15 minutes for about 8 years (from Sep. 2005 to Oct. 2012).

In order to achieve a precise IDF relation, the observed record of hourly (or other finer resolution) data should be collected. For this reason, at first, 15, 30, 60, 120 and 720 minutes rainfall data are extracted from the observed record 15-minute rainfall data and then an IDF relation, which fitted all the data, will be produced. After that, this relation will be calibrated by the observed record of the daily data.

## 2.3 Distribution identification

In order to find return periods of extreme values that were not apparent during the relatively short period of observation, the fitted distribution can be used (interpolate and extrapolate).

To find some good fitted distributions, the following statistical equations (skewness test) will be used (Mahdavi, 2003):

$$m_3 = \frac{1}{n}\sum_{i=1}^{n}(X_i - \overline{X})^3 \qquad (2\text{-}1)$$

$$H = 1.96 \times s^3 \left(\sqrt{\frac{6}{n}}\right) \quad (2\text{-}2)$$

Where:

$m_3$: Third central moment

$X_i$: The $i^{th}$ element of the data series

$\overline{X}$: The mean value of the data series

s: The standard deviation of the data series

n: Number of data

(H is always positive).

Now, according to Table 2.2, some good fitted distributions are selected.

Table 2.2: Best fitted distributions for various conditions (Mahdavi 2003)

| **The relation between H and $m_3$** | **Data status** | **Best fitted distribution** |
|---|---|---|
| $-H \leq m_3 \leq +H$ | Symmetric distribution (at 95% confidence) | Normal |
| $m_3 > +H$ | Positive skew distribution | Gumbel, Log-normal II, Log-normal III, Pearson type III, Log-Pearson III, Generalized Extreme Value (GEV) |
| $m_3 < -H$ | Negative skew distribution | Pearson type III |

To find the best fitted distribution for the rainfall data of the Schoeckelbach basin, first, the annual maximum daily rainfall is produced (Figure 2.2). However the process for another rainfall data is the same.

The mean value and the standard deviation of the annual maximum daily series were calculated and then third central moment was obtained as follow:

$\overline{X} = 53.236$ mm, $s = 15.071$, $m_3 = 3546.014$ mm$^3$ $H = 2023.116$

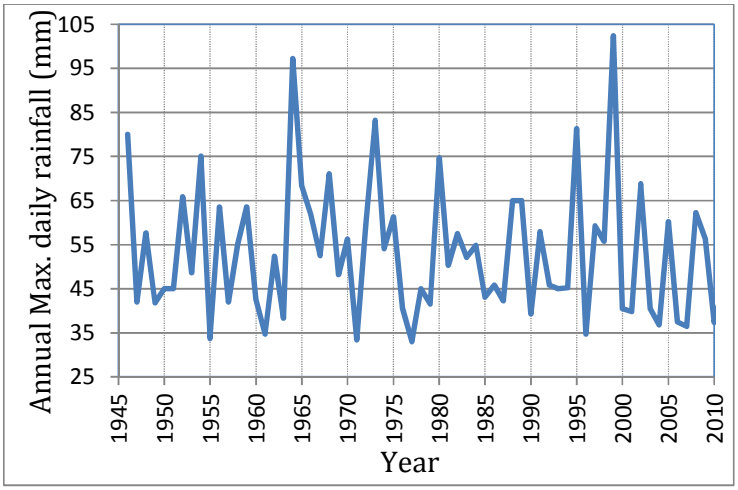


Figure 2.2: The annual maximum daily rainfall

As it can be seen, ($m_3 > +H$), the annual maximum daily series is a positively skewed distribution. Among several distributions which can fit this series, four commonly used probability distributions in rainfall analysis are selected and then the best-fit probability distribution will be determined using L-moments and maximum likelihood methods.

### 2.3.1 L-Moments Method

L-moments statistics are used extensively in many frequency analysis studies and data testing such as homogeneity/heterogeneity of proposed groupings of sites (regions), goodness of fit tests for identifying suitable probability distributions and for solving distribution parameters for the selected probability distributions (L-RAP, 2011).

L-moments is a linear combination of probability weighted moments (Greenwood et al. 1979) which computed from data values:

$$b_0 = \frac{1}{n}\sum_{i=1}^{n} X_i \tag{2-3}$$

$$b_r = \frac{1}{n}\sum_{i=r+1}^{n} \frac{(i-1)(i-2)...(i-r)}{(n-1)(n-2)...(n-r)} X_i \tag{2-4}$$

In which $x_1, x_2, ...x_n$ are arranged in increasing order and n is the number of sample data. The first few L-moments are defined as:

| | |
|---|---|
| $L_1 = b_0$ | The sample mean, a measure of location. |
| $L_2 = 2b_1 - b_0$ | A multiple of Gini's mean difference statistic, a measure of the dispersion of the data values about their mean. |
| $L_3 = 6b_2 - 6b_1 + b_0$ | |
| $L_4 = 20b_3 - 30b_2 + 12b_1 - b_0$ | |

Now by dividing the higher order L-moments by the dispersion measure ($L_2$), the L-moment ratios can be obtained as follows:

| | |
|---|---|
| $\tau_2 = \frac{L_2}{L_1}$ | The coefficient of variation (L-CV) |
| $\tau_3 = \frac{L_3}{L_2}$ | A measure of skewness (L-skewness) |
| $\tau_4 = \frac{L_4}{L_2}$ | A measure of kurtosis (L-kurtosis) |

Tables 2.3 and 2.4 are summarized the general descriptions of relative magnitude of L-CV and L-skewness, respectively (Hosking, 1990).

Table 2.3: General descriptions of relative magnitude of L-CV (L-RAP, 2011)

| | |
|---|---|
| $0.000 < \lvert L-CV \rvert \le 0.025$ | Minimal variability |
| $0.025 < \lvert L-CV \rvert \le 0.075$ | Minor variability |
| $0.075 < \lvert L-CV \rvert \le 0.150$ | Moderate variability |
| $0.150 < \lvert L-CV \rvert \le 0.400$ | Large variability |
| $0.400 < \lvert L-CV \rvert$ | Very large variability |

In this thesis, daily rainfall data which have been recorded for 66 years (1946-2012) was used for analysis (the process for another rainfall data is the same). The annual extreme values are shown in Fig. 2.2. Table 2.5 summarized some information about this data set.

Table 2.4: General description of relative magnitude of L-skewness (L-RAP, 2011)

| | |
|---|---|
| $L-skewness=0.0$ | Symmetrical distribution |
| $0.000<\lvert L-Skw.\rvert\le 0.050$ | Minor skewness |
| $0.050<\lvert L-Skw.\rvert\le 0.150$ | Moderate skewness |
| $0.150<\lvert L-Skw.\rvert\le 0.300$ | Large skewness |
| $0.300<\lvert L-Skw.\rvert$ | Very large skewness (suggestive of volatile or outlier prone Dist.) |

Table 2.5: Information about the annual extreme daily rainfall

| **n** | **Max.** | **Min.** | **Median** | **$L_1$** | **$L_2$** |
|---|---|---|---|---|---|
| 66 | 102.4 | 33 | 51.2 | 53.24 | 8.33 |
| **$L_3$** | **$L_4$** | **$\tau_2$** | **$\tau_3$** | **$\tau_4$** | **Std. Dev.** |
| 1.68 | 0.95 | 0.16 | 0.20 | 0.11 | 15.07 |

Based on Tables 2.3 and 2.4, the annual extreme daily rainfall data has a large skewness and variability data.

### 2.3.2 Parameter estimation using L-moments method

Before the analysis can be carried out, the parameter for each selected distribution needs to be estimated first. In this thesis, L-moments method is used to estimate the parameter of four selected distributions since they are commonly used in rainfall or flood frequency analysis. In all following distributions, $\gamma$ is the location parameter that defines the point where the support set of the distribution begins, $\mu$ is the scale parameter that stretches or shrinks the distribution and $\sigma$ is the shape parameter that effects the shape of the distribution.

#### (a) Generalized Extreme Value (GEV) distribution

The probability density function (pdf) of the GEV is defined as follow:

$$f(x;\mu,\sigma,\gamma)=\frac{1}{\mu}\left[1+\sigma\left(\frac{x-\gamma}{\mu}\right)\right]^{\left(-\frac{1}{\sigma}-1\right)}\exp\left[-\left(1+\sigma\left(\frac{x-\gamma}{\mu}\right)\right)^{\left(-\frac{1}{\sigma}\right)}\right] \qquad (2\text{-}5)$$

where $1+\sigma(x-\gamma)/\mu>0$, $\mu>0$ , $\gamma\in\mathbb{R}$ and $\sigma\in\mathbb{R}$.

The Tr-year return precipitation in this distribution is defined as:

$$R_{Tr} = \gamma + \frac{\mu}{\sigma}\left(1 - \left(-\log\left(\frac{Tr-1}{Tr}\right)\right)^{\sigma}\right) \tag{2-6}$$

where

$$\sigma = 7.8590c + 2.9554c^2 \tag{2-7}$$

$$c = \frac{2}{3+\tau_3} - \frac{\ln 2}{\ln 3} \tag{2-8}$$

$$\mu = \frac{L_2\sigma}{\left(1-2^{-\sigma}\right)\Gamma\left(1+\sigma\right)} \tag{2-9}$$

$$\gamma = L_1 - \frac{\mu\left(1-\Gamma\left(1+\sigma\right)\right)}{\sigma} \tag{2-10}$$

and $\Gamma$ denotes the Gamma function.

**(b) The Gumbel Distribution**

The general formula for the probability density function (pdf) of the Gumbel (maximum) distribution is as follow:

$$f\left(x;\mu,\gamma\right) = \frac{1}{\mu}\exp\left(-\frac{x-\gamma}{\mu}\right)\exp\left[-\exp\left(-\frac{x-\gamma}{\mu}\right)\right] \tag{2-11}$$

The Tr-year return precipitation in this distribution is defined as:

$$R_{Tr} = \gamma + \mu Y_{Tr} \tag{2-12}$$

In which:

$$\gamma = L_1 - 0.5772\mu \tag{2-13}$$

$$\mu = \frac{L_2}{\log 2} \tag{2-14}$$

$$Y_{Tr} = -\ln\left(-\ln\left(\frac{Tr-1}{Tr}\right)\right) \tag{2-15}$$

**(c) Log-Pearson type III (LP III) Distribution**

The probability density function (pdf) of the LP III is defined as follow:

$$f(x;\mu,\sigma,\gamma)=\frac{1}{\mu^{\sigma}\Gamma(\sigma)}\left(\frac{x-\gamma}{\mu}\right)^{(\sigma-1)}\exp\left(-\frac{x-\gamma}{\mu}\right) \tag{2-16}$$

Where $\mu,\sigma>0$ , $x>\gamma$ and $\Gamma$ denotes the Gamma function.

The parameters of LP III are defined as follows:

$$\mu=L_1 \tag{2-17}$$

$$\gamma=\frac{2}{\sqrt{\alpha}}sign(\tau_3) \tag{2-18}$$

$$\sigma=\frac{L_2\Gamma(\alpha)\sqrt{\pi\alpha}}{\Gamma(\alpha+0.5)} \tag{2-19}$$

In which:

$$\begin{aligned} &if \quad 0<|\tau_3|<\frac{1}{3} \quad then \quad z=3\pi{\tau_3}^2 \\ &\alpha=\frac{1+0.2906z}{z+0.1882z^2+0.0442z^3} \end{aligned} \tag{2-20}$$

$$\begin{aligned} &if \quad \frac{1}{3}<|\tau_3|<1 \quad then \quad z=1-|\tau_3| \\ &\alpha=\frac{0.36067z-0.59567z^2+0.25361z^3}{1-2.78861z+2.56096z^2-0.77045z^3} \end{aligned} \tag{2-21}$$

**(d) 3-Parameter Log-Normal (LN III) distribution**

The probability density function (pdf) of the LN III is defined as follow:

$$f(x;\mu,\sigma,\gamma)=\frac{1}{(x-\gamma)\sigma\sqrt{2\pi}}\exp\left[-\frac{\left[\ln(x-\gamma)-\mu\right]^2}{2\sigma^2}\right] \tag{2-22}$$

where $0\le\gamma<x$, $-\infty<\mu<+\infty$ and $\sigma>0$.

Hosking (1990) developed a set of approximate relations for estimation of parameters for LN III (Yuanfang et al., 2004). The relative error of these relations may be less than $10^{-6}$. The following relations were arranged by Yuanfang et al., 2004.

$$L_1 = \gamma + \exp\left(\mu + \frac{\sigma^2}{2}\right) \tag{2-23}$$

$$L_2 = -\exp\left(\mu + \frac{\sigma^2}{2}\right) \times \left(1 - 2\Phi\left(\frac{\sigma}{\sqrt{2}}\right)\right) \tag{2-24}$$

$$\tau_3 = \sigma \frac{A_0 + A_1\sigma^2 + A_2\sigma^4 + A_3\sigma^6}{1 + B_1\sigma^2 + B_2\sigma^4 + B_3\sigma^6} \tag{2-25}$$

In which $\Phi(x)$ indicates distribution function of a standard normal distribution. All other parameters can be obtained from Table 2.6.

If $(L_1, L_2, \tau_3)$ are known, the distribution parameters may be easily obtained by the following equations (only when $|\tau_3| \le 0.94$ and $|\sigma| \le 3$ ):

$$\sigma = \tau_3 \frac{E_0 + E_1{\tau_3}^2 + E_2{\tau_3}^4 + E_3{\tau_3}^6}{1 + F_1{\tau_3}^2 + F_2{\tau_3}^4 + F_3{\tau_3}^6} \tag{2-26}$$

$$\mu = \ln\left(\frac{-L_2 \exp\left(-\frac{\sigma^2}{2}\right)}{1 - 2\Phi\left(\frac{\sigma}{\sqrt{2}}\right)}\right) \tag{2-27}$$

$$\gamma = L_1 - \exp\left(\mu + \frac{\sigma^2}{2}\right) \tag{2-28}$$

All other parameters are presented in Table 2.6. These relations are suitable to LN III with positive skewness.

### 2.3.3 Parameter Estimation using Maximum Likelihood Method

One of the most common ways to estimate the probability distribution parameters in statistical modeling is the maximum likelihood method which simply maximizes the likelihood function to estimate model parameters.

Table 2.6: All parameters in Eqs 2-25 and 2-26.

| $A_0$ | $A_1$ | $A_2$ | $A_3$ |
|---|---|---|---|
| 0.4886025 | 4.44931E-3 | 8.80271E-4 | 1.15071E-6 |

| $E_0$ | $E_1$ | $E_2$ | $E_3$ |
|---|---|---|---|
| 2.0466534 | -3.6544371 | 1.8396733 | -0.2036024 |

| $B_1$ | $B_2$ | $B_3$ |
|---|---|---|
| 6.46629E-2 | 3.30904E-3 | 7.42907E-5 |

| $F_1$ | $F_2$ | $F_3$ |
|---|---|---|
| -2.0182173 | 1.2420401 | -0.2174180 |

In rainfall data because of existing only positive values, the maximum values of the likelihood function and the logarithm of the likelihood function always are the same magnitudes of the distribution parameters. Therefore, instead of the likelihood function, it is more convenient to use the logarithm of the likelihood function as follow (Seckin 2010):

$$LLF = \sum \ln\left(f\left(x_i;\sigma,\mu,\gamma\right)\right) \tag{2-29}$$

The logarithm of the likelihood functions for the mentioned distributions are defined as follows:

**(a) GEV**

$$LLF = -n\ln\left(\mu\right) - \left(1-\sigma\right)\sum y_i - \sum \exp\left(-y_i\right) \tag{2-30}$$

In which

$$y_i = \frac{-\ln\left[1-\sigma\left(\frac{x_i-\gamma}{\mu}\right)\right]}{\sigma} \tag{2-31}$$

**(b) LP III**

$$LLF = -n\ln\left(\left|\mu\right|\right) - n\ln\left[\Gamma\left(\sigma\right)\right] - \sum \ln\left(x_i\right) - \frac{1}{\mu}\sum\left[\ln\left(x_i\right)-\gamma\right] + \left(\sigma-1\right)\sum \ln\left[\frac{\ln\left(x_i\right)-\gamma}{\mu}\right] \tag{2-32}$$

**(c) LN III**

$$LLF = -\frac{n}{2}\ln(2\pi) - n\ln(\sigma) - \sum \ln(x_i - \gamma) - \sum \frac{\left[\ln\left(\frac{x_i - \gamma}{\mu}\right)\right]^2}{2\sigma^2} \quad (2\text{-}34)$$

### 2.3.4 Goodness of Fit tests

The goodness of fit of a statistical model describes how well it fits a set of observations. Measures of goodness of fit typically summarize the difference between observed values and the values expected under the model in question. Such measures can be used in statistical hypothesis testing such as to test for normality of residuals (RMSE test), to test whether two samples are drawn from identical distributions (Kolmogorov-Smirnov test) or whether outcome frequencies follow a specified distribution (Chi-squared test) [Wikipedia[1]]. In this thesis, these three tests are carried out on the data.

**(a) Chi-Squared test**

This test is applied to binned data, so the value of the test statistic depends on how the data is binned (EasyFit 5.5). This thesis employs the following empirical formula:

$$k = 1 + \log_2 N \quad (2\text{-}34)$$

Where:

k: The number of bins

N: The sample size

The Chi-Squared statistic is defined as:

$$\chi^2 = \sum_{i=1}^{k} \frac{(O_i - E_i)^2}{E_i} \quad (2\text{-}35)$$

Where:

1- http://en.wikipedia.org/wiki/Goodness_of_fit

$O_i$: The observed frequency for bin i

$E_i$: The expected frequency for bin i calculated by:

$$E_i = F(x_2) - F(x_1) \tag{2-36}$$

Where:

F: The cumulative distribution function of the probability distribution being tested

$x_1$, $x_2$: The limits for bin i.

**(b) Kolmogorov-Smirnov test**

Assume that there is a random sample $x_1$, ... , $x_n$ from some distribution with cumulative distribution function F(x). The empirical cumulative distribution function is denoted by:

$$F_n(x) = \frac{[N \le x]}{n} \tag{2-37}$$

In which

N: The number of observations.

The Kolmogorov-Smirnov statistic (D) is based on the largest vertical difference between the theoretical and the empirical cumulative distribution function (EasyFit):

$$D = \max_{1 \le i \le n} \left[ F(x_i) - \frac{i-1}{n}, \frac{i}{n} - F(x_i) \right] \tag{2-38}$$

**(c) The Root Mean Square Error (RMSE) test**

The Root Mean Square Error (RMSE) (also called the root mean square deviation, RMSD) is a frequently used measure of the difference between values predicted by a model and the values actually observed from the environment that is being modeled (these individual differences are also called residuals). The RMSE is calculated using the following relation (Haan 2002):

$$RMSE = \left[ \frac{\sum_{i=1}^{n} (R_m - R_i)^2}{n - m} \right]^{0.5} \quad (2\text{-}39)$$

In which, $R_m$ is the modeled rainfall depth (using fitted probability distribution), $R_i$ is the $i^{th}$ observed rainfall depth, n is the number of data and m depends on the number of parameters in the fitted probability distribution (for LP III, LN III and GEV are 3 and for the Gumbel distribution is 2).

### 2.3.5 The Quartile-Quartile Plot (Q-Q Plot)

When the input (observed) data values plotted against the theoretical (fitted) distribution quartiles in a graph, the Quartile-Quartile (Q-Q) plot is produced. Both axes of this graph are in units of the input data set. The quartile-quartile graphs are produced by plotting the observed data values $x_i$ (i = 1, ... , n) against the X-axis, and the following values against the Y-axis (EasyFit 5.5):

$$F^{-1}\left( F_n(x_i) - \frac{0.5}{n} \right) \quad (2\text{-}40)$$

In which:

$F^{-1}(x)$: Inverse cumulative distribution function

$F_n(x)$: Empirical cumulative distribution function

n: Sample size.

The Q-Q plot will be approximately linear if the specified theoretical distribution is the correct model.

### 2.3.6 Probability Difference Plot (P-D Plot)

This graph (very similar to Q-Q plot) can be used to determine how well the theoretical distribution fits to the observed data and compare the goodness of fit of several fitted distributions. The probability difference graph is a plot of the difference

between the empirical cumulative density function and the theoretical cumulative density function as follow (EasyFit 5.5):

$$PDif(x) = F_n(x) - F(x) \tag{2-41}$$

### 2.3.7 The Best-Fit Probability Distribution

Based on the previous statements, all mentioned distributions were analyzed and the final results are described here. For determining all distributions, first distribution parameters should be obtained. The optimized distribution parameters were computed for each distribution and they are shown in Table 2.7. Based on these parameters, probability density function (pdf) for each distribution was computed and they are shown in Fig. 2.3.

Table 2.7: The optimized distribution parameters

| **Parameters** | **GEV** | **Gumbel** | **LP III** | **LN III** |
|---|---|---|---|---|
| $\gamma$ (Location) | 46.044 | 46.401 | 2.6549 | 25.475 |
| $\mu$ (Scale) | 11.473 | 11.841 | 0.05616 | 3.1774 |
| $\sigma$ (Shape) | 0.04801 | - | 22.849 | 0.55143 |

In next step, the goodness fit tests were done and the results are shown in Table 2.8. As it can be seen in this table, the results are a little complicated because the results of the Kolmogorov-Smirnov test are very closed to each other for different distributions and their ranks in this test are very different with Chi-Square method and a little with RMSE method. This table also described that the Gumble distribution is the best fit distribution in both Chi-Square and RMSE tests. Also, the results of Chi-Square test are shown that the values for LN III, GEV and LP III are much closed whereas the value for Gumbel distribution is very smaller than the others (also in RMSE method). For more information about the distribution and in order to arrange all distributions, there is a need to continue our analysis in Q-Q plot and P-D Plot. These two important diagrams are shown in Figures 2.4 and 2.5, respectively. As it can be seen in Fig. 2.4, for x>50, the Gumbel distribution is very close to the fitted line and then GEV, LP III and LN III. As an alternative method, Figure 2.5 illustrates that the Gumble distribution is the best one and GEV, LN III and LP III are in subsequent ranks.

Table 2.8: The results of the goodness fit tests and final decision rank

| Distribution | Chi-Squared | | RMSE | | Kolmogorov-Smirnov | | Final Decision |
|---|---|---|---|---|---|---|---|
| | Value | Rank | Value | Rank | Value | Rank | |
| Gumbel | 0.87164 | 1 | 2.04 | 1 | 0.10534 | 4 | 1 |
| GEV | 2.7235 | 3 | 10.22 | 3 | 0.09448 | 2 | 2 |
| LN III | 2.9641 | 4 | 6.18 | 2 | 0.08165 | 1 | 3 |
| LP III | 2.6844 | 2 | 14.40 | 4 | 0.09764 | 3 | 4 |

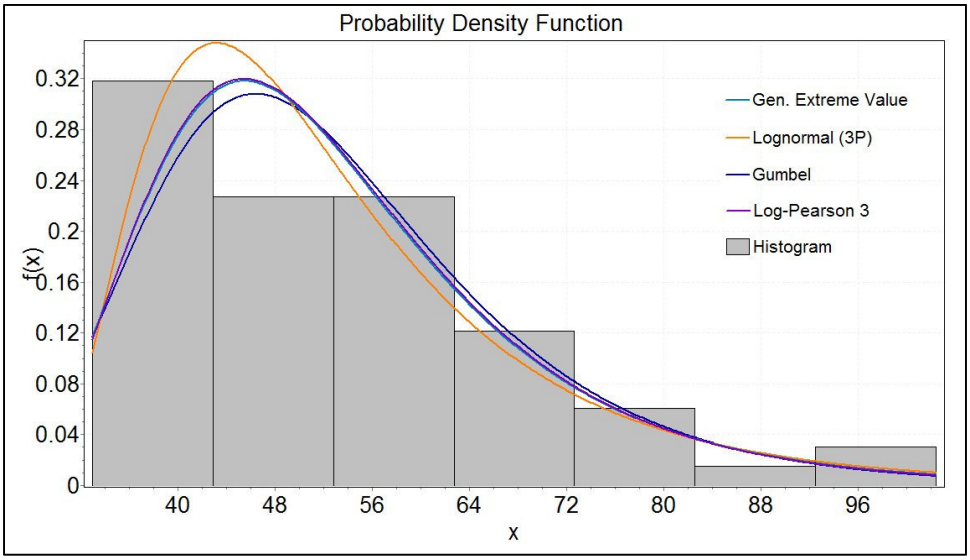


Figure 2.3: Probability density function (pdf) for all distributions

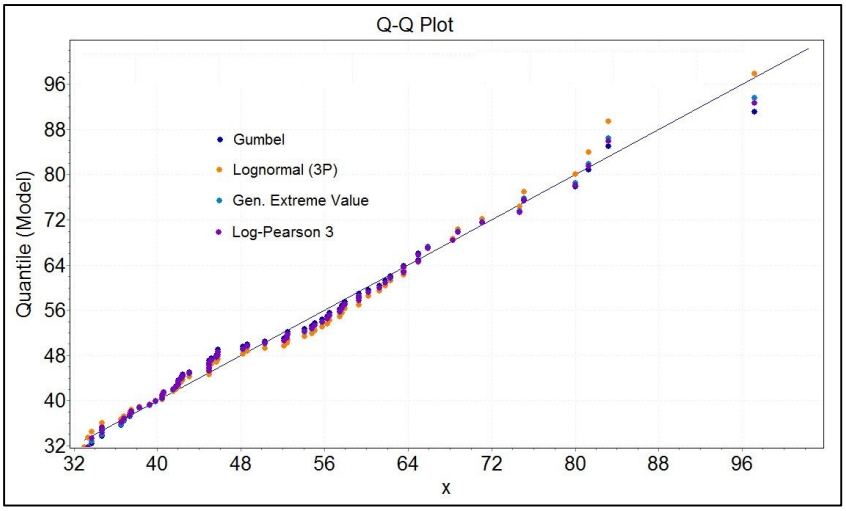


Figure 2.4: Q-Q plot for all distributions

As a final comparison, the sorted observed rainfall and all modeled rainfalls with various distributions are plotted in Figure 2.6. Also box-plots of these series are shown in Figure 2.7. As these figures show, the Gumbel distribution is completely fitted the observed data whereas the LP III is almost far from the observed data especially for the maximum and minimum values in the sorted data. GEV and LN III are almost fitted the observed data but LN III gave smaller values and GEV gave greater values. Due to this reason, GEV is better than LN III and finally these distributions are ranked as they are shown in table 2.8.

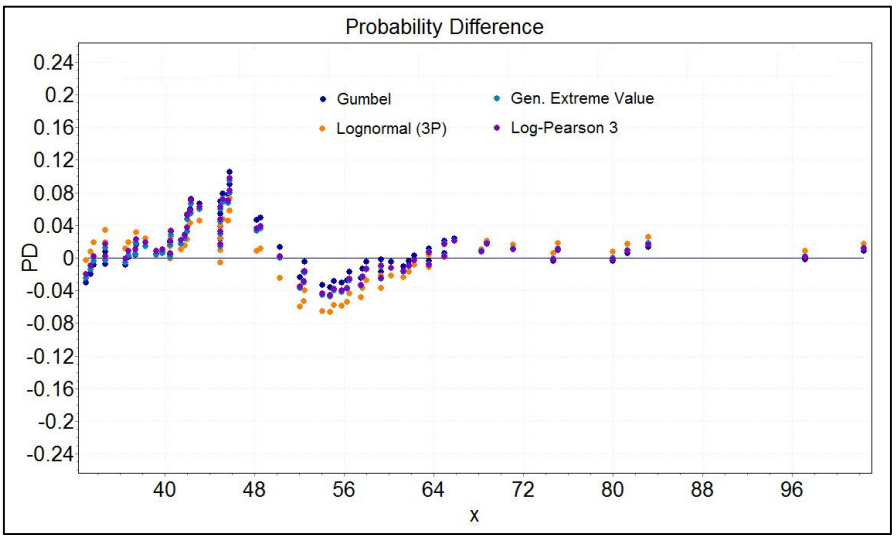


Figure 2.5: Probability difference plot for all distributions

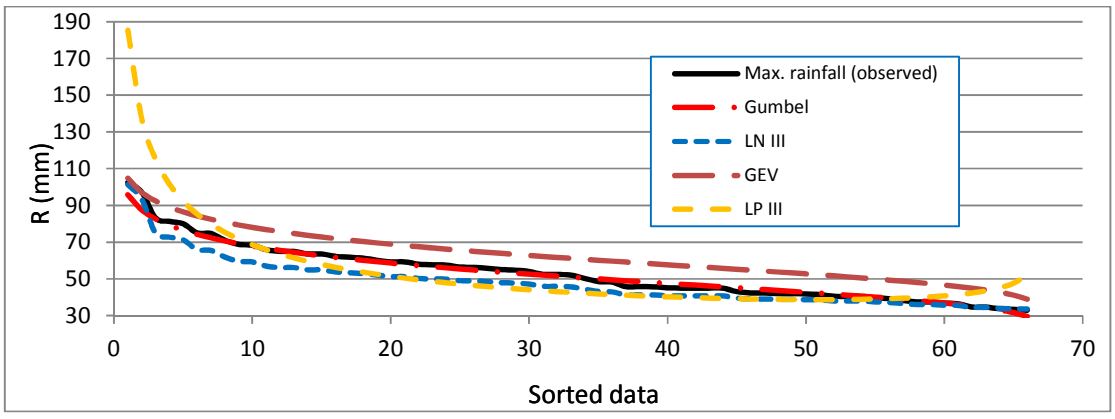


Figure 2.6: A comparison between the sorted observed data and all distributions

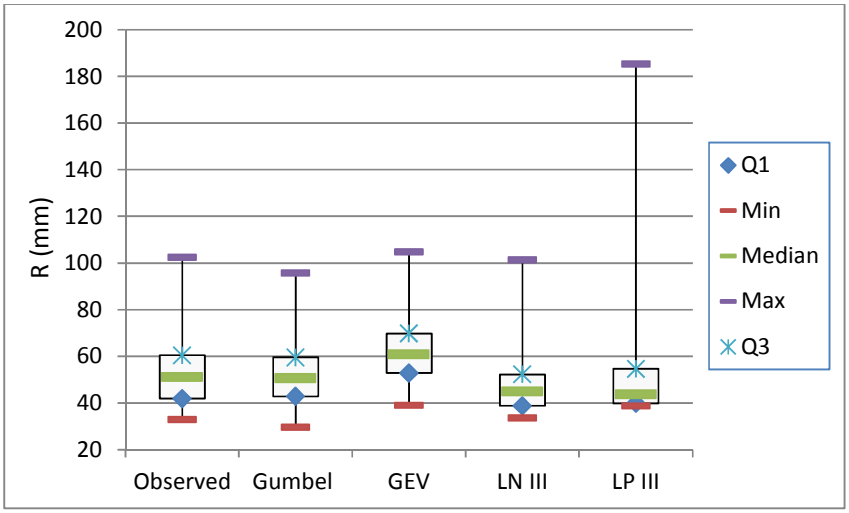


Figure 2.7: Box-plots for all series

## 2.4 Statistical Confidence limit

In order to represent the uncertainty in an estimate of a curve or function based on limited or noisy data, a confidence analysis is used in statistical modeling. Confidence analyses are often used as part of the graphical presentation of results in a statistical modeling.

The confidence limits are expressed as follow (Mahdavi 2003):

$$X_{Tr,u} = X_{Tr} + S\Delta X \tag{2-42}$$

$$X_{Tr,l} = X_{Tr} - S\Delta X \tag{2-43}$$

in which $X_{Tr}=x_t$ (the Gumbel's distribution parameter)

$$\Delta X = \frac{a\delta}{\sqrt{n}} \quad \text{and} \quad a = (1 + 1.3K + 1.1K^2)^{0.5}$$

where:

S: is a constant (for 90% confidence=1.645)

δ: the standard deviation

n: number of data

K: the Gumbel's parameter

$X_{Tr,u}$ and $X_{Tr,l}$: upper and lower confidence limits for the return period of Tr

Based on these equations, a 90% confidence analysis was constructed and the final result is shown in Figure 2.8. As it can be seen in this figure, the best-fit probability distribution which were obtained in the previous section, is fitted precisely the observed data and can be used for rainfall-runoff analysis of the Schoeckelbach basin and, of course, for north part of Graz.

To know how the confidence limits were calculated, the procedure is briefly explained in table 2.9.

Table 2.9: The 90% confidence analysis for the best-fit probability distribution (only the results of some return periods are shown)

| **The confidence limit parameters** | **Return periods (Tr : year) (n=66 and $S_{90\%}$=1.645)** | | | |
|---|---|---|---|---|
| | **Tr=2** | **Tr=5** | **Tr=10** | **Tr=20** |
| K | -0.16428 | 0.71948 | 1.30460 | 1.86587 |
| $X_{Tr}$ | 50.76 | 64.08 | 72.90 | 81.36 |
| a | 0.903395 | 1.582636 | 2.137327 | 2.693553 |
| $\Delta X$ | 1.675943 | 2.936045 | 3.965086 | 4.996974 |
| $X_{Tr,u}$ | 53.51736 | 68.90972 | 79.42111 | 89.5776 |
| $X_{Tr,l}$ | 48.00351 | 59.25013 | 66.37598 | 73.13755 |

Note that in Figure 2.8 the exceedance probability to the observed annual maximum daily series was calculated using Weibull (1939) relation:

$$P\% = \frac{m}{n+1} \times 100 \qquad (2\text{-}44)$$

where:

m: The rank of a value in a list ordered by descending magnitude

n: Total number of data.

This procedure is briefly explained in Table 2.10.

Table 2.10: the exceedance probability distribution to the annual maximum daily rainfall series (only some maximum years are shown)

| **Year** | **Annual max. daily rainfall (mm)** | **Sorted data (mm)** | **m** | **P% (n=66)** | **Tr=100/P (year)** |
|---|---|---|---|---|---|
| … | … | 102.4 | 1 | 1.493 | 67 |
| 1964 | 97.2 | 97.2 | 2 | 2.985 | 33.5 |
| … | … | 83.2 | 3 | 4.478 | 22.33 |
| 1973 | 83.2 | 81.3 | 4 | 5.970 | 16.75 |
| … | … | … | … | … | … |
| 1977 | 33 | … | … | … | … |
| … | … | … | … | … | … |
| 1995 | 81.3 | … | … | … | … |
| … | … | … | … | … | … |
| 1999 | 102.4 | … | … | … | … |
| ... | … | 33 | 66 | 98.508 | 1.02 |

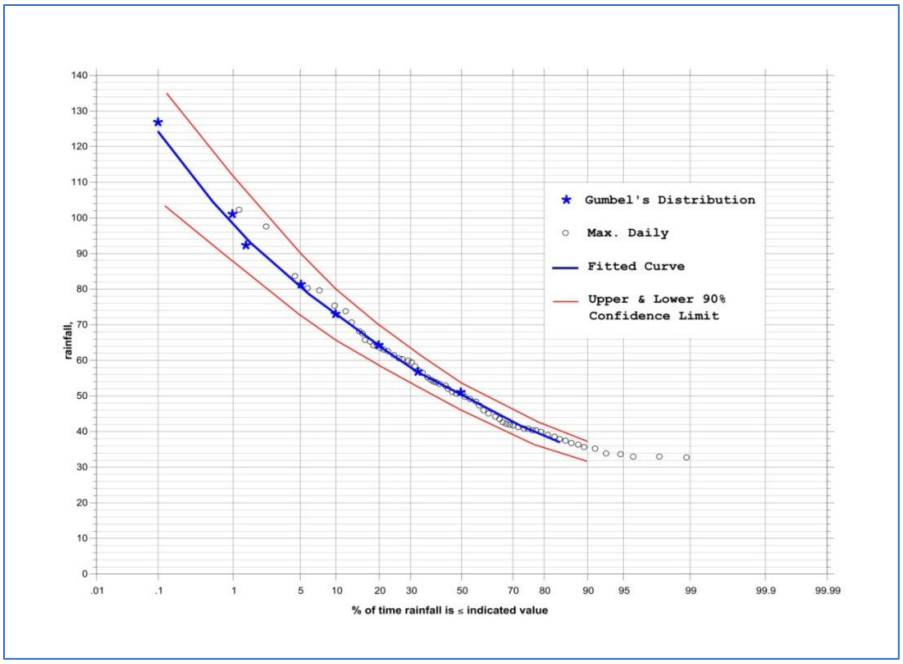


Figure 2.8: Confidence analysis (90%) for the best-fit probability distribution

## 2.5 Estimation of IDF parameters

Storms can be determined with some parameters. The characteristics of a rainstorm are as follow:

1. Intensity (mm/hour),
2. Duration (min, hour, or days),
3. Frequency (once in 5 years or once in 10, 20, 40, 60 or 100 years),
4. Areal extent (area over which it is distributed).

When a number of storms with different intensities and various durations are collected as a series, then a relation may be obtained by plotting the intensities against durations of storms either on the natural graph paper, or on a double log (log-log) paper (Raghunath, 2006). A more general and common Intensity-Duration–Frequency (IDF) relationship is defined as (Sherman Eq.):

$$i = \frac{KTr^m}{(t+B)^n} \tag{2-45}$$

Where

i: Intensity (mm/hr),

t: Duration (min),

Tr: Return period (year),

$K, m, B, n$: are constants for a given catchment.

Let, $A = KTr^m$, then by taking logarithms on both sides of Eq. (2-45),

$$\log(i) = \log(A) - n\log(t+B)$$

This is equation of a straight line if i and (t+B) are plotted on a log-log paper. Then slope of the straight line plot gives the constant n. Also by trial and error, the value of B for the lines of best fit can be obtained. A is i-intercept (value of i, when (t+B)=1 in log-log paper) and should be consider for each line. After that, by taking logarithms on both side of A,

$$\log(A) = \log(K) + m\log(Tr)$$

This is again in the form of a straight line if A and Tr are plotted on a log-log paper. The slope of this straight line gives the constant m. K is A-intercept (value of A, when Tr=1 in log-log paper) of this line.

In this section, IDF parameters are estimated from (15, 30, 60, 120 and 720) minute rainfall and then it will be calibrated by the annual maximum daily rainfall. This is because of this fact that the IDF relation at first is estimated using the short time series (8 years) and then it can be calibrated using the long time series (66 years).

Table 2.11 shows how these series (15, 30 and 60) are produced from 15-minute rainfall data. The procedure for 120 and 720 minute are the same.

Table 2.11: Generation of new rainfall series from 15-minute rainfall data (only a portion of series are shown)

<table>
<tr><th rowspan="2">15-min (mm)</th><th colspan="6">New rainfall series</th></tr>
<tr><th>15-min R (mm)</th><th>15-min i (mm/hr)</th><th>30-min R (mm)</th><th>30-min i (mm/hr)</th><th>60-min R (mm)</th><th>60-min i (mm/hr)</th></tr>
<tr><td>1.5</td><td>1.5</td><td>6</td><td rowspan="2">3.1</td><td rowspan="2">6.2</td><td rowspan="4">4.9</td><td rowspan="4">4.9</td></tr>
<tr><td>1.6</td><td>1.6</td><td>6.4</td></tr>
<tr><td>1.1</td><td>1.1</td><td>4.4</td><td rowspan="2">1.8</td><td rowspan="2">3.6</td></tr>
<tr><td>0.7</td><td>0.7</td><td>2.8</td></tr>
<tr><td>0.1</td><td>0.1</td><td>0.4</td><td rowspan="2">0.5</td><td rowspan="2">1.0</td><td rowspan="4">0.7</td><td rowspan="4">0.7</td></tr>
<tr><td>0.4</td><td>0.4</td><td>1.6</td></tr>
<tr><td>0.2</td><td>0.2</td><td>0.8</td><td rowspan="2">0.2</td><td rowspan="2">0.4</td></tr>
<tr><td>0.0</td><td>0.0</td><td>0.0</td></tr>
</table>

After generating the new series, the annual maximum series for each new series will be developed. Then the Gumbel's distribution will be produced for each annual maximum series as it mentioned in the previous section. The final results of this step are shown in Table 2.12.

Table 2.12: The Gumbel's distribution for each annual maximum series

| **Duration (min)** | **Intensity for various return period (Tr : year) i (mm/hr)** | | | |
|---|---|---|---|---|
| | **Tr=2** | **Tr=5** | **Tr=10** | **Tr=20** |
| 15 | 74.417 | 107.9358 | 130.1238 | 151.4243 |
| 30 | 50.54497 | 71.51077 | 85.38929 | 98.71266 |
| 60 | 29.09406 | 39.80178 | 46.88986 | 53.69441 |
| 120 | 19.89161 | 24.81854 | 28.07997 | 31.21094 |
| 720 | 4.238735 | 5.406145 | 6.178922 | 6.920789 |

Now, intensities are plotted against durations in a log-log paper. To obtain the parameter of B, using trial and error, B=10 converts these curves into straight lines. Figure 2.9 shows the influence of parameter B on the curves in two conditions.

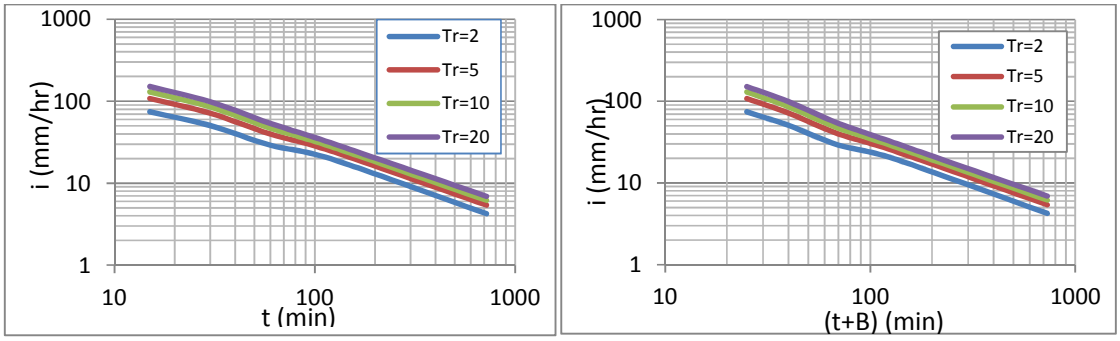


Figure 2.9: The influence of parameter B on the curves, (left) B=0 and, (Right) B=10

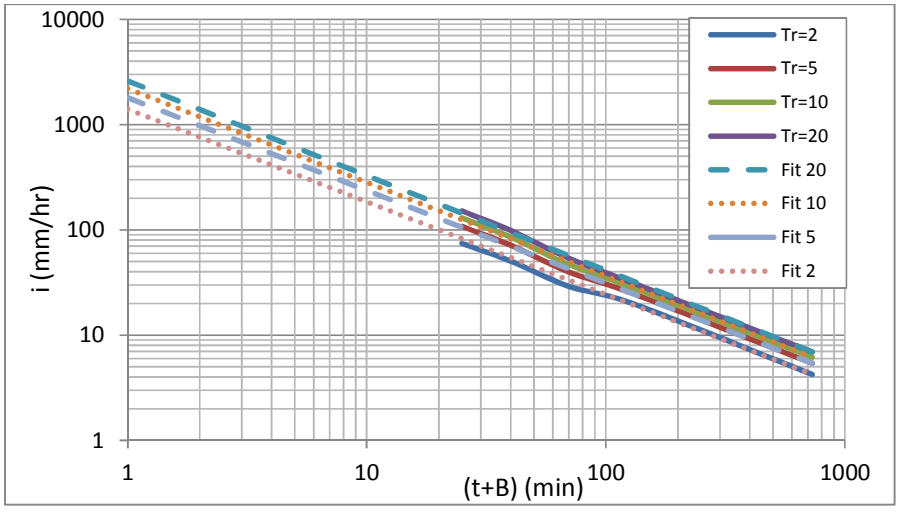


Figure 2.10: Intensities versus durations; calculation of the parameters of A and n

Parameters (A [for each line] and n) are calculated using Figure 2.10 as follows:

$A_{Tr=2}$=1400

$A_{Tr=5}$=1800

$A_{Tr=10}$=2200

$A_{Tr=20}$=2600

$n = \frac{\log(1400)-\log(4.2387)}{\log(730)-\log(1)} = 0.88$ (Slope of a fitted line)

As a same procedure, the parameters of A are plotted against the return periods in a log-log paper. Figure 2.11 illustrates the final result of this step. The final parameters (K and m), using Figure 2.11, will be obtained as follow:

K =1100

$m = \frac{\log(2600)-\log(1100)}{\log(20)-\log(1)} = 0.287$ (Slope of the fitted line)

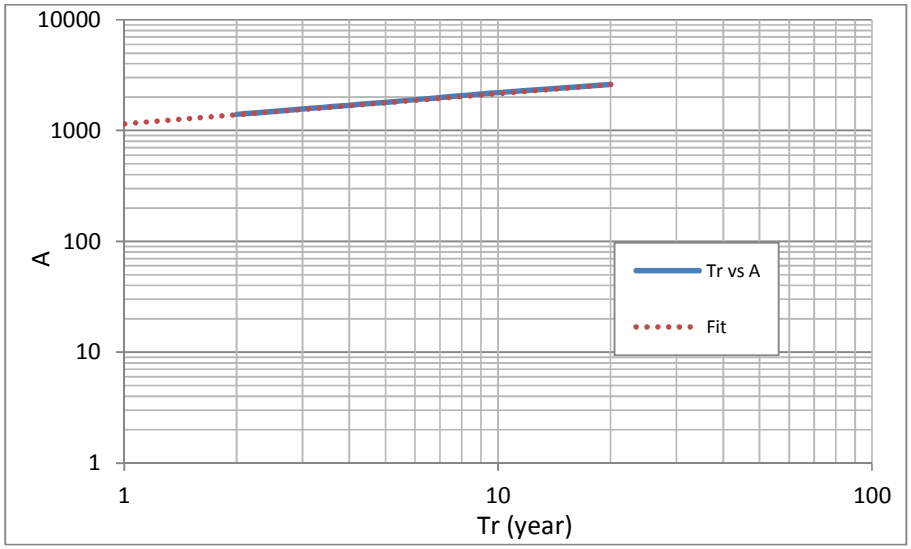


Figure 2.11: Return period versus parameter A; calculation of parameters K and m

At the final of this step an IDF relation can be obtained as follow:

$$i = \frac{1100 Tr^{0.287}}{(t+10)^{0.88}} \qquad i: \left(\frac{mm}{hr}\right), \quad t: (min), \quad Tr: (year)$$

But this is not the final IDF relation of the basin. This relation should be calibrated with respect to the annual maximum daily rainfall which is a continuous series for 66 years. For this reason, the Gumbel's distribution for the annual maximum daily rainfall was generated as it carried out for other series. Figure 2.12 illustrates intensity for various return periods which obtained from the Gumbel's distribution for this series.

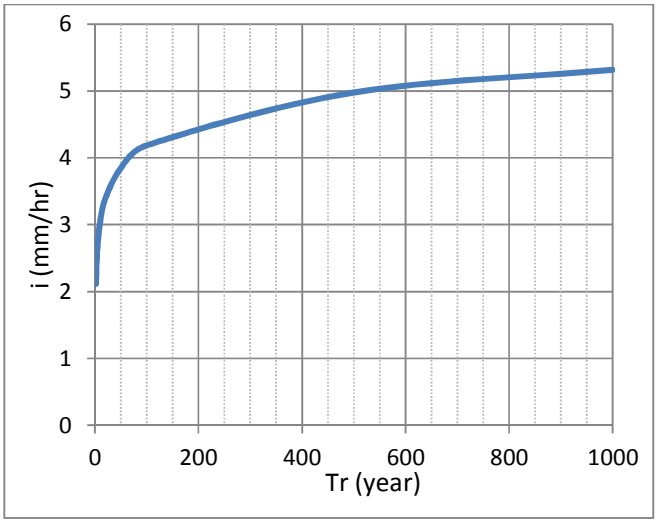


Figure 2.12: The Gumbel's distribution for the annual maximum daily rainfall

Now by calibrating the IDF relation, it is possible to obtain the best curve which is fitted the curve shown in Figure 2.12.

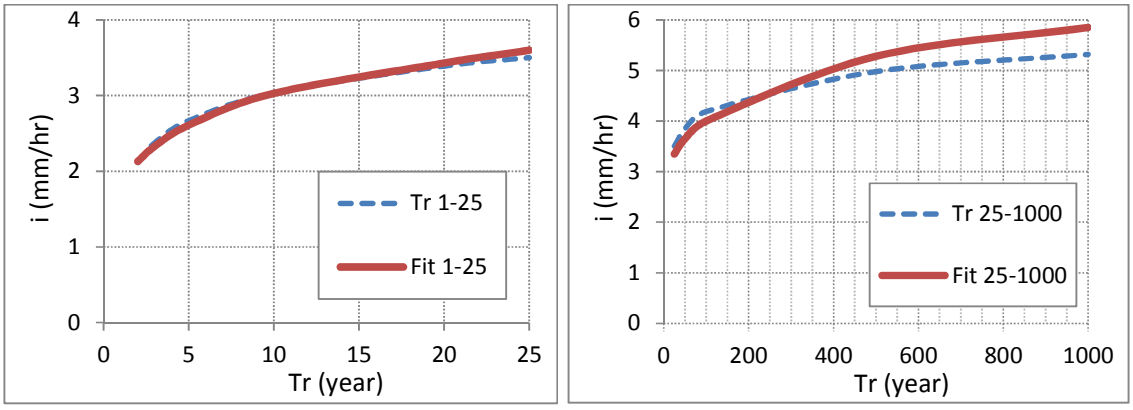


Figure 2.13: The Gumbel distribution (annual maximum daily rainfall) and the fitted (calibrated) IDF curve (left) (Eq. 2-46) for Tr<=25 and (right) (Eq. 2-47) for Tr>25

In this step, to increase the accuracy, the calibrated IDF relation is dissected into two separated equations as follow:

$$i = \frac{1100 Tr^{0.22}}{(t+10)^{0.879}} \qquad \text{for } Tr \leq 25 \tag{2-46}$$

$$i = \frac{1000 Tr^{0.187}}{(t+10)^{0.88}} \qquad \text{for } Tr > 25 \tag{2-47}$$

Figure 2.13 illustrate the above equations. The rainfall-runoff modeling of the Schoeckelbach basin will be done using these two equations.

## 2.6 Sources of Error in Rainfall Estimation

One of the largest sources of error in the runoff modeling process is the rainfall data (Berndtsson and Niemczynowicz, 1988; Schilling and Fuchs, 1986). In fact, in rainfall-runoff modeling process, often, measurements for only a limited number of points (rain gauges) within the watershed are used as conditions over the entire watershed and it can provide error.

### 2.6.1 Error in Estimating Watershed Rainfall Amount by Using One Gauge

The result of a study indicated that the peak outflow simulated using only one gauge in the watershed may frequently differ from the peak flow estimated using the true spatial rainfall by over 50%, even on small watersheds less than 20 $km^2$ (Niemczynowicz, 1988).

Since, in this thesis some additional rain gauge data which could increase the accuracy of the modeling were not available, rainfall-runoff modeling is carried out using only one gauge.

# Chapter 3

# Terrain Analysis

## 3.1 Introduction

The aim of terrain analysis is to derive the basin characteristics and to collect the dataset for runoff modeling in Hec-HMS. A Digital Elevation Model (DEM) is required as input for terrain analysis.

Digital Elevation Model (DEM) is a raster file which consists elevation and location information for all points of the area. In general, when the spatial resolution of the DEM (the distance between two adjacent cells) is finer then the accuracy of the DEM is higher. In this thesis, a very high resolution DEM (1×1 m) is used (Micro-scale) in order to reduce the numerical errors and to extract basin characteristics precisely. Table 3.1 explains the various DEM resolution range and the application of each.

Table 3.1: Typical application scales of DEM (Oksanen, 2006)

| Scale | Resolution | data sources | Examples of application |
|---|---|---|---|
| Micro-scale | 0.1-5 m | Field survey, LIDAR | Civil engineering, Large-scale mapping, Ortho-rectification of aerial photographs, Detailed hydrological modeling, Precision agriculture |
| Fine topo-scale | 5-50 m | Photogrammetry, Map digitization, InSAR, LIDAR | Spatial hydrological modeling, Spatial analysis of soil properties, Ortho-rectification and radiometric corrections of aerial photographs |
| Coarse topo-scale | 50-200 m | Photogrammetry, Map digitization, InSAR | Broad scale hydrological modeling, Sub-catchment analysis for lumped parameter hydrological modeling and assessment of biodiversity |
| Meso-scale | 200-5000 m | Map digitization | Elevation-dependent representations of surface temperature and precipitation |
| Macro-scale | 5-500 km | Map digitization | Global circulation models |

There are several tools available for terrain pre-processing. In this thesis, Hec-GeoHMS (version that works with Arc-GIS 9.3) is used.

The results will be used to create input files for Hec-HMS.

### 3.2 Terrain pre-processing

Terrain pre-processing contains several steps which should be done step by step as follows (USACE, 2009):

1. DEM reconditioning: The DEM Reconditioning function modifies Digital Elevation Models (DEMs) by imposing linear features onto them (river network/burning/fencing).
   Input file: DEM + River network.
2. Fill sinks: The Fill Sinks function fills sinks in a grid. If a cell surrounded by higher elevation cells, the water is trapped in that cell and cannot flow. The Fill Sinks function modifies the elevation value to eliminate these problems.
   Input file: DEM reconditioning (or only DEM).
3. Flow direction: this step computes the corresponding flow direction grid. The values in the cells of the flow direction grid indicate the direction of the steepest descent from that cell.
   Input file: Hydro DEM.
4. Flow Accumulation: It computes the associated flow accumulation grid that contains the accumulated number of cells upstream of a cell, for each cell in the input grid.
   Input file: Flow direction (Fdr).
5. Stream network: this step creates a Stream Grid for a user-defined threshold. This threshold is defined either as a number of cells (default 1%) or as a drainage area in square kilometers.
   Input file: Flow accumulation (Fac).
6. Stream segmentation: creates a grid of stream segments that have a unique identification. A segment may be either a head segment, or a segment between two segment junctions.
   Input file: Flow direction (Fdr) + Stream network (Str).
7. Catchment grid delineation: creates a grid in which each cell carries a value (grid code) indicating to which catchment the cell belongs. The value

corresponds to the value carried by the stream segment that drains that area, defined in the input Link grid.

Input file: Flow direction (Fdr) + Stream segmentation (StrLnk).

8. Catchment polygon processing: it converts catchment grid delineation into a catchment polygon feature class.

   Input file: Catchment grid (cat).

9. Drainage line processing: converts the input Stream Link grid into a Drainage Line feature class. Each line in the feature class carries the identifier of the catchment in which it resides.

   Input file: Stream network (StrLnk) + Flow direction (Fdr).

10. Drainage point processing: allows generating the drainage points associated to the catchments.
11. Watershed aggregation: this step aggregates the upstream sub-basins at every stream confluence. This is a required step and is preformed to improve computational performance for interactively delineating sub-basins and to enhance data extraction when defining a Hec-GeoHMS project. This step does not have any hydrologic significance.

    Input file: Drainage line (DrainageLine) + Catchment polygon (Catchment)

12. Longest flow path for catchments: generates the longest flow path for each catchment in the input Catchment feature class.
13. Slope: allows generating the slope grid in percent for a given DEM.
14. Slope greater than 30: allows generating a grid where the cells having a slope greater than or equal to 30% have a value of 1, and all the others 0. It requires as input a slope grid containing the slope in percent.
15. Slope greater than 30 and facing north: allows generating a grid where the cells having a slope greater than or equal to 30% and facing north have the value 1. All other cells take the value 0.
16. Weighted flow accumulation: used to compute the runoff or the load for each cell. This function takes as input a flow direction grid and a weight grid. It computes the associated weighted flow accumulation grid that contains the

accumulated values (weight) of cells upstream of a cell, for each cell in the input flow direction grid.

Some of these steps are typically shown in Fig. 3.1.

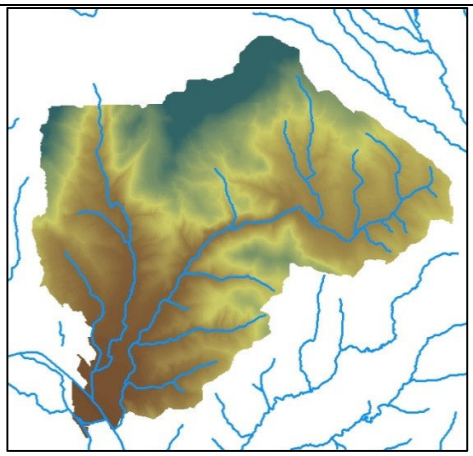

Unprocessed DEM + River network

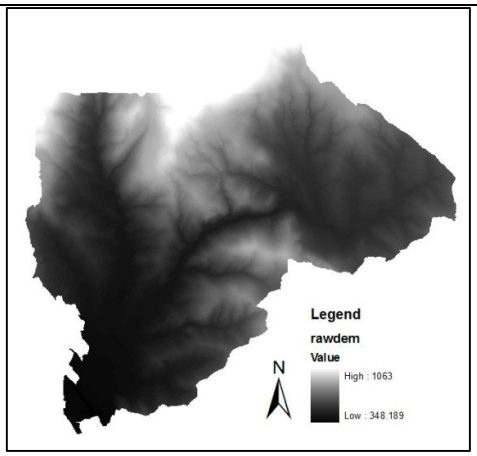


DEM reconditioning

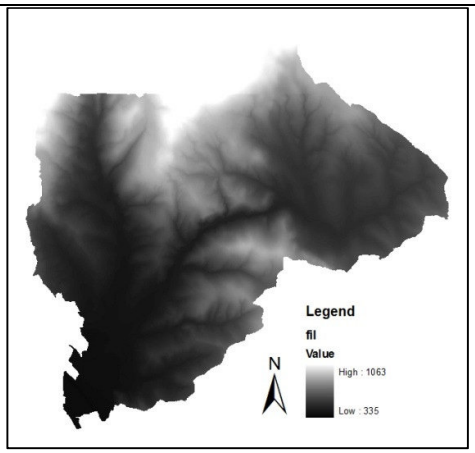


Fill sink

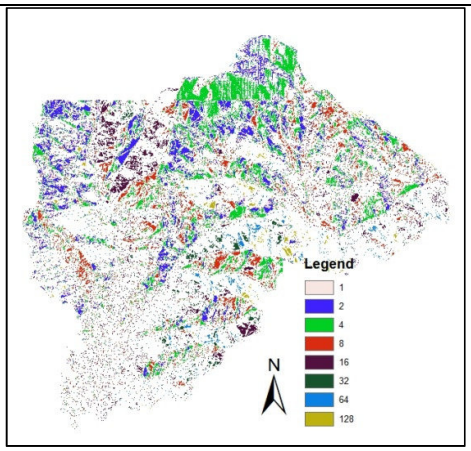


Flow direction

Figure 3.1: Terrain pre-processing for the Schoeckelbach basin (to be continued)

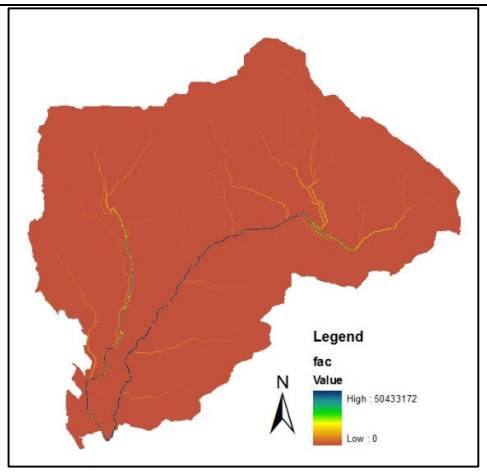


Flow accumulation

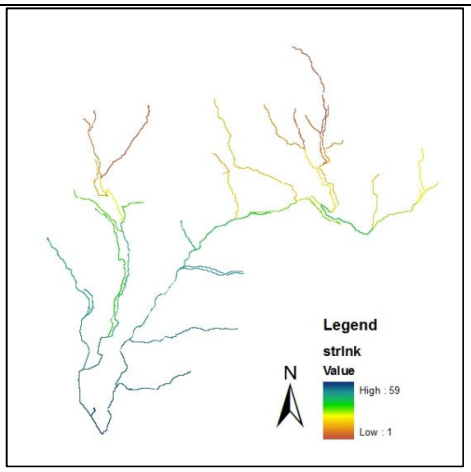


Stream network

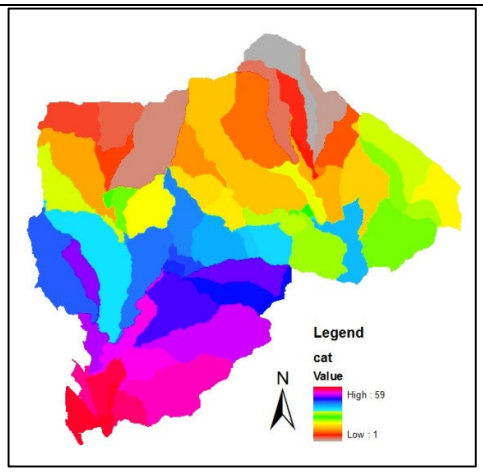


Catchment delineation

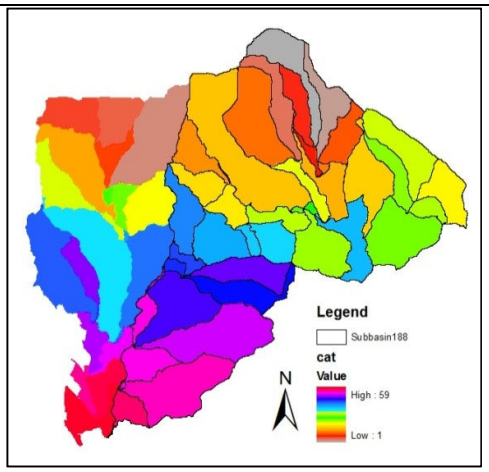


Boundary identification

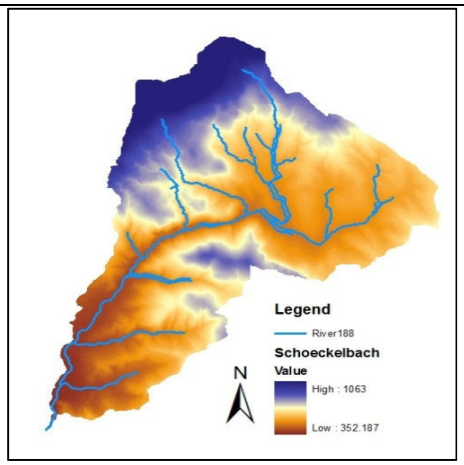


Schoeckelbach basin

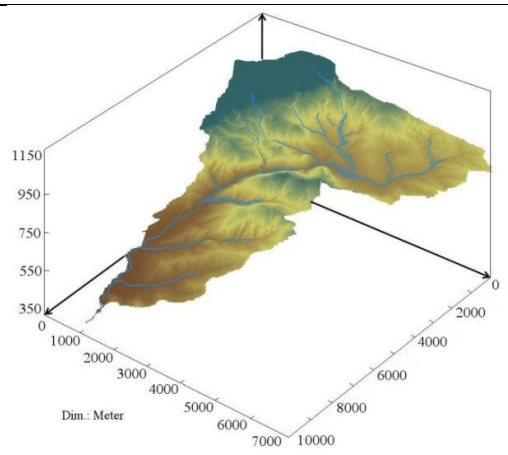


3D view

Figure 3.1: Terrain pre-processing for the Schoeckelbach basin

### 3.2.1 DEM errors

There are many potential sources of errors in DEMs. DEMs are often derived from contours (topographic data). These topographic data are usually derived using photogrammetric methods. The results of a study indicated that for (8×10) inch photography (gathered at 1:50,000 scale), these methods can conduct to raise errors of ±0.6 m for spot heights, and ±0.7 m for contours just from random errors in the photogrammetric process (Fryer, 1994). This could conduct to contour displacement of 140 m on a flood plain with 0.5% slope.

However, the amount of errors in a high resolution DEM (Micro-scale) are insignificant and most of the time they can be neglected.

## 3.3 Basin model

The basin model contains all physical characteristics of the model, such as basin areas, river reach connectivity, or reservoir data. In HEC-HMS, there are seven different watershed elements for construction of the basin model: sub-basins, reach, junction, source, sink, reservoir and diversion (Hec-HMS user's manual, 2010).

Prior to obtain the basin model, stream and sub-basin characteristics should be analyzed. This step contains (Hec-GeoHMS user's manual, 2009):

1. River length: it computes the river length for all routing reaches (or a selected one) in the river network.
2. River slope: this step computes the slope of each river using upstream and downstream elevation of a river reach.
3. Basin slope: this step computes the average basin slope in the watershed.
4. Longest flow path: this step computes the longest flow length, upstream elevation, downstream elevation and slope between the endpoints.
5. Basin centroid: in this step, the centroid of each sub-basin will be determined.
6. Centroid elevation: this step computes the elevation for each centroid point using the DEM.

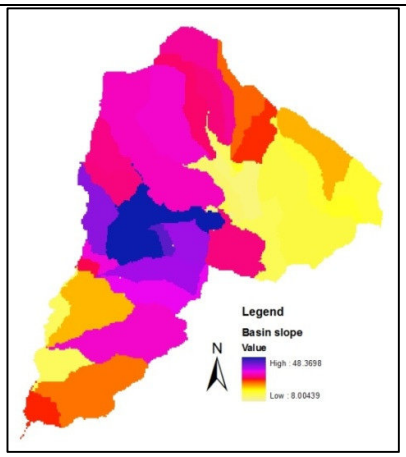


Basin slope

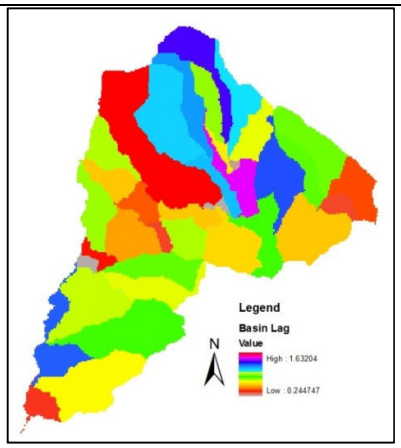


Basin Lag

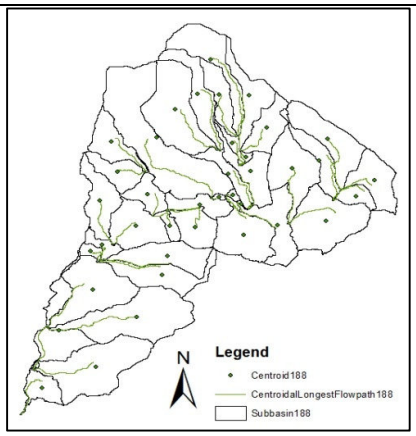


Centroid longest flow path

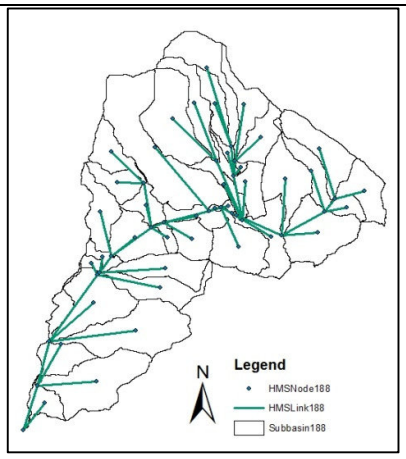


Hec-HMS links

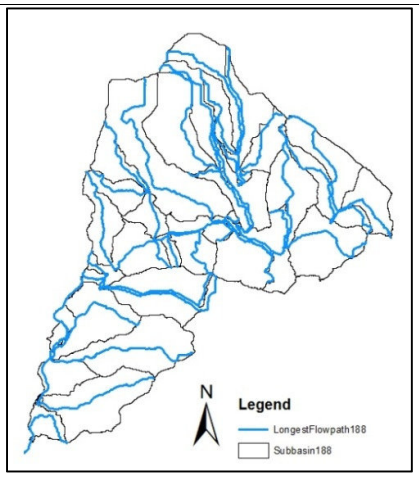


Longest flow path

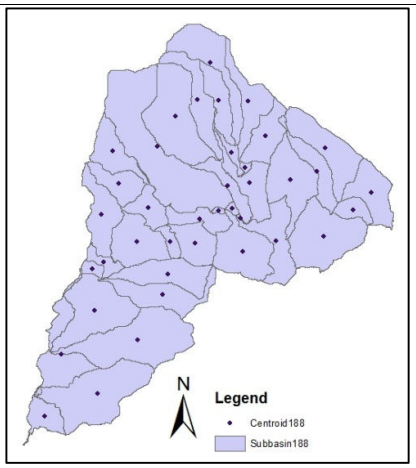


Basin centroid

Figure 3.2: Stream and sub-basin characteristic analysis

7. Centroid flow path: this step computes the centroid flow path by projecting the centroid onto the longest flow path. The centroid flow path is measured from the projected point on the longest flow path to the sub-basin outlet.

The final results of these steps are typically shown in Fig. 3.2.

### 3.4 Time of concentration

Time of concentration is defined as the time it takes for runoff to travel from the hydraulically most distant part of the watershed basin to the basin outlet or point of analysis (concentration point) (Hec-HMS user's manual, 2010). The units for time of concentration are time, in hours. Time of concentration is calculated using one of three equations (SCS Upland method).

These three equations can be found in Appendix B.

### 3.5 Stream flow routing

When a flood wave propagates along a river, its magnitude and length may be changed because of storage in the reach between two sections. When the water surface is not uniform, the storage in the reach can be divided into two parts prism storage and wedge storage (Fig. 3.3). Prism storage defines as the volume that would be stored in the reach if the flow were uniform (water surface parallel to bed channel). The volume stored between this parallel line and the actual water surface profile is called wedge storage. When inflow is increased, the wedge storage volume is also increased (positive) because the outflow actually cannot increase simultaneously. The wedge storage is become negative when inflow is decreased more rapidly than outflow.

In Hec-HMS, there are several methods available for stream routing as follows:

1. **Lag model**; which is the simplest routing method and widely used in urban drainage channels. In this method the inflow and outflow hydrographs are the same but the outflow hydrograph is lagged by a specified duration. Since the magnitude and length of inflow hydrograph is changed during propagation in channel, this method is not selected.

2. **Modified Puls method**; which is based on continuity equation and momentum equation. The method assumes that the lateral inflow is insignificant. In Hec-HMS, this method is calculated using a trial and error procedure. This method is widely used in reservoir routing.
3. **Muskingum method**; which is based on the continuity equation. In this method, storage is modeled as the sum of prism storage and wedge storage. This method includes parameters that are not physically based and they are difficult to estimate.
4. **Muskingum-Cunge method**; which is very similar to Muskingum method but overcomes the Muskingum method limitations. This method also considers the lateral inflow and is very easy to use.
5. **Kinematic-wave model**; which is based on the continuity and momentum equations. Hec-HMS uses this model for very limited shape of the cross section such as trapezoidal, rectangular and circular.

Based on the above statements, for stream flow routing, the Muskingum-Cunge method is selected.

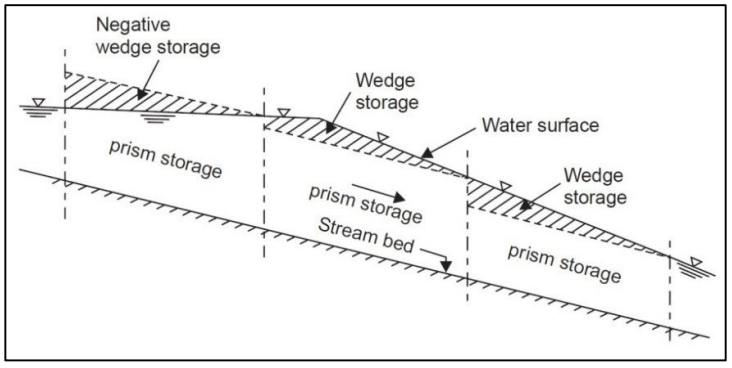


Figure 3.3: Storage in a stream channel during a flood wave (Hec-HMS user's manual, 2010)

### 3.6 The Muskingum-Cunge Method

The Muskingum-Cunge method for channel flood routing has been documented in many textbooks. This method was added as a flood routing option in the HEC-1 program (1990) because it can increase accuracy, consistency and range of physical conditions (the Natural Resources Conservation Service NRCS, 1965 and 1983).

This method can be found in Appendix B.

### 3.7 Using the Muskingum-Cunge method

For this modeling method in Hec-HMS, Channel geometry can be one of the following:

1. Circular
2. Trapezoidal
3. Rectangular
4. Triangular
5. 8 point irregular cross section

In this thesis, 8 point irregular cross section was used. Flow resistance in the channel and overbank flow area is simulated using Manning's roughness coefficients.

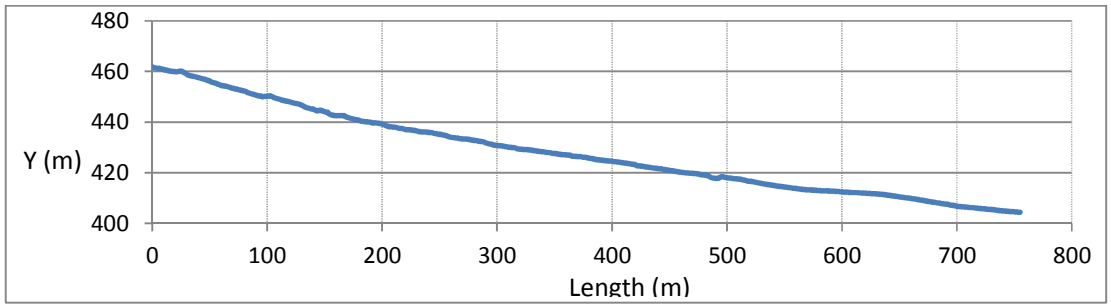


Figure 3.4: (top) the reach location and 8 selected cross sections, (down) river profile

To know how this process was done in this project, a reach is shown here. Figure 3.4 illustrates the location of this reach in the Schoeckelbach basin. To model precisely, several sections on this river were selected and for each of which, 8-point cross section was modeled. Figure 3.5 illustrates the modeled cross sections of the reach (Fig. 3.4) using for the Muskingum-Cunge routing method. For other reaches the method are the same.

### 3.8 Flow routing error considerations

Flow routing errors may occur when its parameters are not estimated correctly. Some of these parameters are as follows:

#### 3.8.1 Channel and floodplain interactions

When flow overtops the channel, roughness and geometrical shape of channel are changed and variations can occur in the hydraulic properties. Sometimes, this process can make instability during channel routing or it can increase the numerical errors.

#### 3.8.2 Changes in roughness

When discharge is increased, roughness can fluctuate which is depend on the channel and overbank characteristics (vegetation, trees, etc.). Most of routing models cannot consider these variations in modeling and it can increase the numerical errors.

#### 3.8.3 Time and Distance Steps

Time step (dt) and distance step (dx) have the main role to control the accuracy of the model and its results. If dt or dx are too large, routing models may be unstable and fail to reach a solution (see sections B.2.3 and B.2.4).

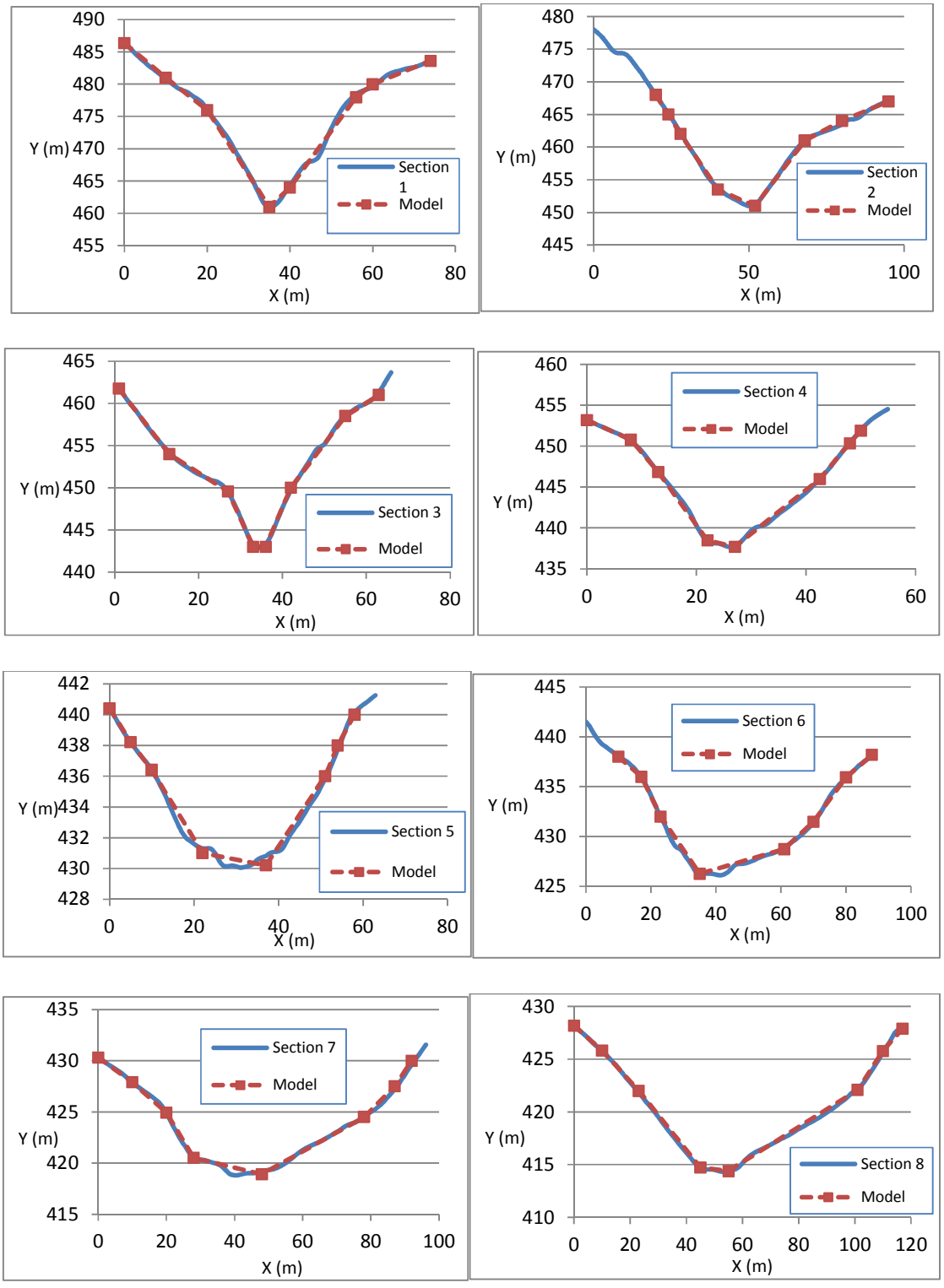


Figure 3.5: the modeled cross sections

# Chapter 4

# Loss Analysis

## 4.1 Introduction

Rainfall loss refers to that portion of the total rainfall that does not become to runoff.

Rainfall losses can be divided into three processes:

1. Rainfall interception by plants,
2. Water depression storage,
3. Infiltration of water into the ground.

Among these three processes, only infiltration can be calculated by some equations (Raghunath, 2006). In Hec-HMS, there are several options in order to model the cumulative losses as follows (Hec-HMS user's manual, 2010):

1. **The initial and constant-rate loss model:** This model assumes that the maximum potential rate of precipitation is constant during rainfall event. Because of low accuracy, this model is not used in this thesis.
2. **The deficit and constant-rate loss model**: is very similar to the previous one.
3. **The SCS CN (Soil Conservation Services, Curve Number) loss method:** This is a simple, predictable and stable conceptual method for estimation of losses. It relies on only one parameter, CN which depends on a function of cumulative precipitation, soil type, land cover and antecedent moisture. This method is a widely used method for estimating direct runoff from rainfall on small to medium-sized un-gauged basins and it gives very good results when a basin covered with homogenous soil and land cover.
4. **The Green and Ampt loss method:** This method is a conceptual model of infiltration in a basin. Infiltration rate in time interval of t depends on some parameters of soil such as saturated hydraulic conductivity, volume moisture deficit, wetting front suction and cumulative loss at time t. This is a good method for estimating of losses but it needs more information about soil cover when compared with SCS CN method.
5. **Continuous soil moisture accounting (SMA) model:** which is a continuous model and it is the only method which can simulate both wet and dry weather behavior. This model considers the basin as a series of storage layers and by

using precipitation and potential evapotranspiration data as input, can simulate surface runoff, groundwater flow, losses due to evapotranspiration and deep percolation over the basin. This is a very good method for estimation of losses but it needs meteorological data as input and should be calibrated with real observed data.

Based on the above statements, because of its simplicity and considering the available data for the Schoeckelbach basin, SCS CN method is used in this thesis. The basic reference for SCS CN method is the National Engineering Handbook, Section 4, Hydrology (1964) (USDA-TR-55, 1986).

CN can be determined using the hydrologic soil group (HSG), cover type, treatment, hydrologic condition, and antecedent runoff condition (TR55, 1986).

These factors and SCS CN method can be found in Appendix B.

The only problem in using CN may be happened when soils outside the USA are classified into the four hydrological soil groups A, B, C and D, and the determination of the antecedent moisture condition (AMC), which is an index of basin wetness (TR55, 1986). This is because of this fact that the available tables which give hydrological soil groups are classified based on soil types in USA.

## 4.2 Preparing CN map for Schoeckelbach basin in Hec-GeoHMS

Based on the theory of section B.3, CN can be estimated. In this section some data are needed as following:

1. Land use raster data (Fig. 4.1)
2. Soil data (Fig. 4.2)
3. Basin boundary polygon (Fig. 4.3)

### 4.2.1 Land use reclassification and delineation

Origin land use data of the Schoeckelbach has 8 land cover categories. In order to facilitate the process it is needed to simplify the category. To reduce the category raster reclassify is used. Table 4.1 shows the origin land use and also the reclassified data (Codes are shown in Figure 4.1).

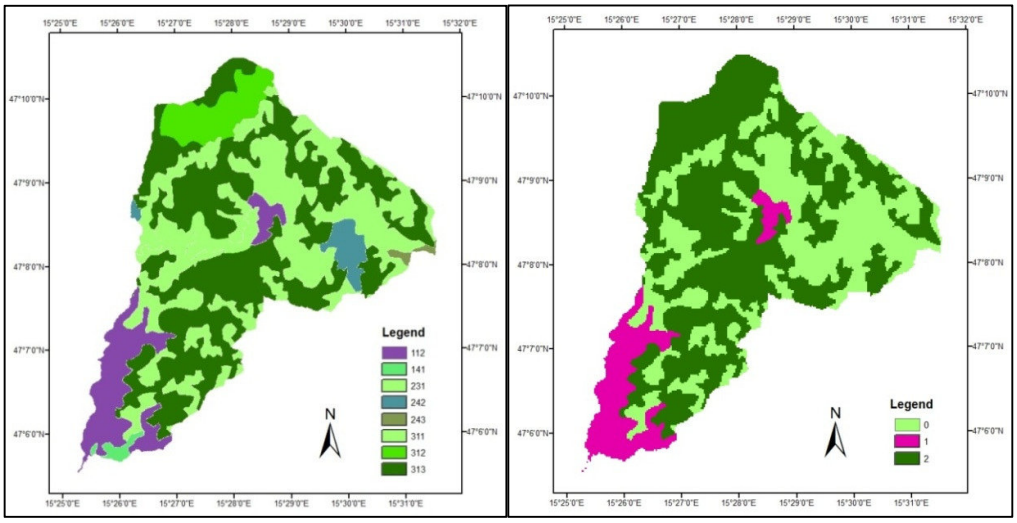


Figure 4.1: left, original raster land use data and right, raster reclassify (30m×30m) (Legend: Table 4.1)

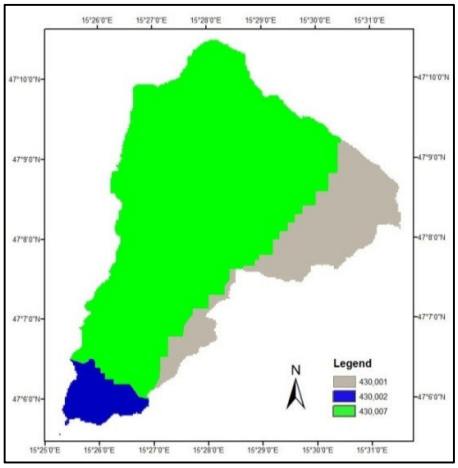


Figure 4.2: Soil data (250m×250m) (Legend: Table 4.4)

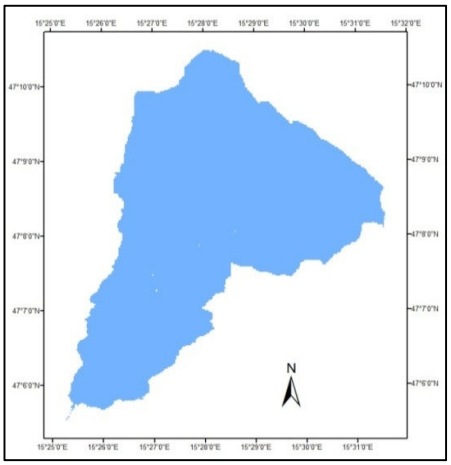


Figure 4.3: Basin boundary polygon

Table 4.1: Land use data

| Code | Land use components | % | % | Reclassify | Status | Code |
|---|---|---|---|---|---|---|
| 313 | Mixed Forest | 43.5 | 52.8 | Forest | High loss | 2 |
| 312 | Evergreen Forest | 6.2 | | | | |
| 311 | Deciduous Forest | 3.1 | | | | |
| 112 | Low Intensity Residential | 9.9 | 10.7 | Urban | Low loss | 1 |
| 141 | Urban/Recreational Grasses | 0.8 | | | | |
| 231 | Pasture (fair) | 33.3 | 36.5 | Pasture | Med. to high loss | 0 |
| 243 | Grasslands | 0.5 | | | | |
| 242 | Grasslands/Herbaceus | 2.7 | | | | |

### 4.2.2 Soil data

The soil data which is available for Graz is a (250×250 m) polygon file. This soil data is clipped from the original file to fit the extent of study area. The clipped map, which is an almost homogenous soil map (Fig. 4.2), consists 3 kinds of soil based on the FAO soil classification. Table 4.2 shows the Schoeckelbach soil types.

The Food and Agriculture Organization of the United Nations (FAO) developed a soil classification, also called World Soil Classification. FAO was classified soils in 30 different categories in 1974.

Table 4.2: The Schoeckelbach soil types

| Soil type | SMU code | FAO90 code | % |
|---|---|---|---|
| Dystric Cambisol (medium) | 430001 | CMd | 20.6 |
| Eutric Cambisol (medium) | 430002 | CMe | 5.9 |
| Rendzic Leptosol (medium) | 430007 | LPK | 73.5 |

SMU: Soil Map Unit, FAO: Food and Agriculture Organization of the UN.

The Schoeckelbach soil map consists:

1. **Cambisols** represent soils of young age in a continuous process of pedological maturation, as revealed by the presence of the cambic horizon (Kapur et al., 2011).

In pedogenic terms they stand between Fluvisols and Luvisols. Cambisols are the most widely distributed soils of the Mediterranean delimiting diverse climatic areas (Kapur et al., 2011). The major Cambisol units are Eutric and Dystric. Cambisols with moderate to deep soil profiles are among the most productive soils of southern Europe. The Eutric Cambisol is an excellent soil used for all types of crops while Dystric Cambisols are used for mixed arable farming, forestry and grazing. Cambisols are developed in medium and fine-textured materials derived from a wide range of rocks, mostly in alluvial, colluvial and aeolian deposits. This type of soil with respect to the land cover is classified as B or C. In this thesis, because most part of the area (which consists Cambisol) is covered by urban area, group C was selected (Table B.3).

2. A **Leptosol** in the FAO World Reference Base for Soil Resources is a very shallow soil over hard rock or highly calcareous material or a deeper soil that is extremely gravelly and/or stony. Leptosols are particularly widespread in mountain areas and they are unattractive soils for rainfed agriculture because of their inability to hold water, but may sometimes have potential for treecrops or extensive grazing (Kapur et al., 2011). Leptosols are best kept under forest. This type of soil with respect to the land cover is classified as A or B. in this thesis, because most part of the area (which consists Leptosol) is covered by forest or agricultural lands, group A was selected (Table B.3).

### 4.2.3 Union soil and land use data

During the union processing, soil data and land use data combined to one shape file. This union file and CNLookup table (table 4.3), are used computing CN grid process in Hec-GeoHMS.

Table 4.3: CNLookup table for the Schoeckelbach basin

| Code | Description | A | B | C | D |
|---|---|---|---|---|---|
| 0 | Pasture | 67 | 77 | 83 | 87 |
| 1 | Urban (medium) | 57 | 72 | 81 | 86 |
| 2 | Forest | 30 | 58 | 71 | 78 |

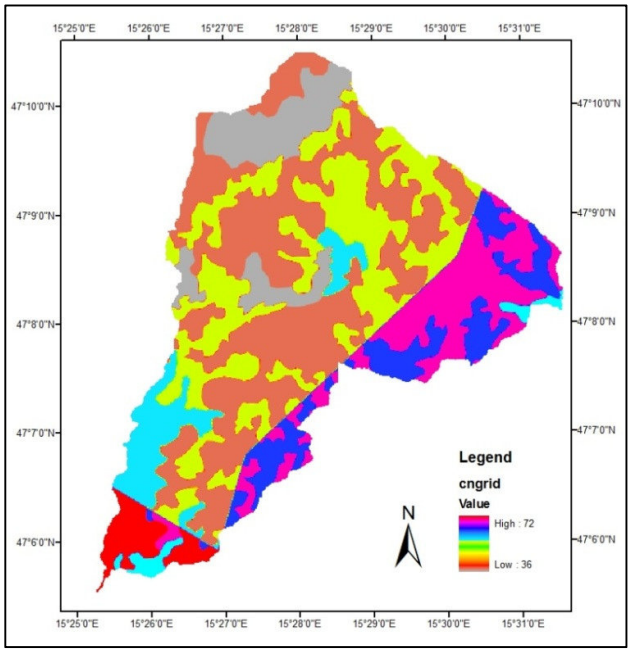


Figure 4.4: The final CN map

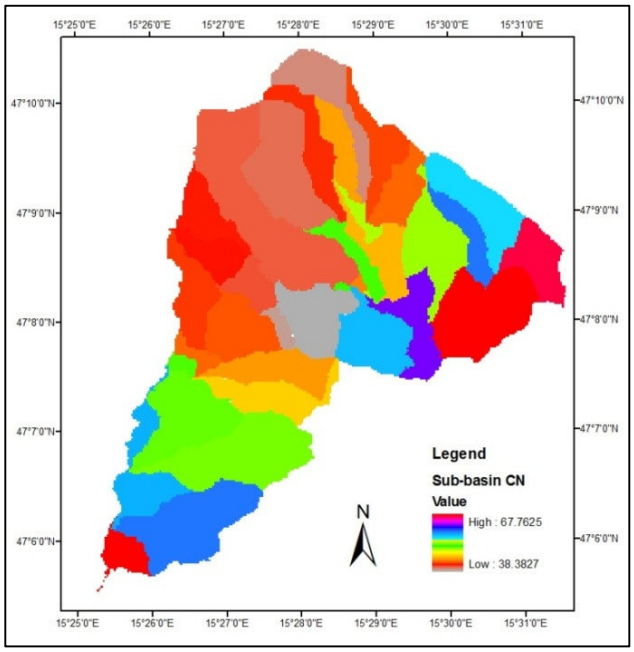


Figure 4.5: The final CN map for importing to Hec-HMS

### 4.2.4 CN modification

After creation of CN values, the CN map should be modified based on the antecedent moisture condition and urban impervious area modifications. This procedure can be

done with raster calculator in ArcGIS. However, the final CN map is shown in Fig. 4.4.

### 4.2.5 CN map for importing to Hec-HMS

Hec-HMS uses the mean CN value for each sub-basin, so, average CN for each sub-basin was calculated as it is shown in Fig. 4.5.

## 4.3 SCS CN errors and limitations

The limitations related to the SCS runoff equation are as follows:

1. SCS CN equation was developed based on daily rainfall data and duration of storms was not considered. It means that all storms which have the same rainfall magnitude but different duration will produce equal amount of direct runoff volume.
2. For a discontinuous storm, this method may give over-predict runoff volume. In this case, the method cannot consider the amount of soil storage which caused by infiltration between two sequential rainfall events. However, the SCS CN modification based on the antecedent moisture condition should be considered.
3. SCS CN equation was developed based on annual maximum one-day runoff data. It means that the CN procedure may give results with low accuracy for small rainfall events.
4. In this method, when duration of rainfall is increased, the infiltration rate will approach zero.
5. The accuracy of the method is very dependent on the accuracy of CN which is the only parameter in this method.
6. SCS CN method gives good results for basins covered by nearly homogenous land use and soil cover, so for other basins in this case, modification should be considered.

# Chapter 5

# Runoff Modeling using Hec-HMS

## 5.1 Introduction

In this chapter, rainfall-runoff modeling of Shoeckelbach basin will be carried out using Hec-HMS software. The main purpose of rainfall-runoff modeling in this thesis is high flood risk management in the basin. For this complete time series of flows are needed and peak discharge values alone are not enough.

In this chapter, all input data which prepared in the previous chapters, will be used to simulate various hydrograph for various storm frequencies in the Schoeckelbach basin. Three model components containing required data for runoff modeling in Hec-HMS are needed as follows:

1. Basin Model
2. Meteorological Model
3. Control Specification Model

These steps will be presented in this chapter.

## 5.2 Basin Model

Basin model is the main component in a rainfall-runoff modeling (USACE, 2000). In fact, in this step some information relevant to the spatial attribute of the model should be provided such as basin area, river reach connectivity or reservoir data. The basin model of the Schoeckelbach catchment was prepared using Hec-GeoHMS and the process was described in the chapter 3. However the basin model is shown in Fig. (5.1). In this step, some parameters should be justified such as basin model properties, hydrologic elements (source, junction, sub-basin, reach, reservoir, diversion and sink), loss method, and transform method. Most of these parameters were described in the previous chapters. Here, only transform method will be described.

In Hec-HMS, there are several options for transform method as follows:

1. **Clark unit hydrograph:** This is a time-area instantaneous unit hydrograph which appoints a relationship between travel time and a part of basin that may contribute runoff during that travel time. In this method isochrones are

produced for the basin and then time-area curve can be determined by calculating the mean travel time for each sub-area (cells). In this method it is necessary to estimate a time-area relationship and a linear reservoir routing coefficient which may be difficult to estimate. However some empirical formulas were produced by U.S army Corps of Engineers.

2. **ModClark:** This is a distributed-parameter model which process and spatial variability of characteristics are considered explicitly (Hec-HMS user's manual, 2000). In this method at first a grid is produced and for each cell, the distance to the outlet and area of cell are specified. Then volume of inflow for each cell is calculated for each time step and then, this inflow is routed through a linear reservoir.
3. **Kinematic wave:** This is a conceptual model of unit hydrograph which considers the basin as a very wide open channel. The inflow to the channel is the excess precipitation and the outflow can be simulated using unsteady shallow water equation. The shallow water equation in this method is approximated with a finite difference method. The type of cross sections in Hec-HMS can be selected as trapezoidal, rectangular, triangular and circular. The accuracy and stability of the model is very dependent on the time and space interval.
4. **Snyder unit hydrograph:** This is a parametric-empirical model of unit hydrograph which can be derived using lag time, peak flow, total time base, basin area and unit hydrograph peaking coefficient. These parameters can be determined using observed data or can be estimated using empirical equations.
5. **User-specified unit hydrograph:** This is an empirical model of the unit hydrograph which is specified directly by user. User hydrograph in this case is derived from observed rainfall and runoff data. In practice, this is an uncommon method because the necessary data for deriving the unit hydrograph are seldom available (Hec-HMS user's manual, 2000).
6. **SCS unit hydrograph:** This is a parametric and dimensionless unit hydrograph which developed by the Soil Conservation Service (SCS) in USA based on averages of great number of unit hydrographs derived from gauged rainfall and

runoff for large number of different sizes and for many different locations. The necessary parameters for this method are basin area, time to peak discharge, peak discharge, the excess precipitation duration (which is often consider as computational time interval) and the basin lag time. All of these parameters can be calculated using available equations and very easy to use. Figure (5.2) illustrates the SCS dimensionless unit hydrograph.

In this thesis, SCS unit hydrograph is used for transform method because of its simplicity and its application in small to medium sized basins. Since the available observed discharge data are as statistical peak discharges in various frequencies, this unit hydrograph can be used to estimate and produce more discharges from the observed peak discharges because all necessary parameters have been already calculated for the basin.

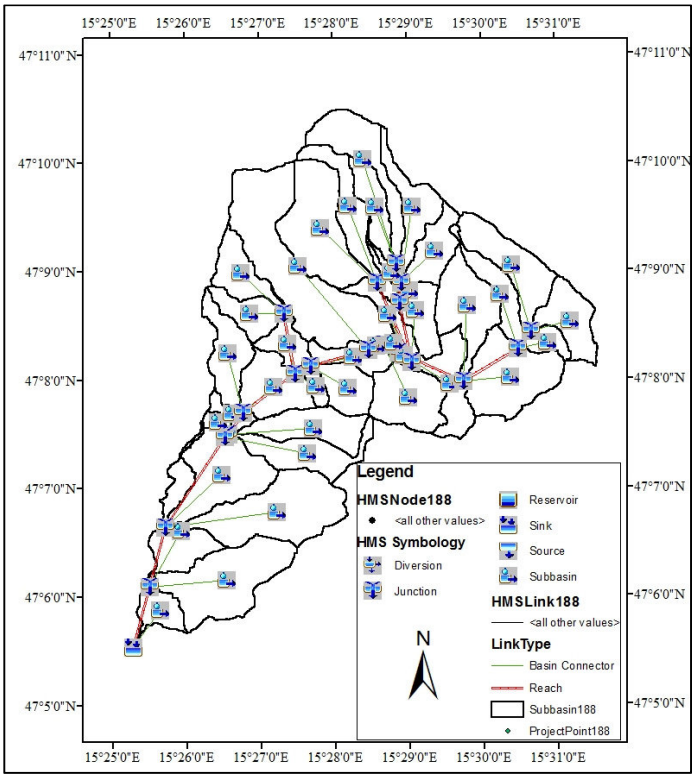


Figure 5.1: Basin model of the Schoeckelbach basin

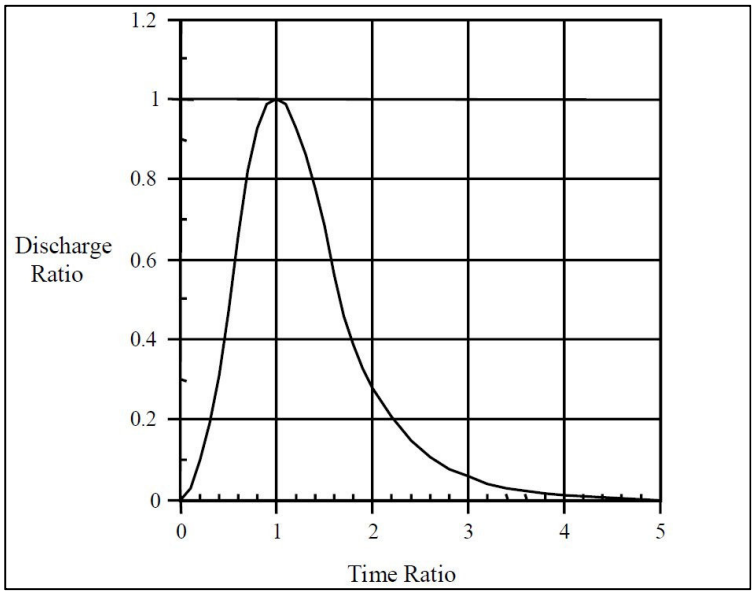


Figure 5.2: The SCS dimensionless unit hydrograph

## 5.3 Meteorological Model

Meteorological model is one of the main components in a project. This model is prepared the meteorological boundary conditions for sub-basins. Meteorological model includes all climatic information such as precipitation, evapotranspiration and snowmelt methods (Hec-HMS user's manual, 2010). Hec-HMS provides several methods in the HMS model to generalize observed rainfall over the basin such as frequency storm, user gauge weighting, gridded precipitation, inverse distance, SCS storm and specified hyetograph. Since the observed discharges in the Schoeckelbach basin are based on peak discharges for various frequencies, among these meteorological methods, Storm frequency method and user gauge weighting method (for Continuous simulation) are selected for this thesis.

## 5.4 Control specification model

Control specification is used to control simulation runs. The main purpose of using control specification model is to specify the start and end of the computation period and the computation time interval (Hec-HMS user's manual, 2010). In this thesis, control specification model of each simulation will be described in that simulation.

## 5.5 Runoff modeling

In this section, rainfall – runoff modeling for the Schoeckelbach basin is done for 1-day rainfall with return periods of 2, 5, 10, 20, 30, 50 and 100 year. In this section a frequency storm is used in the meteorological model because the observed discharges are based on the peak discharges for various frequencies.

### 5.5.1 Frequency storm model

For frequency storm model in Hec-HMS there are several options available in order to define the rainfall parameters such as probability, intensity duration, storm duration, intensity position and rainfall depths. It should be noted that Hec-HMS uses the alternating block method to develop a hyetograph from the rainfall depths. This method positions the block of maximum incremental depth at the middle of the required duration and remaining blocks are arranged then in descending order (Hec-HMS user's manual, 2010). For example, Figure 5.3 illustrates the hyetograph of 100-year 1-day storm for the Schoeckelbach basin.

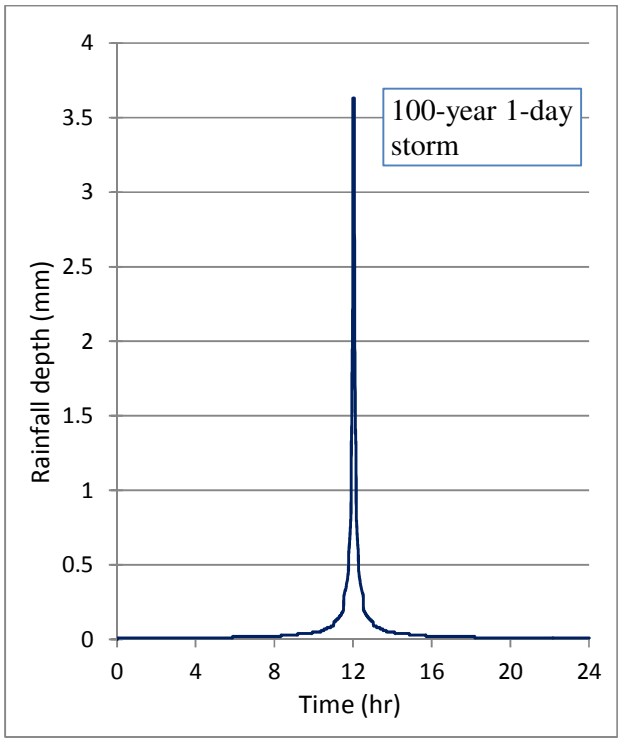


Figure 5.3: Hyetograph for 100-year 1-day storm (Schoeckelbach basin)

Also, the intensity position in Hec-HMS is adjusted on 50 percent as default. The intensity position can be changed by user but in this thesis 50 percent is used.

The rainfall depths for various return periods and durations are computed using IDF relation which was obtained in chapter 2. Table 5.1 summarizes the final details.

Table 5.1: Rainfall depths for various frequencies and durations (mm)

| **Duration** | **Tr=2** | **Tr=5** | **Tr=10** | **Tr=20** | **Tr=30** | **Tr=50** | **Tr=100** |
|---|---|---|---|---|---|---|---|
| 5 min | 9.88 | 12.08 | 14.07 | 14.46 | 14.52 | 15.98 | 18.19 |
| 15 min | 18.91 | 23.14 | 26.95 | 27.07 | 27.80 | 30.58 | 34.81 |
| 1 hr | 30.6 | 37.44 | 43.61 | 44.05 | 44.93 | 49.43 | 56.27 |
| 2 hr | 35.52 | 43.46 | 50.61 | 51.31 | 52.12 | 57.34 | 65.28 |
| 3 hr | 38.17 | 46.96 | 54.39 | 54.90 | 55.98 | 61.59 | 70.12 |
| 6 hr | 42.49 | 51.98 | 60.55 | 61.73 | 62.28 | 68.52 | 78.00 |
| 12 hr | 46.76 | 57.21 | 66.64 | 67.50 | 68.50 | 75.36 | 85.80 |
| 24 hr | 51.17 | 62.59 | 72.91 | 73.42 | 74.90 | 82.40 | 93.80 |

### 5.5.2 Observed discharge data

The only observed discharge data for the Schoeckelbach basin are as a number of peak discharges for various frequencies which were calculated statistically. These observed peak discharges and the statistical method can be found in Sackl, 2009.

The position where observed data were gathered is illustrated in Figure 5.4 and those observed data are also shown in Fig. 5.5 to 5.11. It should be mentioned that from these peak discharges, it is possible to estimate hydrograph of flow in the river because all necessary parameters were calculated such as basin area, time of concentration, peak discharge and etc. SCS unit hydrograph can be used for this reason and the observed data which are illustrated in Fig. 5.5 to 5.11 are calculated based on this method.

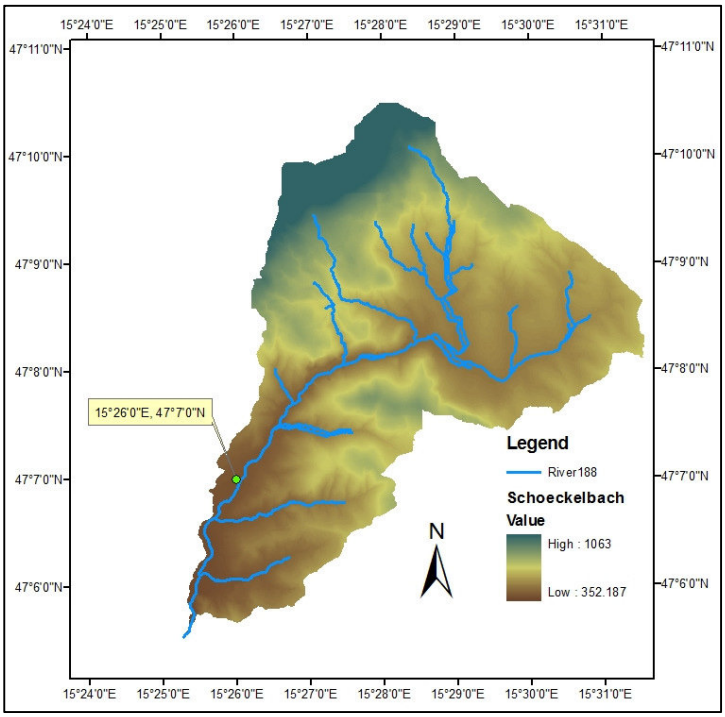


Figure 5.4: The observed data come from this position (R480)

### 5.5.3 Calibration

The final results of modeling are illustrates in Fig. 5.5 to 5.11 (the right hand side pictures). It should be mentioned that these pictures illustrate model data for the position where the observed data were gathered and these are not discharges for the outlet of Schoeckelbach basin.

As it can be seen in these figures, this model should be calibrated because for Tr>10 year the model and observed data are not matched each other.

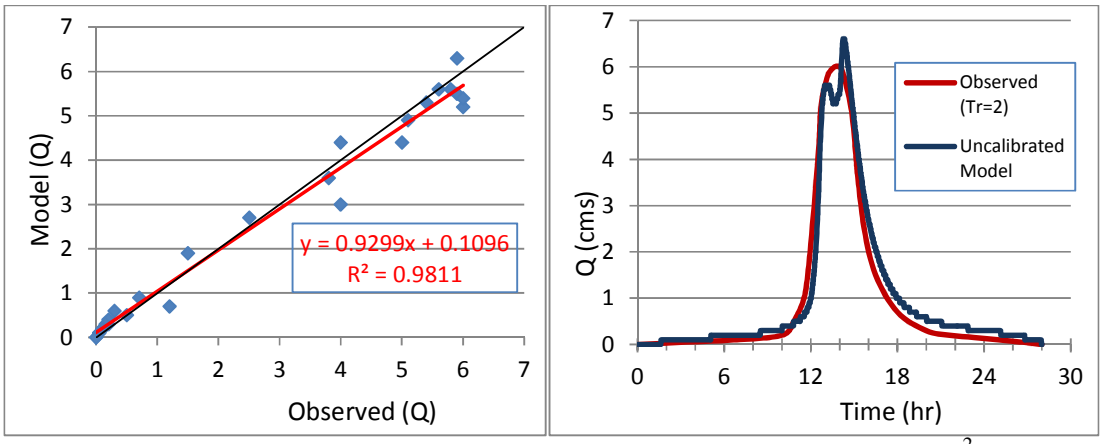


Figure 5.5: (right) Runoff modeling (uncalibrated) for Tr=2 year, (left) $R^2$ test

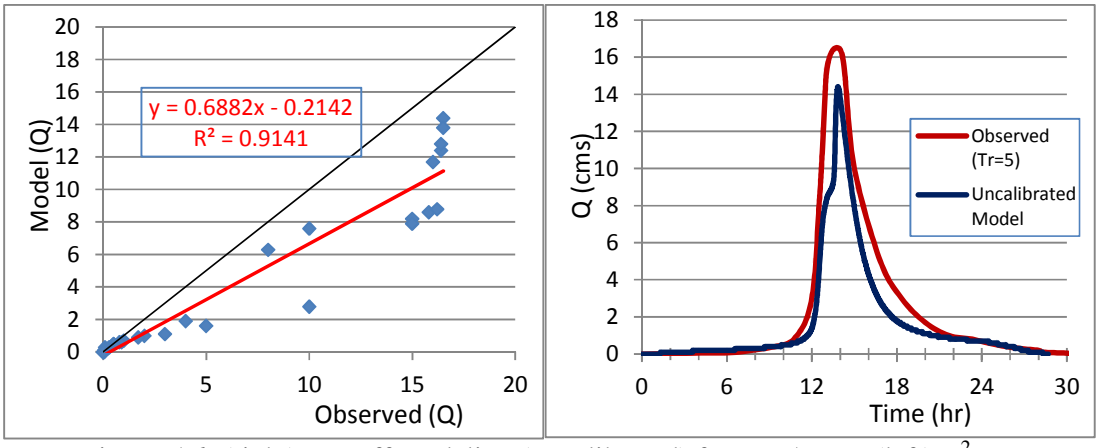


Figure 5.6: (right) Runoff modeling (uncalibrated) for Tr=5 year, (left) $R^2$ test

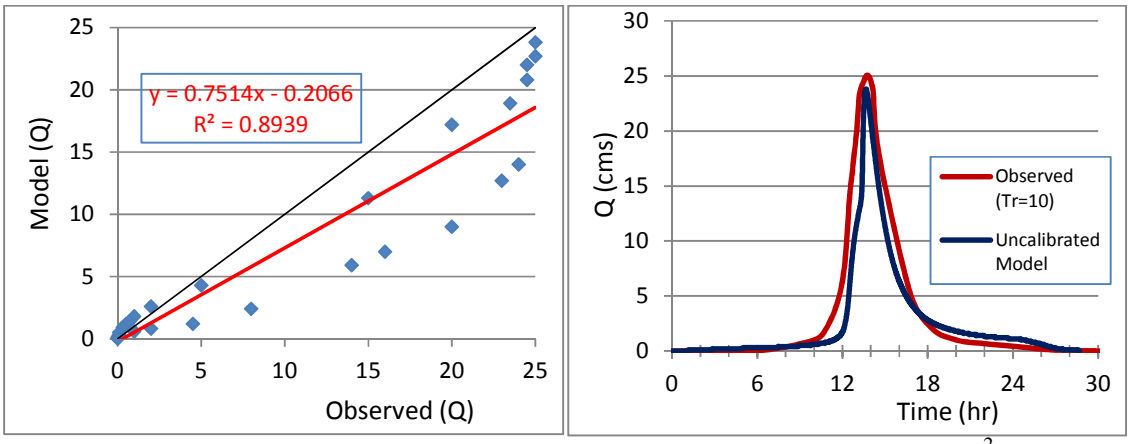


Figure 5.7: (right) Runoff modeling (uncalibrated) for Tr=10 year, (left) $R^2$ test

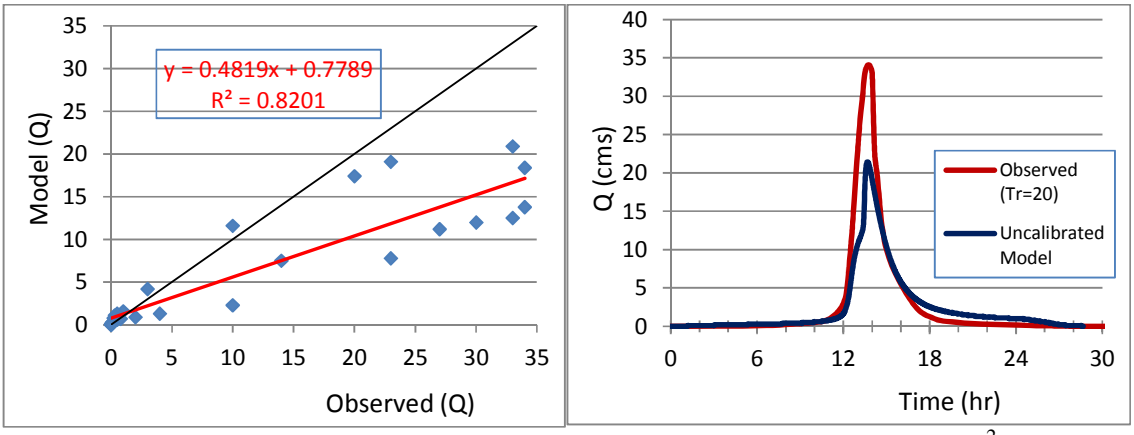


Figure 5.8: (right) Runoff modeling (uncalibrated) for Tr=20 year, (left) $R^2$ test

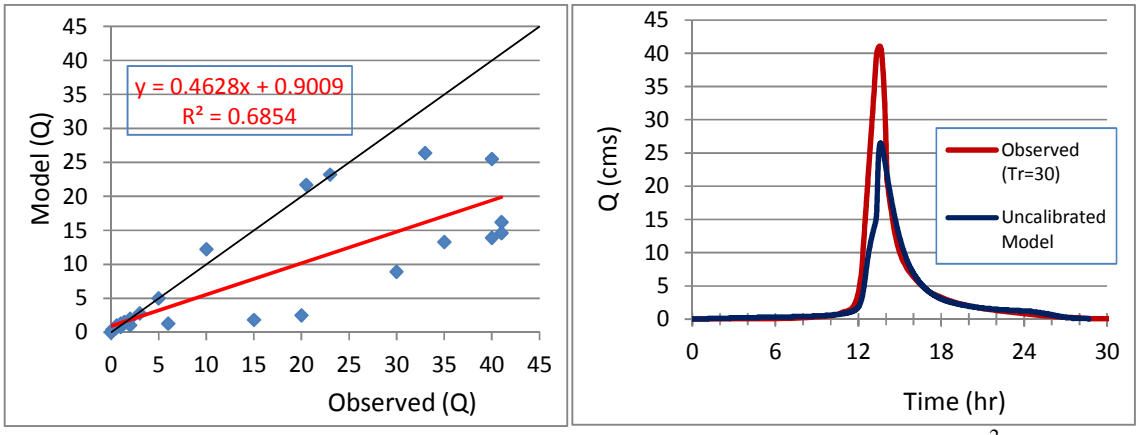


Figure 5.9: (right) Runoff modeling (uncalibrated) for Tr=30 year, (left) $R^2$ test

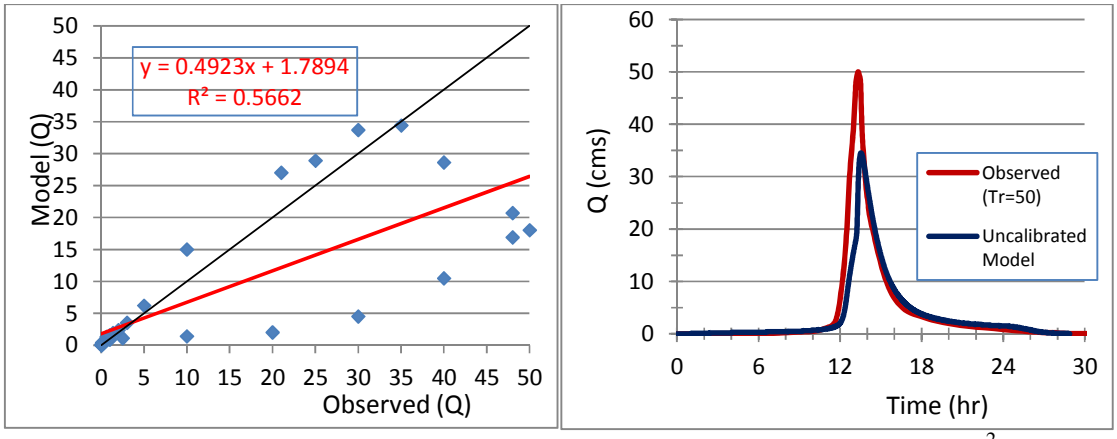


Figure 5.10: (right) Runoff modeling (uncalibrated) for Tr=50 year, (left) $R^2$ test

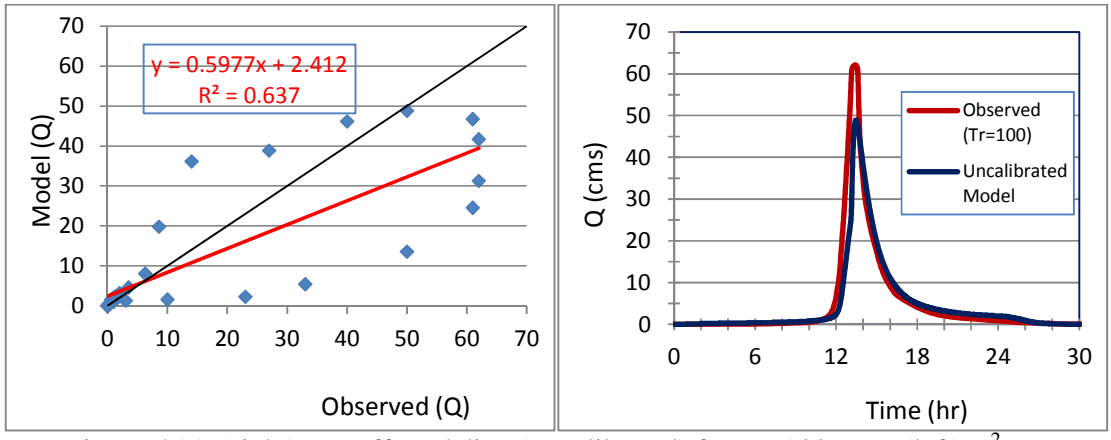


Figure 5.11: (right) Runoff modeling (uncalibrated) for Tr=100 year, (left) $R^2$ test

Model calibration is one of the most important steps in every numerical modeling. In the rainfall-runoff models, this function measures the degree of variation between computed and observed time series flows. When the objective function is minimized,

it means that the optimal parameter values are determined and calibration process is completed (USACE, 2000). The calibration process can be done manually or automatically. There are five functions available in Hec-HMS which allows the automated model calibration. In this thesis, peak-weighted root mean square error (PWRMSE) is selected which is defined as follow:

$$PWRMSE = \sqrt{\frac{\sum_{t=1}^{N}(Q_O(t) - Q_M(t))^2 \frac{Q_O(t) + Q_A}{2Q_A}}{N}} \quad (5\text{-}1)$$

$$Q_A = \frac{1}{N}\sum_{t=1}^{N} Q_O(t) \quad (5\text{-}2)$$

Where $Q_O$ and $Q_M$ are the observed and modeled flow at time t respectively and $Q_A$ is the average observed flow.

Seven rainfall-runoff events were chosen for the calibration of the hydrologic model. These models were shown in Fig 5.5 to 5.11. During the manual calibration it was found that for Tr>10 year, the model hydrographs were smaller than the observed hydrographs whereas for Tr<10 the model and observed data are almost the same.

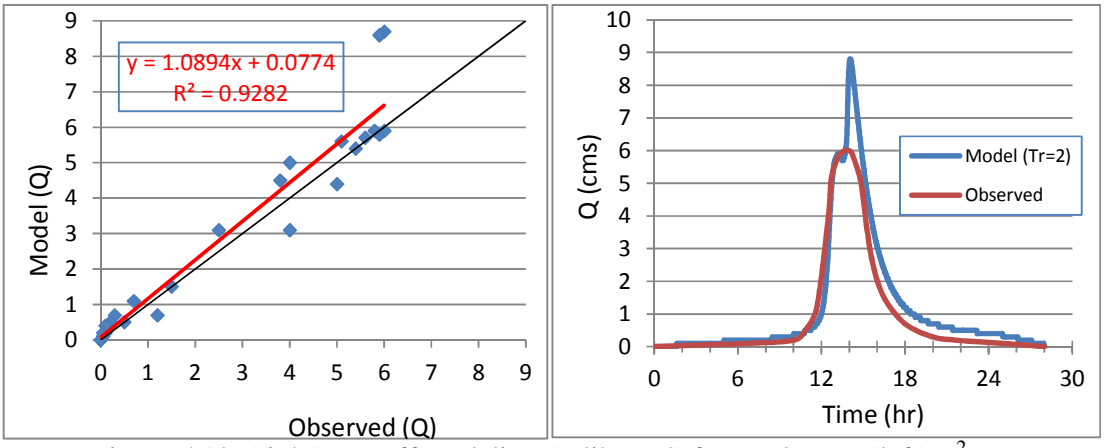


Figure 5.12: (right) Runoff modeling (calibrated) for Tr=2 year, (left) $R^2$ test

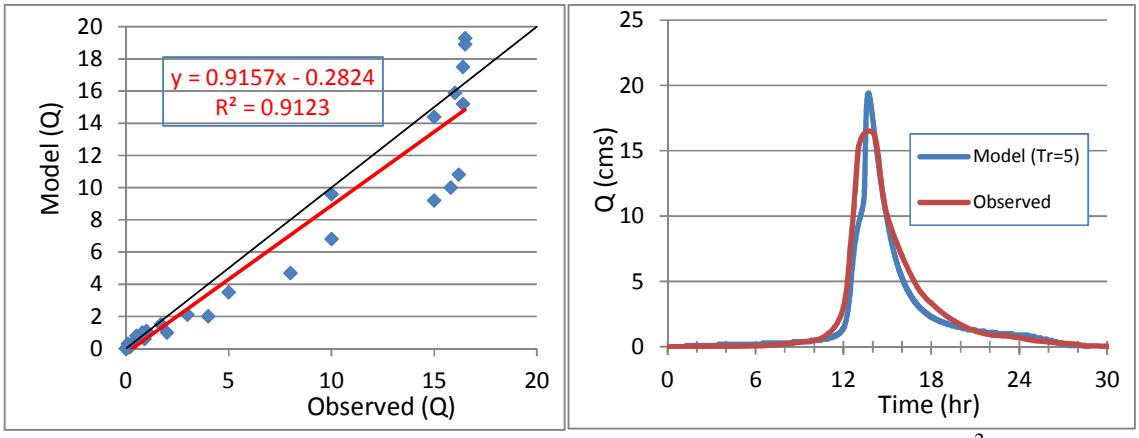


Figure 5.13: (right) Runoff modeling (calibrated) for Tr=5 year, (left) $R^2$ test

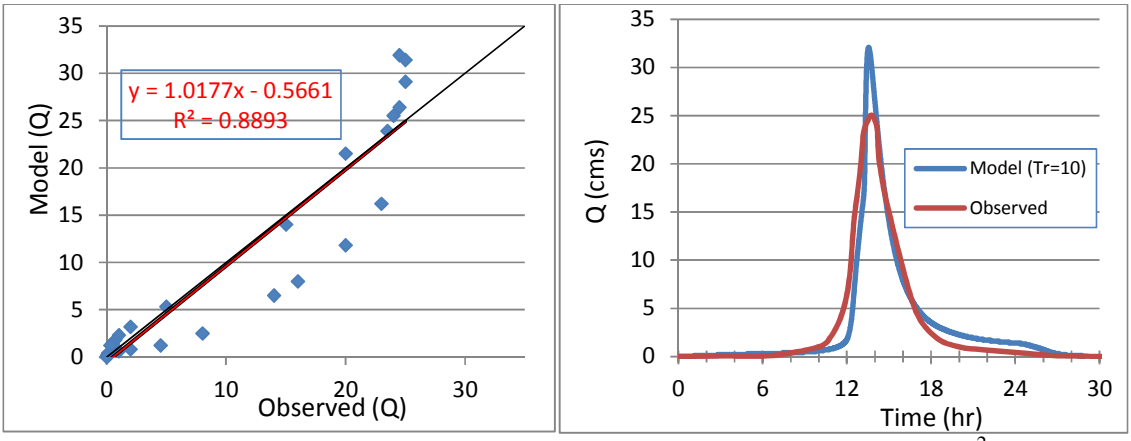


Figure 5.14: (right) Runoff modeling (calibrated) for Tr=10 year, (left) $R^2$ test

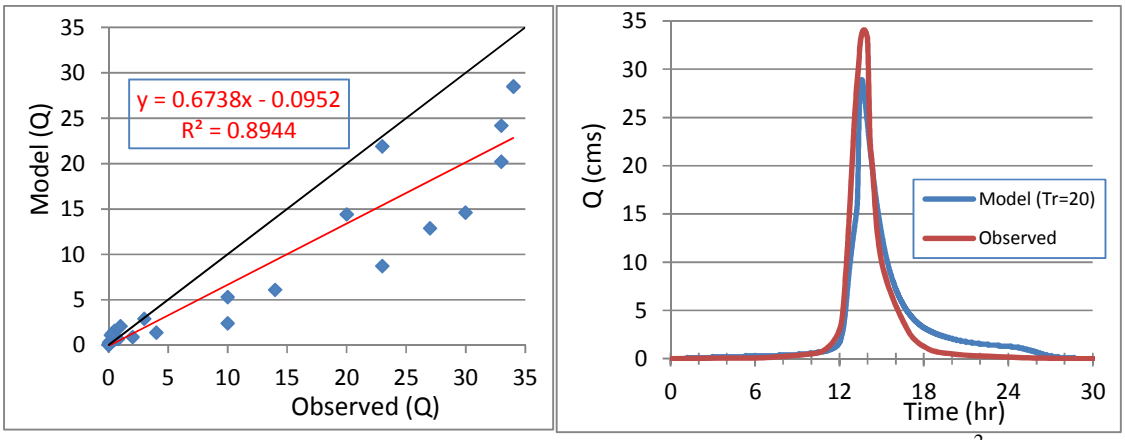


Figure 5.15: (right) Runoff modeling (calibrated) for Tr=20 year, (left) $R^2$ test

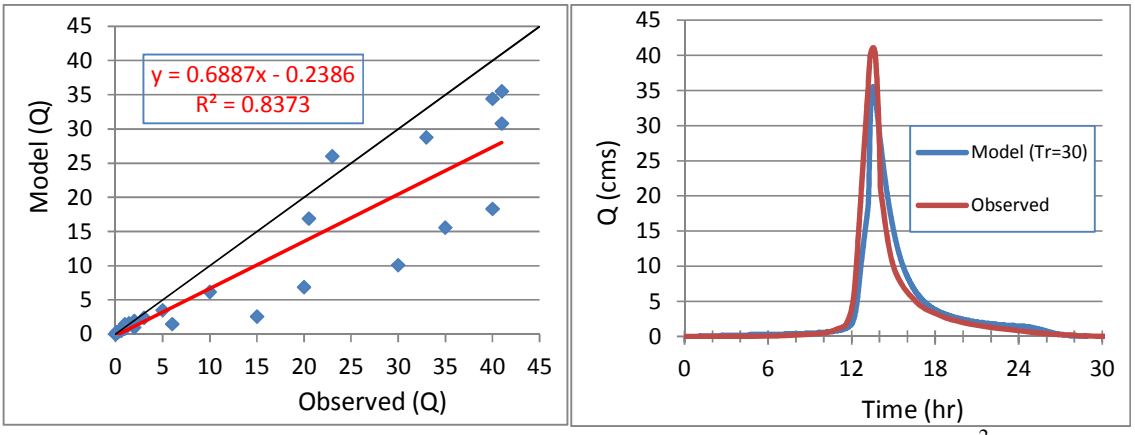


Figure 5.16: (right) Runoff modeling (calibrated) for Tr=30 year, (left) $R^2$ test

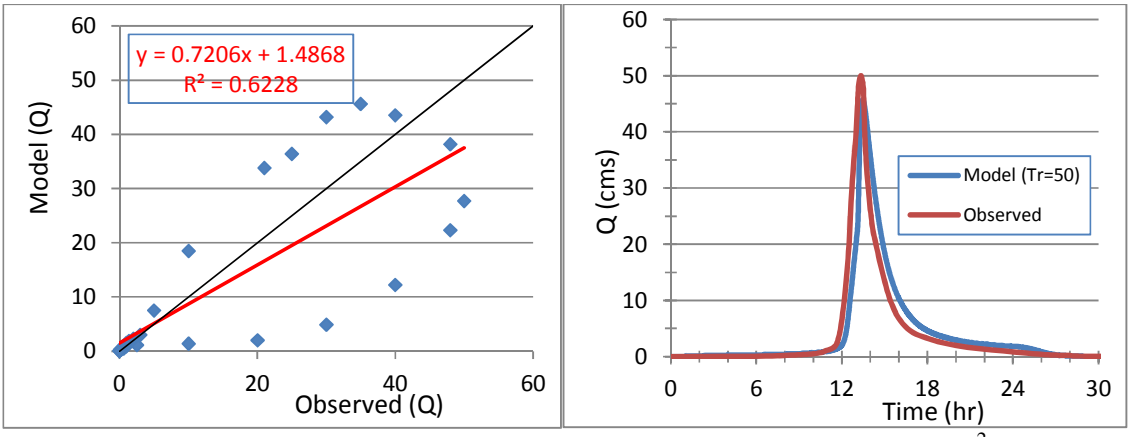


Figure 5.17: (right) Runoff modeling (calibrated) for Tr=50 year, (left) $R^2$ test

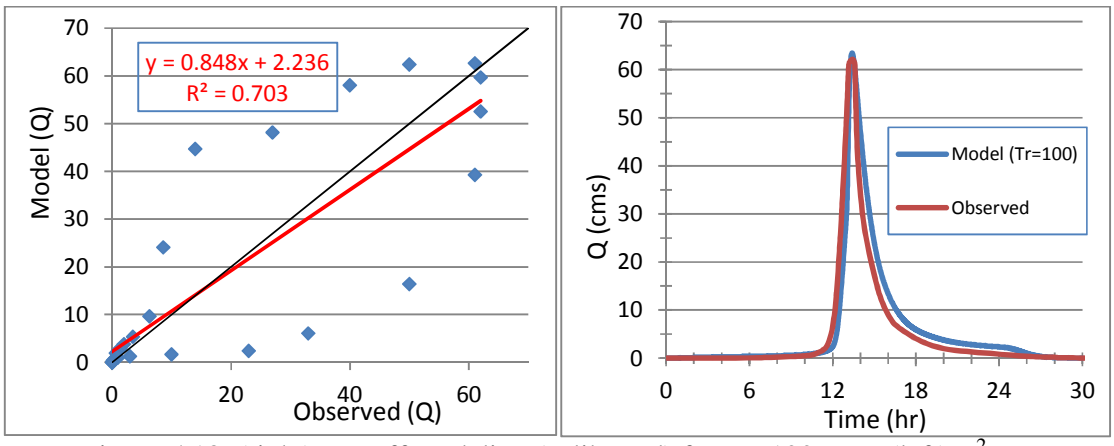


Figure 5.18: (right) Runoff modeling (calibrated) for Tr=100 year, (left) $R^2$ test

The $R^2$ tests which were shown in the left hand side of Figures 5.5 to 5.11 also showed that the model and observed data did not match each other. In those pictures the red

line denotes the best fitted line and the black line denotes the exact results. As it can be seen, the red lines and the black ones are not adjusted.

Using the calibration method (manual and automated) these 2 lines were accosted. The final results are shown in the left hand side of Figures 5.12 to 5.18.

Figure 5.19 shows the $R^2$ test for all simulations before and after the calibration process. As it can be seen in this picture, the value of $R^2$ is changed from 0.6481 to 0.8067 and this means that the differences between modeled data and observed data are reduced.

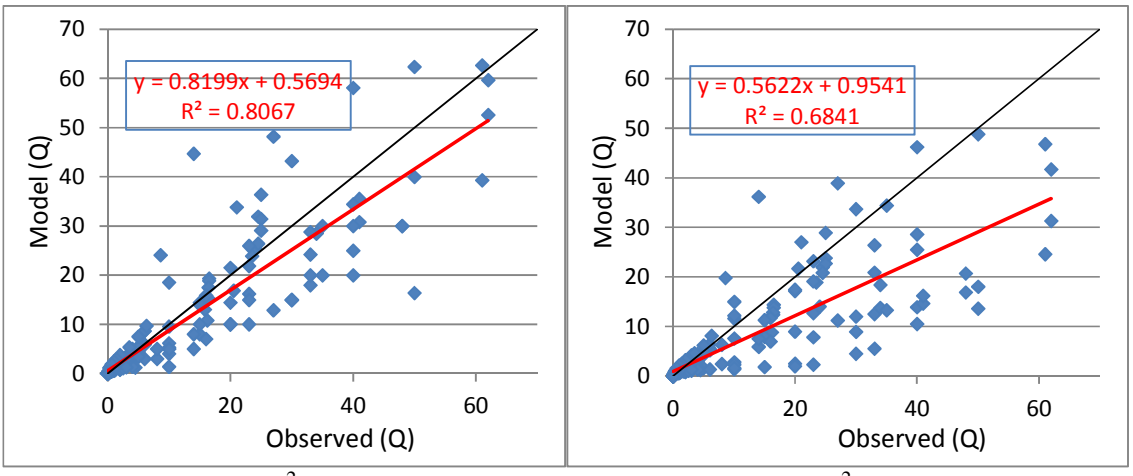


Figure 5.19: (right) $R^2$ test for all un-calibrated simulations, (left) $R^2$ test for all calibrated simulations

Although, the peak discharges of the calibrated model for Tr=2, 5 and 10 year are a little more than the peak discharges of the observed data, but the model hydrographs for Tr>20 year are almost similar to the observed hydrographs especially for Tr=50 and 100 year.

Now it is possible to use this model for other kinds of modeling which will be discussed in the rest of this chapter.

### 5.6 Analysis of land use change

One of the most important research areas in hydrology to model rainfall-runoff process is land use and land cover change. Since one of the major factors in rainfall runoff

modeling is land use, land use change has a significant impact on the peak discharge and hydrograph of the basin. In this section, the results of a research (Martijn Snelder, Dr. Eric Kooman and Dr. Kees Kasse, Vrije Univ., Aug. 2010) which was done in Netherlands about the land use change in Austria between 1990 and 2000 are used. Also, the report of CIA world factbook[1] about urbanization rate in Austria is used here.

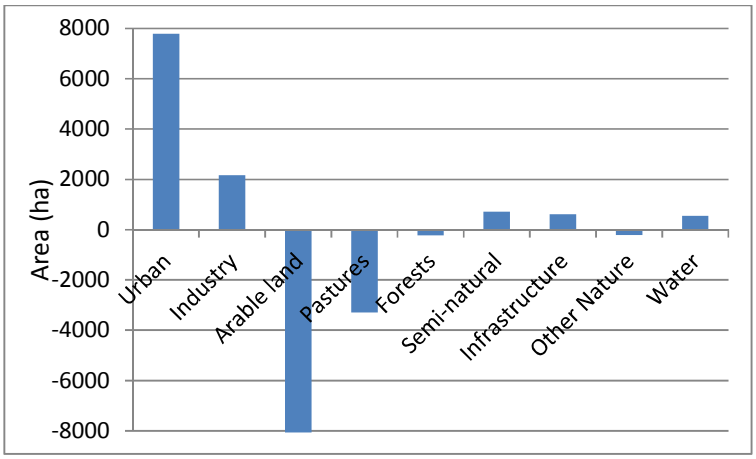


Figure 5.20: Land use change between 1990 and 2000 in Austria

Table 5.2: Land use change between 1990 and 2000 in Austria

| Land use | 1990 | | 2000 | | Transition |
|---|---|---|---|---|---|
| | Area (ha) | % | Area (ha) | % | % |
| Urban | 317581 | 3.78 | 325362 | 3.88 | +0.10 |
| Industry | 17137 | 0.2 | 19293 | 0.23 | +0.03 |
| Arable land | 1520974 | 18.12 | 1512912 | 18.02 | -0.10 |
| Pastures | 1196644 | 14.26 | 1193360 | 14.22 | -0.04 |
| Forests | 3758362 | 44.77 | 3758133 | 44.77 | 0.00 |
| Semi-natural | 586994 | 6.99 | 587705 | 7.0 | +0.01 |
| Infrastructure | 5567 | 0.07 | 6172 | 0.07 | 0.00 |
| Other nature | 921253 | 10.97 | 921030 | 10.97 | 0.00 |
| Water | 69744 | 0.83 | 70289 | 0.84 | +0.01 |

The land use transitions between 1990 and 2000 are shown in table 5.2. This Table shows that the most important part of land use change in Austria is urbanization.

1- https://www.cia.gov/library/publications/the-world-factbook/geos/au.html

Figure 5.20 illustrates that 44% of the total amount of land use change can be considered urbanization. Most urbanizing on the land use maps happens near current urban land use and close to some of the bigger cities. In Austria, a large amount of the urbanization can be observed around Vienna, Graz and Linz.

Also, CIA world factbook reported that the rate of urbanization in Austria is 0.6% annual rate change between 2012 and 2015. If this ratio is considered constant up to 2020, the forest area of the Schoeckelbach basin will be decreased about 6% and the urban area will be increased about 6% between 2010 and 2020. This changing in land use will change the peak discharge and hydrograph of the basin. The land use change analysis is shown that the peak discharge for a 100-year 1-day rainfall is increased about 4 ($m^3$/sec). In this analysis, CN for the Schoeckelbach basin is modified based on the urbanization rate and a rainfall runoff modeling is carried out. It should be noticed that this peak discharge is very depend on the position of the urbanization in the Schoeckelbach basin and in this analysis it is assumed that the urbanization is increased in the vicinity of the current urban areas .

## 5.7 Analysis of Climate Change

In this section, a climate change analysis is carried out in the Schoeckelbach basin. Because of lack of the necessary information, climate change analysis is done using information of the Intergovernmental Panel on Climate Change IPCC.

As it is obvious from the recorded temperatures during the last century, the global temperature has increased between 1-2 °C especially in the last 50 years (IPCC, 2007). Figure 5.21 illustrates the changes in global surface temperature for each continent separately.

The change of temperature and precipitation cause a number of direct and indirect effects on the environment and the society. Some of these effects are as follows:

1. Biodiversity
2. Water resources
3. Agriculture

4. Forestry
5. Urbanization
6. Electricity
7. Regional and settlement development

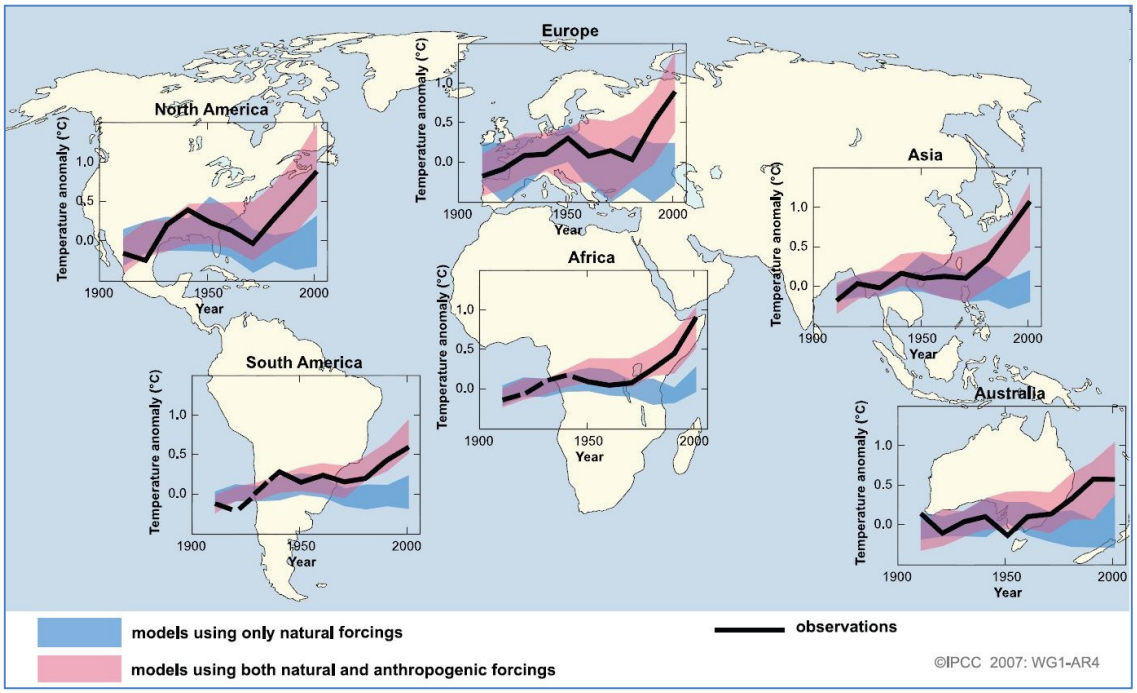


Figure 5.21: Changes in global surface temperature (IPCC 2007)

As the world warms, rainfall will increase overall but changes in distribution will increase droughts as well as floods.

Since, the temperature and precipitation data are very important for statistical modeling of climate change and temperature data were not available for us, the temperature data which were available in some websites (such as www.maplecroft.com) and reports (such as IPCC 2007) were used in this thesis to carry out an approximate modeling of influence of climate change in rainfall-runoff modeling of the Schoeckelbach basin.

In this thesis, effects of three probable SRES scenarios, namely A2 (high), A1B (medium) and B1 (low) on the rainfall-runoff process in a small basin in austria are investigated (see these senarios in Appendix B).

Figure 5.22 illustrates the surface temperature changes for the early and late 21st century relative to the period 1980-1999. As it can be seen in this figure, temperature changes in Austria for the period 2020-2029 is between 0.5-1 °C and for the period of 2090-2099 is relatively high (3-5 °C) based on these three SRES scenarios.

Based on the changes in the global temperature, the global precipitation also has been changed, for example in Austria; the precipitation has increased by 10-15% in the last 40 years with the exception of southeast Austria (including the Schoeckelbach basin) that became drier. Figures A.28 to A.31 illustrate the global drought changes which were statistically simulated based on the precipitation and temperature data recorded in the last century (Dai 2010).

As it can be seen in these figures, Austria will have relatively bad conditions especially in the southern and southeastern part. Based on these conditions, a website (www.maplecroft.com) reported that Austria in the vulnerability of climate change was classified as medium to high risk (Figure A.32). Also, IPCC released a model (scenario A1B) of the global precipitation changes which was based on the observed data during 1900-2000. Figure 5.23 illustrates this report for period 2090-2099 relative to 1980-1999. This figure shows that for Austria, the relative precipitation for December to February (DJF) is a little increased but for June to August (JJA) is intensively decreased.

Based on these reports, rainfall-runoff modeling of the Schoeckelbach basin was carried out including three SRES scenarios (A2, A1B and B1). For this reason, similar to the method which was employed in (Mohammadnejad, 2010), the precipitation data with respect to the Figures (A.28 to A.31), were considered as -5%, +5% and +10% repectively. Also because of changing in land use especially forests, the CN numbers were increased as +5%, +10% and +20% respectively.

However, the final results are summarized in Table 5.3. It should be mentioned again that this table shows the results approximately (more than 90% of the models agree in the sign of the change) because the observed temperature data (in the last century) were not accessible and these data were obtained from some websites and IPCC reports approximately.

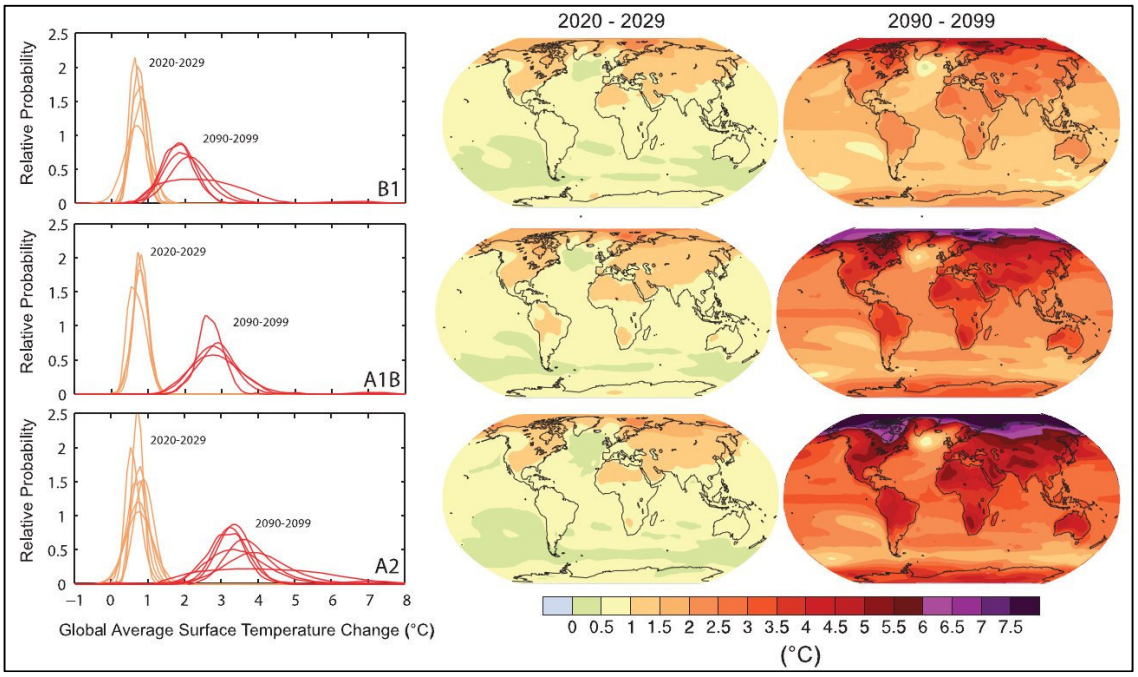


Figure 5.22: The global surface temperature changes for the early and late 21st century relative to the period 1980-1999 (IPCC 2007)

Table 5.3: Final results of climate change analysis (JJA) relative to 1990-2012 (Max. discharge $m^3$/sec)

| SRES Scenario | 1990-2000 | 2030-2039 | 2060-2069 | 2090-2099 |
|---|---|---|---|---|
| A2 (high) | 80.2 | 88.7 | 98.3 | 95.8 |
| A1B (medium) | 80.2 | 77.2 | 74.1 | 73.5 |
| B2 (low) | 80.2 | 69.1 | 79.6 | 74.4 |

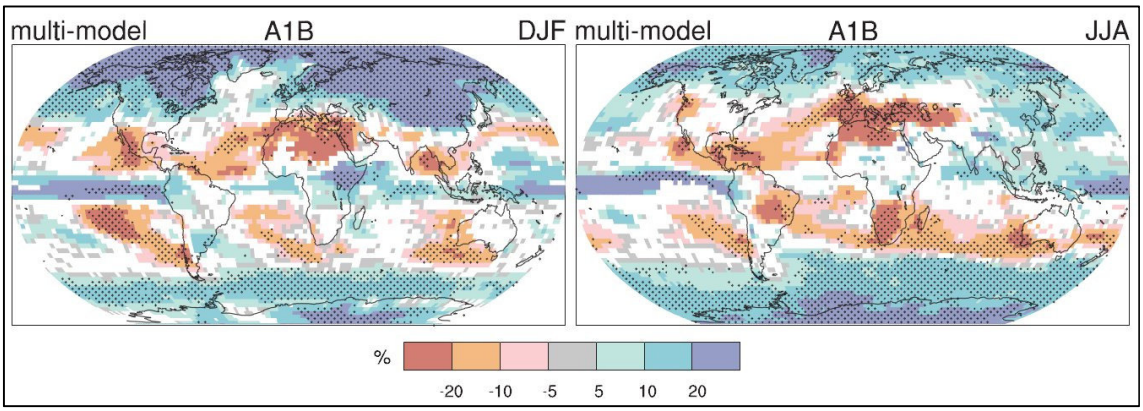


Figure 5.23: Relative changes in precipitation (in percent) for the period 2090–2099, relative to 1980–1999. Stippled areas are where more than 90% of the models agree in the sign of the change (IPCC 2007)

Since, climate change in Austria (especially southeastern Austria) effects on drought severity, Schoeckelbach basin will lose some forest areas and due to this reason, the peak discharges can be increased.

As it can be seen in the table, the estimated peak discharges will be decreased except for A2 scenario. It should be mentioned that for climate change modeling of the Schoeckelbach basin the effect of land use change (reduction of forest coverage) was considered.

### 5.8 Continuous simulation model

The continuous simulation is used when a long time modeling for a decade or more is needed. For this reason a continuous record of rainfall with an appropriate time interval is required (McEnroe, 2010). For the Schoeckelbach basin, the continuous model was developed from data recorded at a gauge which was shown in chapter 2. The rainfall data was gathered in two kinds:

1- from 1947 to 2012 every days
2- from 2005 to 2012 every 15 minutes

For continuous simulation of the Schoeckelbach basin the second data was used.

Because small watersheds respond quickly to rainfall, a short computational time step is needed to obtain a realistic stream flow hydrograph (USACE, 2000). Since in Hec-HMS, time interval cannot be greater than [0.29×lag(t)] for the smallest river and in Schoeckelbach basin there are some small rivers with [0.29×lag<5 min], a computational time step of 1 minutes is possible. However, with such a small time step, the computational time will be increased too much. For this reason, the continuous simulation was limited to 1 year (01 Aug. 2011 to 01 Sep. 2012). The results of some months with high amount of rainfall are shown in Figures A.33 to A.35.

# Chapter 6

# Flood Management using Hec-RAS

## 6.1 Introduction

Floods are occurred in rivers when the flow rate exceeds the capacity of the river channel. Floods are often considered as catastrophic events because they usually make major infrastructure failures. In order to assess the consequences of floods, a flood modeling should be carried out to find the high flood risk regions in the basin. There are several models available to do this process but in this thesis Hec-RAS is used. This is because of this fact that the results of Hec-HMS which are necessary data for flood modeling can be imported to Hec-RAS as an input file. Also, all channel characteristics can be derived using Hec-GeoRAS which is an extension for ArcGIS and these information can be imported to Hec-RAS directly. Here, inundation areas are modeled for 100-year 1-day rainfall.

## 6.2 Inundation areas for 100-year 1-day rainfall

The 100-year 1-day rainfall modeling was shown in Fig. 5.18. Most of the models which are used for flood modeling employ a stage-discharge relation for flood modeling. This relationship is investigated in the next section.

### 6.2.1 Stage-Discharge Relation

The relationship between the water level and the simultaneous flow discharge in an open channel is known as stage-discharge relation (Rantz et al., 1982). This relation is used in order to simulate the inundation areas along an open channel.

The most commonly used stage discharge relation is a parabolic equation which is given by (Herschy, 1995; Kennedy, 1984; Rantz et al., 1982):

$$\mathrm{Q} = \mathrm{a}(H - b)^c \tag{6-1}$$

In which:

Q: discharge ($m^3$/sec)

$H$: water depth in river (m)

*a, b, c*: calibration coefficients which depend on the river condition

*a* is the discharge value when the effective depth of flow (H-b) is equal to 1 (on log-log paper); *b* is the gauge height when there is no flow; *c* is the slope of the rating curve (on logarithmic paper).

To know how it is possible to obtain this relation for a river, by taking logarithms on both sides of Eq. (6-1), the following relation is arrived:

$$\log(Q)=\log(a)+c.\log(H-b)$$

which is in the form of a straight line if Q and (H-b) are plotted on a log-log paper, the slope, of the straight line plot gives the constant c. Also by trial and error, the value of b for the line can be obtained while by changing b, the curve becomes straight line. Parameter a, is Q-intercept (value of Q when (H-b)=1 in log-log paper).

It should be noted that river cross section directly effect on the stage-discharge relation. If the cross section is a compound section, for this river, there are more than one stage-discharge relations. Figure 6.1 shows the cross section of river R480 (see also Fig. 5.4) in Schoeckelbach basin. As it can be seen, because of a compound cross section, there are two stage-discharge relations for this river. Figure (6.2) shows how the stage-discharge parameters can be obtained for this river.

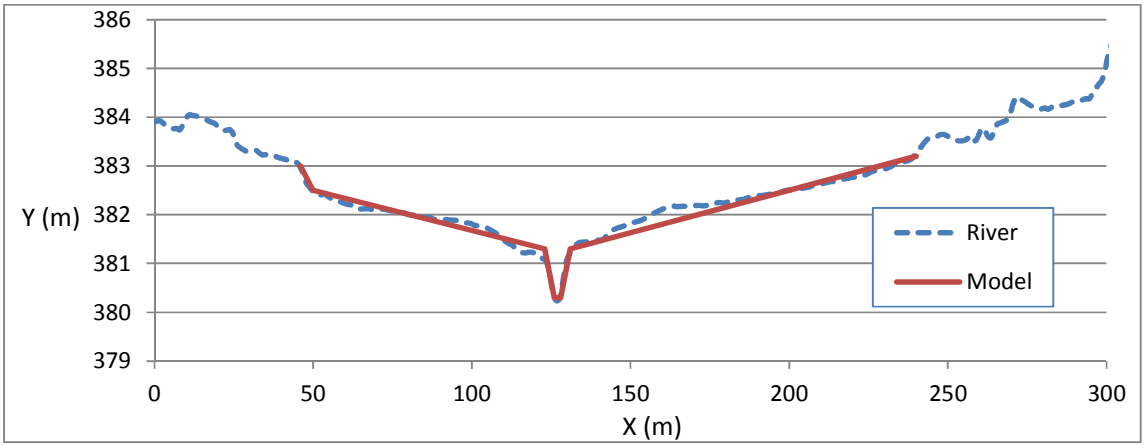


Figure 6.1: The river cross section (R480)

Table (6.1) shows some calculated discharges (using Manning's formula) and simultaneous stages in this river (R480).

Because the cross section is a compound cross section (H<=1m and H>1m), the stage-discharge relation for this river is splitted up to two relations as shown in Figures (6.3) and (6.4).

$$Q = 9.3378(H)^{1.856} \qquad H \leq 1\ m \tag{6-2}$$

$$Q = 12(H - 0.25)^{4.044} \qquad H > 1\ m \tag{6-3}$$

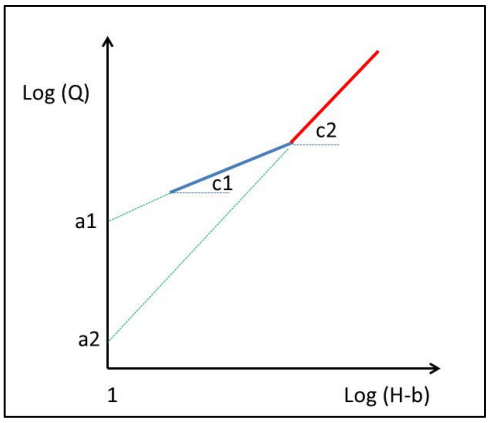


Figure 6.2: The stage-discharge relation for a compound cross section (R480)

Now, using these equations, it is possible to compute the stages and the width of water surfaces for various observed peak discharges. Figure (6.5) shows the final results. As the picture illustrates, for a 100-year 1-day rainfall ($Q_p$=62 $m^3$/sec) the width of water surface can reach to up to 130 m. This analysis shows that all structures should be constructed away from the main river (at least 65 meter from each side).

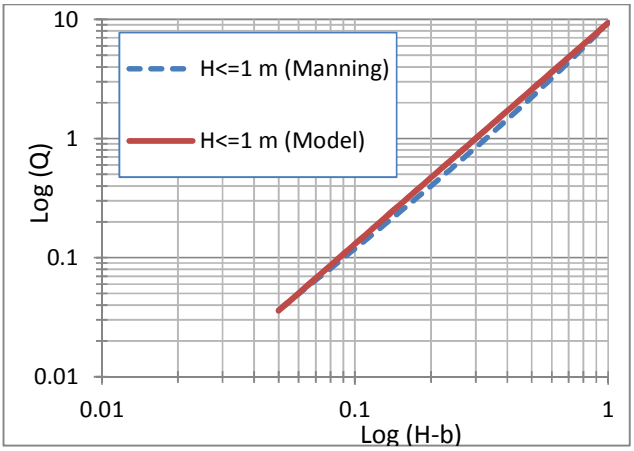


Figure 6.3: The stage-discharge relation for H<=1 m (Eq. 6-2)

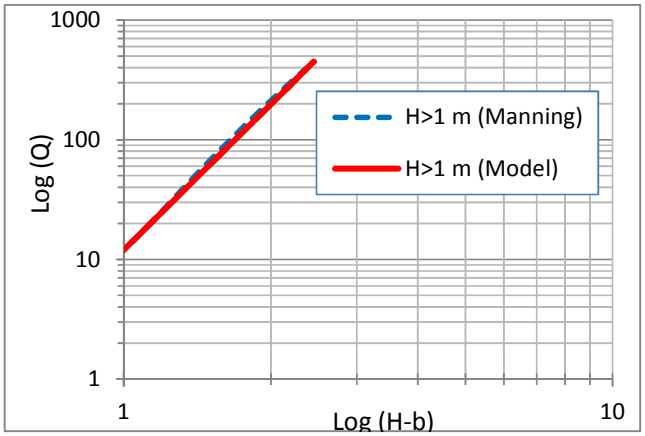


Figure 6.4: The stage-discharge relation for H>1 m (Eq. 6-3)

Table 6.1: The stage-discharge values calculated from Manning's formula

| H (m) | A ($m^2$) | P (m) | n | R (m) | S (m/m) | Q ($m^3/s$) |
|---|---|---|---|---|---|---|
| 0.1 | 0.23 | 2.6325 | 0.035 | 0.0874 | 0.008431 | 0.1188 |
| 0.5 | 1.75 | 5.1623 | 0.035 | 0.3390 | 0.008431 | 2.2321 |
| 0.8 | 3.52 | 7.0597 | 0.035 | 0.4986 | 0.008431 | 5.8066 |
| 1 | 5.00 | 8.3246 | 0.035 | 0.6006 | 0.008431 | 9.3379 |
| 1.5 | 23.19 | 65.0952 | 0.035 | 0.3563 | 0.008431 | 30.5742 |
| 2 | 69.76 | 121.8658 | 0.035 | 0.5725 | 0.008431 | 126.1769 |
| 2.5 | 144.72 | 178.6364 | 0.035 | 0.8101 | 0.008431 | 329.9205 |

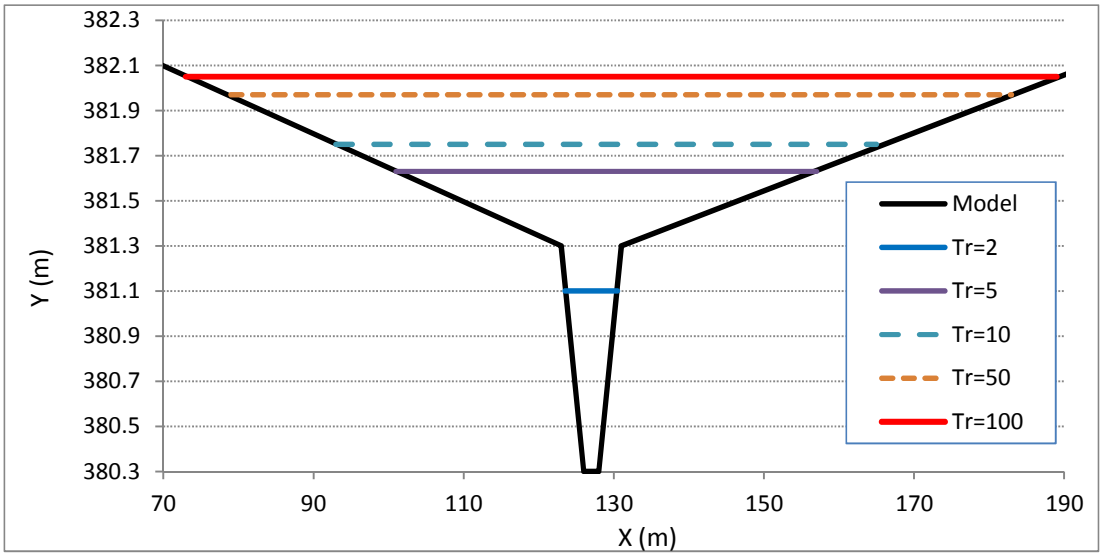


Figure 6.5: The stages for various observed discharges (R480)

### 6.2.2 Flood management map

As it represented before, one of the most important usages of the rainfall-runoff modeling is its application as a management tool, for example, in the management of flood in urban area. When a rainfall-runoff modeling is completed, it is possible to evaluate the value of floods in all river tributaries and also sub-basins. Using these data, it is possible to make a flood map and to specify the high flood risk regions.

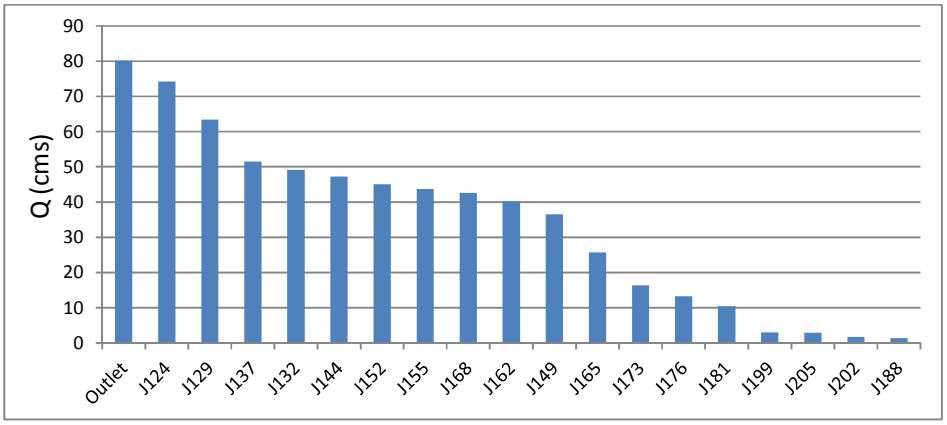


Figure 6.6: The discharges for 100-year 1-day rainfall modeling at the river tributaries

This process was done for the Schoeckelbach basin for a 100-year 1-day rainfall-runoff model. Figure 6.6 illustrates the amount of flood discharges at the river tributaries. The river tributaries also are shown in Fig. 6.7.

As it was predictable, the flood discharges for the tributaries in the north part of Schoeckelbach are very low because most of forests are placed at the north part of Schoeckelbach with high amount of losses and low amount of runoff.

Also, Fig 6.8 illustrates the flood map of Schoeckelbach basin. As it can be seen in this picture, the sub-basins with high flood risk are placed at southern Schoeckelbach where the urban area is placed there (Red border in Fig. 6.7). This was predictable, because of existing impervious regions in urban areas the amount of losses is low and the amount of runoff is high. The amounts of peak discharges for the regions that situated at the north and the middle part of the basin are almost low because most of these regions are covered by forests. Also, the amounts of discharges for the regions

that situated at the east part of the basin are almost high because of their soil type (Dystric Cambisol).

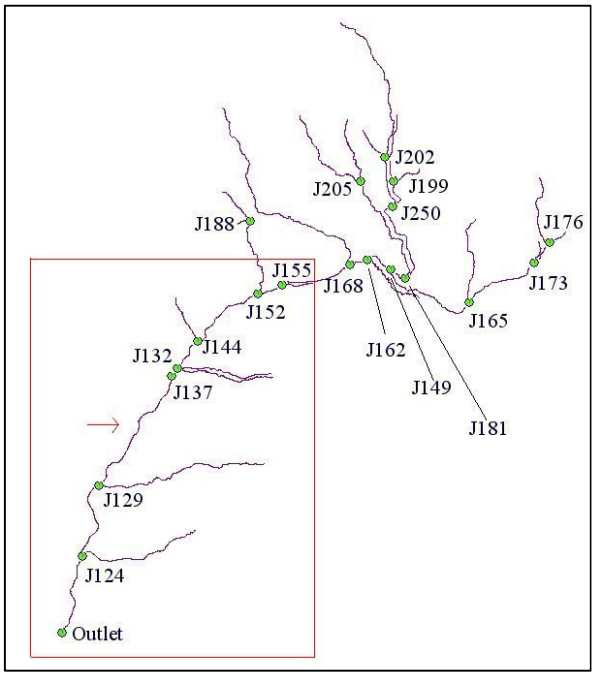


Figure 6.7: The name of river tributaries in the Schoeckelbach basin (red border: critical reaches)

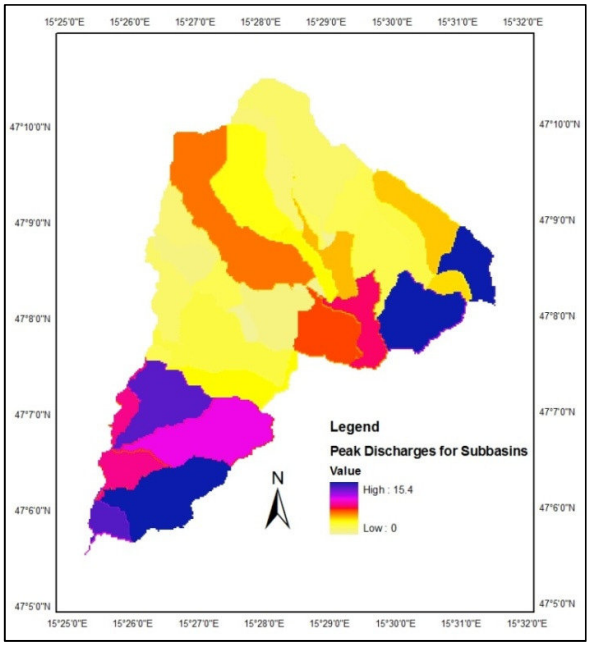


Figure 6.8: The discharge map for each sub-basin in the Schoeckelbach basin for a 100-year 1-day rainfall

## 6.3 Flood control using Hec-RAS

The procedure for preventing the harmful effects of flood waters is called flood control. There are a number of methods to control the consquenses of floods. These methods are the construction of levees, lakes, dams, reservoirs or retention ponds to hold extra water during times of flooding.

In this section two methods of them (levee and retention pond) are investigated.

### 6.3.1 Control of high flood risk regions in the basin using levee

As it was shown in the previous section, the most of regions with high flood risk are situated at the southern Schoeckelbach basin. This part of the basin is very important for flood risk management because urban area is also placed here (green area in Fig. A.5 right). In order to manage the consequences of probable floods in this part, the rivers with high flood risk are investigated using Hec-RAS. Figure A.5 (left) illustrates a river including five reaches (R390, R400, R480, R520 and R590) and Figure A.5 (right) illustrates that river after installing levee in order to reduce flood regions.

The river characteristics and also detail of sections are imported from Hec-GeoRAS to Hec-RAS. Detail of high discharges (100-year 1-day rainfall) and also boundary conditions are imported from Hec-HMS to Hec-RAS.

Water surface profile, velocities, hydraulic grade line and energy line are computed using Hec-RAS in two conditions: 1- River before installing levee, 2- River after installing levee.

Figure A.6 illustrates the longitudinal profile of the river, water surface and energy line in two conditions: (top) river before installing levee, and (bottom) river after installing levee.

Results of Hec-RAS show that for the river before installing levee, almost all reaches, water flow can come out of the banks. These results are shown in Figures A.7, A.8, A.9, A.10 and A.11 (top) for reaches R390, R400, R480, R520 and R590 respectively. Also in each Figure, a section which have the widest cross section is shown. As it was

discussed in the previous section, reach R480 have the most critical condition and width of water surface can reach to up to 150 meters (Fig. A.9, top).

In order to reduce the high flood risk regions along this river, levees are installed on the banks. The height of these levees are varied between 1 to 2 meters depend on the water level along the reaches. The results are shown in Figures A.7, A.8, A.9, A.10 and A.11 (bottom) for reaches R390, R400, R480, R520 and R590 respectively.As it can be seen in these Figures, levees can prevent water flowing through the banks and they reduce the high flood risk areas.

It should be noted that installation of levees increase the water velocity in the reaches. Figure A.12 illustrates velocities which increase between 0.2 and 0.9 m/sec in all reaches. Although in some reaches it is possible to decrease the distance between levees on the right and left banks but it is not recommended because it could increase the velocities more than the present one.

### 6.3.2 Flood control using retention dam

A retention dam is constructed in order to reduce storm water runoff and to prevent flooding. There are two kinds of retention pond; dry pond and wet pond. Dry pond is a temporarily stores water after a storm and wet pond is like a permanent pool.

Table 6.2: The retention dam information[1]

| | |
|---|---|
| Dam name | Weinitzen |
| Dam type | Retention dam |
| Dam height | 8.5 m |
| Dam length | 222 m |
| Maximum volume of storage | 215,000 $m^3$ |
| Maximum water surface area | 78,900 $m^2$ |
| Maximum water elevation | 439.5 m.a.s.l |
| Dam operation | Reduction of the incoming flood peak runoff by nearly 50% |

2- http://wasser.graz.at/cms/beitrag/10124679/2551353/

In this section, hydraulic operation of an existing retention basin (dry pond) which has been constructed recently in the Schoeckelbach basin is investigated. All available information about this retention basin can be found in Table 6.2. The dam is located at upstream of the high flood risk regions in the area (red border in Fig. 6.7).


Figure 6.9: Satellite map for the Weinitzen retention dam (red line)

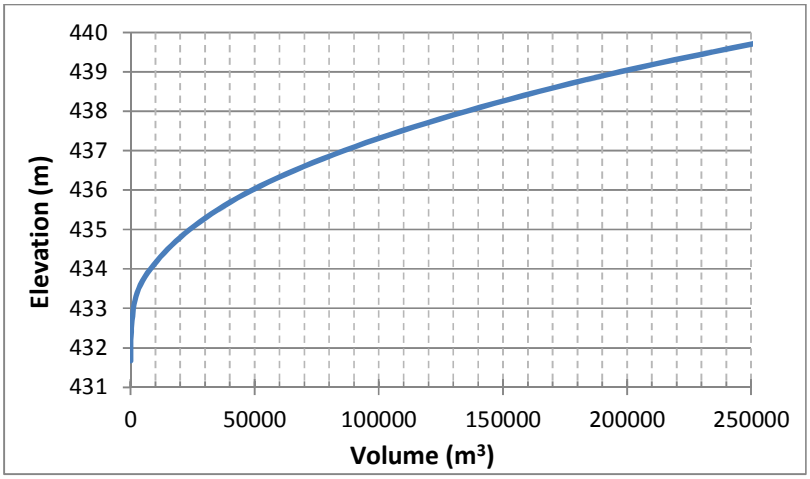


Figure 6.10: Elevation-Volume curve

Figure A.13 illustrates dam position in the Schoeckelbach basin in 2D and 3D views. Also, Figure 6.9 illustrates position of this dam in a satellite map as schematic because this dam has been constructed recently and it was not in any available satellite map.

Figures 6.10 and 6.11 illustrates Elevation-Volume and Elevation-Area curves respectively. In order to analyze the hydraulic operation of the dam, first, a reservoir routing should be carried out. For this reason, Puls reservoir routing method is used.

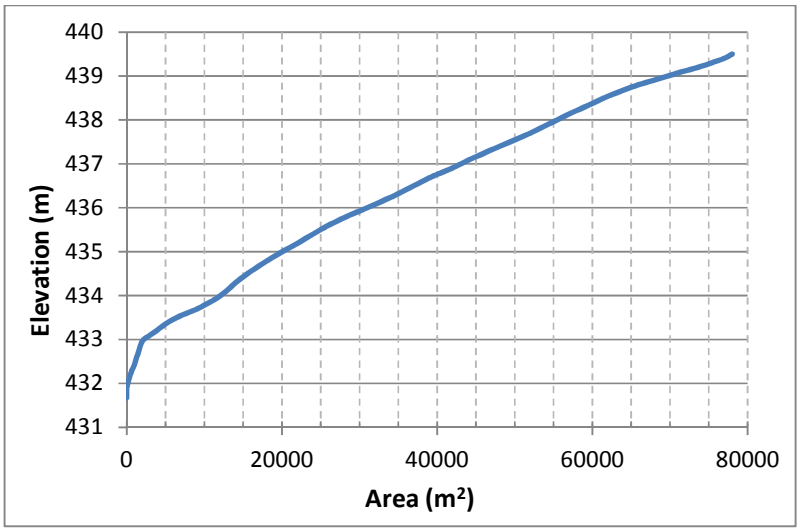


Figure 6.11: Elevation-Area curve

### 6.3.2.1 Puls reservoir routing

This method is based on the continuity equation and an empirical or analytical relationship between discharge and storage within the reach. The simplest form of the continuity equation can be written as follow:

$$I - O = \frac{\Delta S}{\Delta t} \tag{6-4}$$

Where:

*I*: the average inflow to the reach during $\Delta t$

*O*: the average outflow from the reach during $\Delta t$

*S*: storage within the reach

In reservoir routing, the inflow hydrograph is known, and the outflow hydrograph from the reservoir is unknown. Equation (6-4) can be rewritten as follow:

$$\frac{I_1 + I_2}{2} - \frac{O_1 + O_2}{2} = \frac{S_2 - S_1}{\Delta t} \tag{6-5}$$

And with rearranging it becomes:

$$I_1 + I_2 + \left(\frac{2S_1}{\Delta t} - O_1\right) = \frac{2S_2}{\Delta t} + O_2 \tag{6-6}$$

In this equation, all parameters on the left side are known and the others are unknown. To find these unknown parameters, a relationship between storage and discharge is needed as follow:

$$S = f(Q) \tag{6-7}$$

This depends on the geometry of the reservoir and its outlet. For this reason, discharges for various water elevations in the reservoir should be calculated. Then storage-outflow function (SOF) $[(2S/\Delta t) + Q_O]$ should be computed. Now, it is possible to route the inflow hydrograph using equation (6-6) and SOF curve.

Figure 6.12 illustrates dam inflow and outflow (outlet radius=0.9 m). As it can be seen in this Figure, the peak discharge is reduced about 60% and maximum volume of storage in the reservoir is reached 104,400 $m^3$.

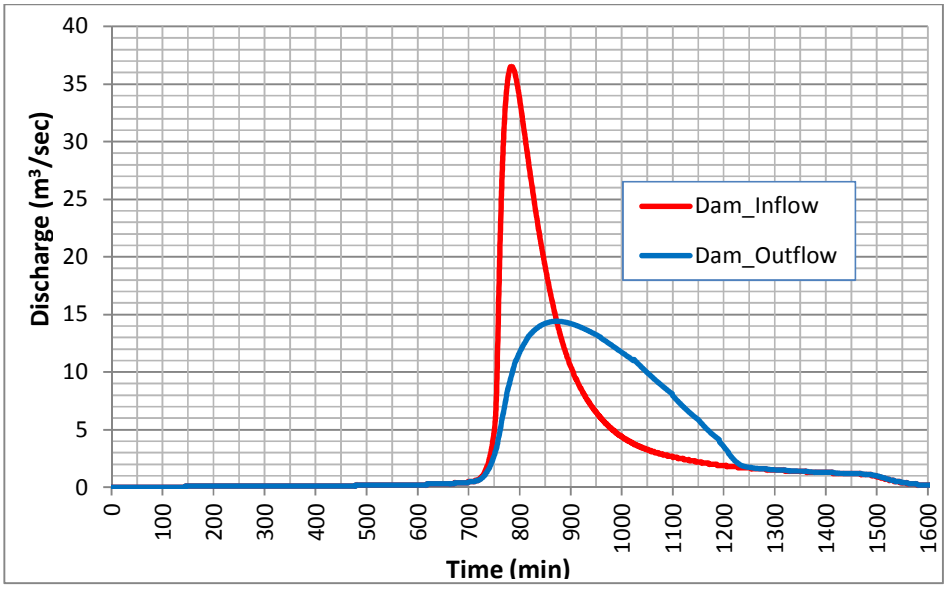


Figure 6.12: Dam inflow and outflow (time from the beginning of the rainfall), R=0.9 m, volume of storage=104,400 $m^3$

Figures A.16 to A.22 illustrate the effect of this retention dam on the outflow hydrograph from the downstream junctions of the retention dam. Figure A.14 illustrates the maximum water surface in the reservoir for 100-year 1-day rainfall.

In order to use whole capacity of the reservoir for a 100-year rainfall, it is possible to reduce the radius of the dam outlet pipe. Figure A.15 illustrates dam inflow and outflow if radius is decreased to 0.4 m. In this case, maximum volume of storage can be reached to 206,900 $m^3$. Figures A.16 to A.22 illustrate the effect of this new radius on the outflow hydrograph from the downstream junctions of the retention dam. As it can be seen in Figure A.22 the influence of these two pipes (0.4 and 0.9 m) in maximum discharge at the outlet of the Schoeckelbach basin is not too much and they just effect on the falling limb of the hydrograph. For this reason, an additional retention dam between the outlet of the Schoeckelbach basin and current retention dam is needed.

In order to understand better the effect of these two pipes on flood control in the Schoeckelbach basin, the inundation areas with these new hydrographs are investigated. Figures A.23 to A.27 illustrate the inundation areas for reaches that were shown in Fig. A.5. As it can be seen in these Figures, this retention dam can control the inundation areas until downstream of reach of R400.

Section 6.3 has been shown that both levee and retention dam can control the flood and reduce the inundation areas. In the Schoeckelbach basin the length of river with high flood risk is about 7 km. Construction of levee on this river is costly so, retention dam is better than levee for this basin. If an additional retention dam is constructed, the urban area at the southern basin can be protected against floods.

## 6.4 A comparison between inundation areas in Model and HORA[2]

In order to evaluate the accuracy of the model in estimating the high flood risk regions, this model is compared with Natural Hazard Overview and Risk Assessment Austria (HORA). Figure 6.13 shows a view of southern Schoeckelbach in HORA. Figure 6.14

2- http://hora.gv.at/

illustrates the high flood regions in HORA and model in the same scale. As it can be seen in this figure, inundation areas are completely the same.

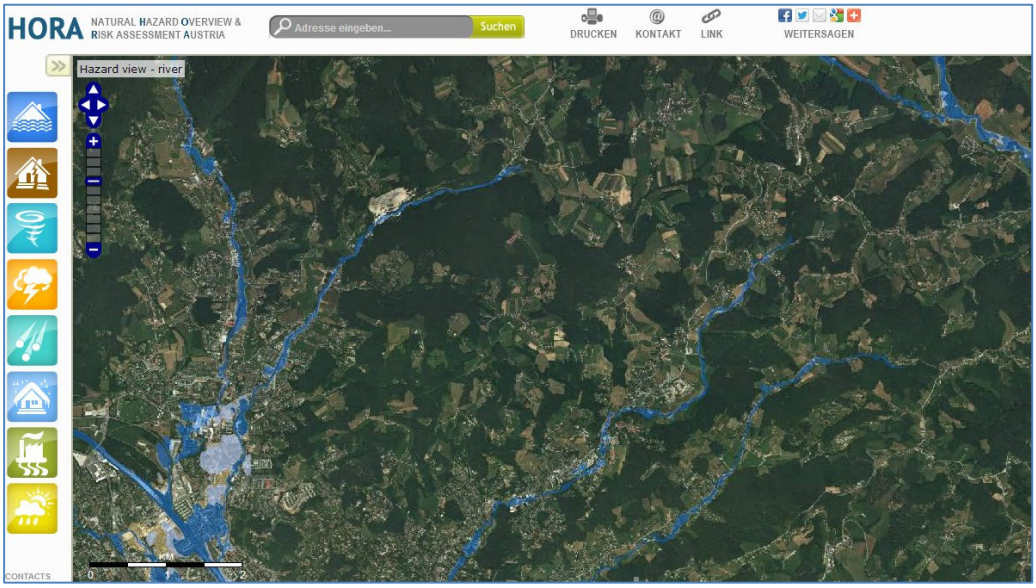


Figure 6.13: The view of southern Schoeckelbach in HORA

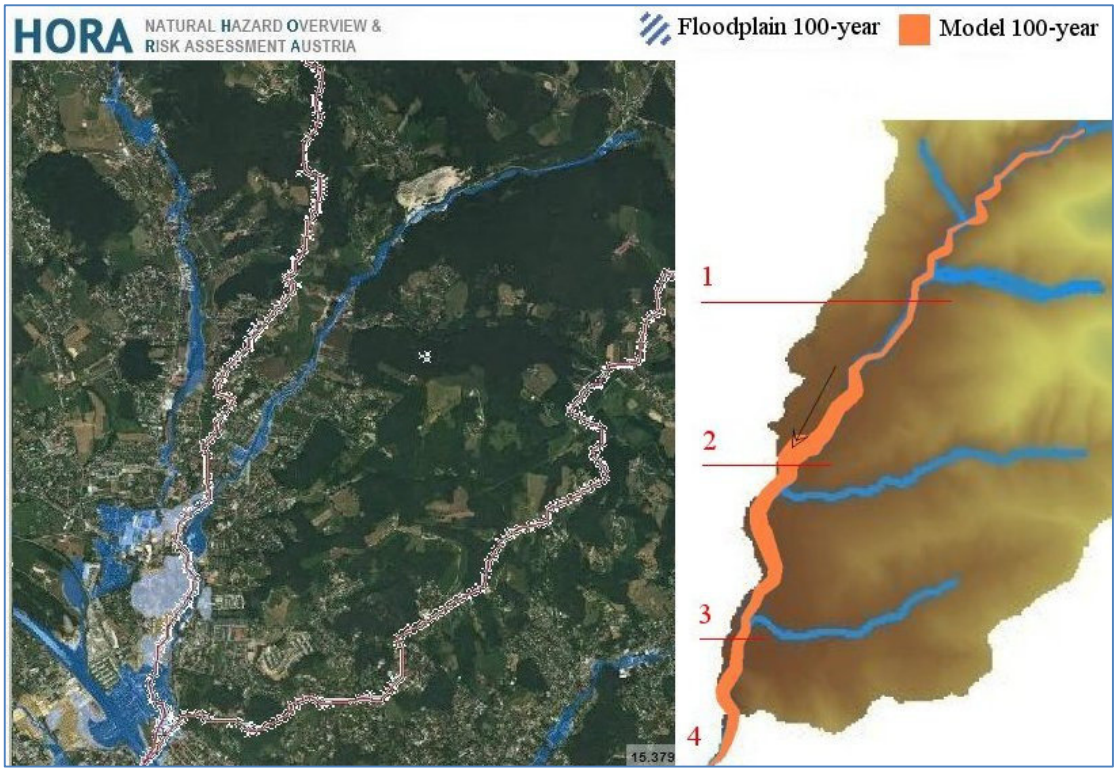


Figure 6.14: The boundary of Schoeckelbach basin in Model and HORA

In order to show more details, the inundation area in Fig. 6.14 is dissected into 4 parts and each of which, is shown in a separated Figure. Figures A.1, A.2, A.3 and A.4 (see Appendix A) illustrate parts 1, 2, 3 and 4 respectively. Note that the scale in each Figure for left side and right side of the Figure is the same. These Figures show that the inundation areas for the Schoeckelbach basin in HORA are the same as inundation areas obtained by the model.

HORA gives inundation areas for return periods of 30, 100 and 300 years. There is no any further information in this website about how these data were constructed.

**Summary**

This thesis has described the process of determining high flood risk regions using a rainfall-runoff modeling in a small catchment area in Austria. The process can be summarized as follows:

1. For rainfall analysis and in order to achieve the best fit probability distribution, in this thesis, four commonly distributions used in hydrology were compared as GEV, Gumbel, LP III and LN III. For this reason, distribution parameters were estimated using L-moments and maximum likelihood methods. The rainfall analysis was shown that the best-fit probability distribution for the rainfall data recorded at the northern Graz is Gumbel distribution. After that, parameters of the IDF relation are estimated using Gumbel distribution and a simple graphical method. This IDF relation is used as input for Hec-HMS.
2. For hydrological and also hydraulic analysis in a basin, the catchment characteristics are required. This process which is called terrain analysis was done in Hec-GeoHMS. For this reason, a very high resolution DEM (micro-scale: 1m×1m) was used. For stream routing, the Muskingum-Cunge method was used. Stream network in this method, was modeled with 8-point cross section.
3. To evaluate the amount of losses in the basin, SCS-CN method was used. For this reason soil map and land use were combined and then by using SCS CN tables, a CN map was produced in Hec-GeoHMS. Then, this CN map was modified based on the antecedent moisture condition using ArcGIS. The final CN map for importing to Hec-HMS was developed using a mean CN value for each sub-basin.
4. The runoff modeling was done using Hec-HMS. All data were imported to Hec-HMS and runoff modeling was done for various storm frequencies. The results were calibrated using some observed data. Also some additional modeling such as impact of land use change, climate change and continuous modeling were also carried out.

5. The final work which was determining the high flood risk regions in the basin was done using Hec-GeoRAS and Hec-RAS. When the rainfall-runoff modeling was completed, flood hydrographs can be imported to Hec-RAS and channel characteristics can be imported from Hec-GeoRAS to Hec-RAS. Then it is possible to model inundation areas for all reaches in the basin. The results have shown that the most critical regions are placed at the southern basin (Shoeckelbach basin) where the urban area is also located there.
6. In order to assess the consequences of the flood at the southern basin, flood control analysis was done. For this reason two structures (levee and retention dam) which are used for control of flood were investigated. For reservoir routing analysis (retention dam), Puls method was used and levee was designed in Hec-RAS. The results have been showed that the existing retention dam cannot control flood in all reaches and additional retention dam is required.

**Recommended Works for the Future**

In this thesis, some additional data which could increase the accuracy of the modeling were not available. For this reason, some extra modeling for the future might be useful as follows:

1- As it was discussed in chapter 2 (section 2.6), rainfall-runoff modeling using only one gauge can rise sources of errors and decrease the accuracy of the rainfall analysis. For this reason, it is strongly recommended to collect more rainfall data from additional rain gauges in the vicinity of the basin and then in rainfall analysis, using regional analysis with time-dependent analysis, an IDF relation may be determined with very high accuracy.
2- SCS Curve Number (CN) method gives good results for a basin covered by homogenous soil type and land cover. Although the soil type of the Schoeckelbach basin is almost homogenous in a 250×250 meter map (the highest resolution map which was available), but it is recommended that loss analysis also carry out using Green and Ampt method in order to increase the accuracy of the modeling and make a comparison with SCS CN method.
3- In order to increase the accuracy of calibration, it is recommended to collect more discharge data in reaches.
4- In order to develop flood alert for constructions which placed in high flood risk regions, it is recommended to collect the map of constructions and using section 6.3 (Chapter 6), make an alert system.

# Appendix A

In this appendix, some additional Figures are provided for more information. All of these Figures were discussed in chapters 5 and 6.

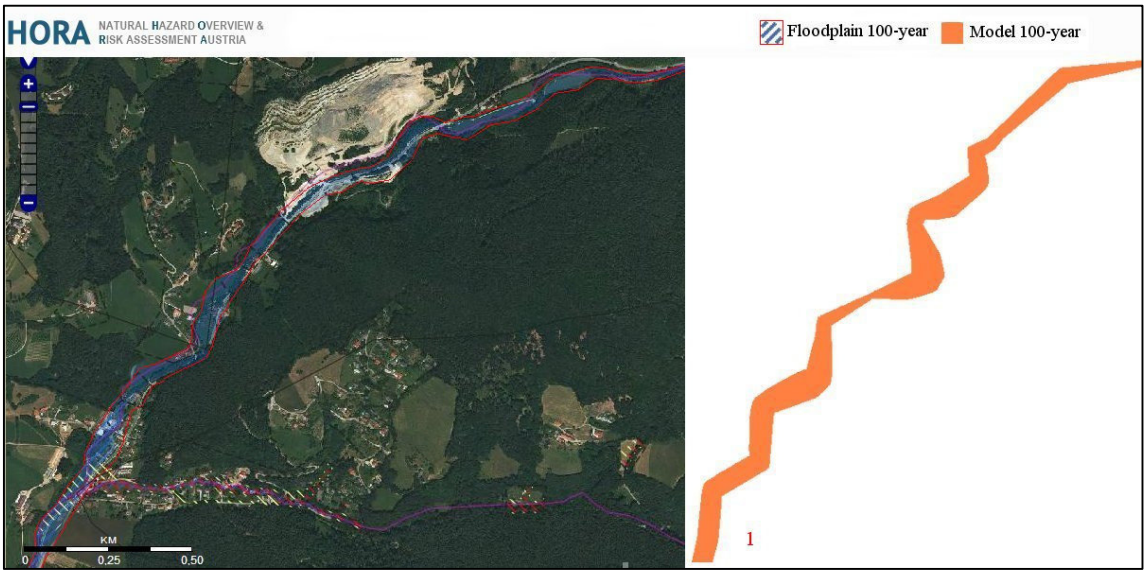


Figure A.1: A comparison between inundation area in Model and HORA (part 1, Fig. 6.14)

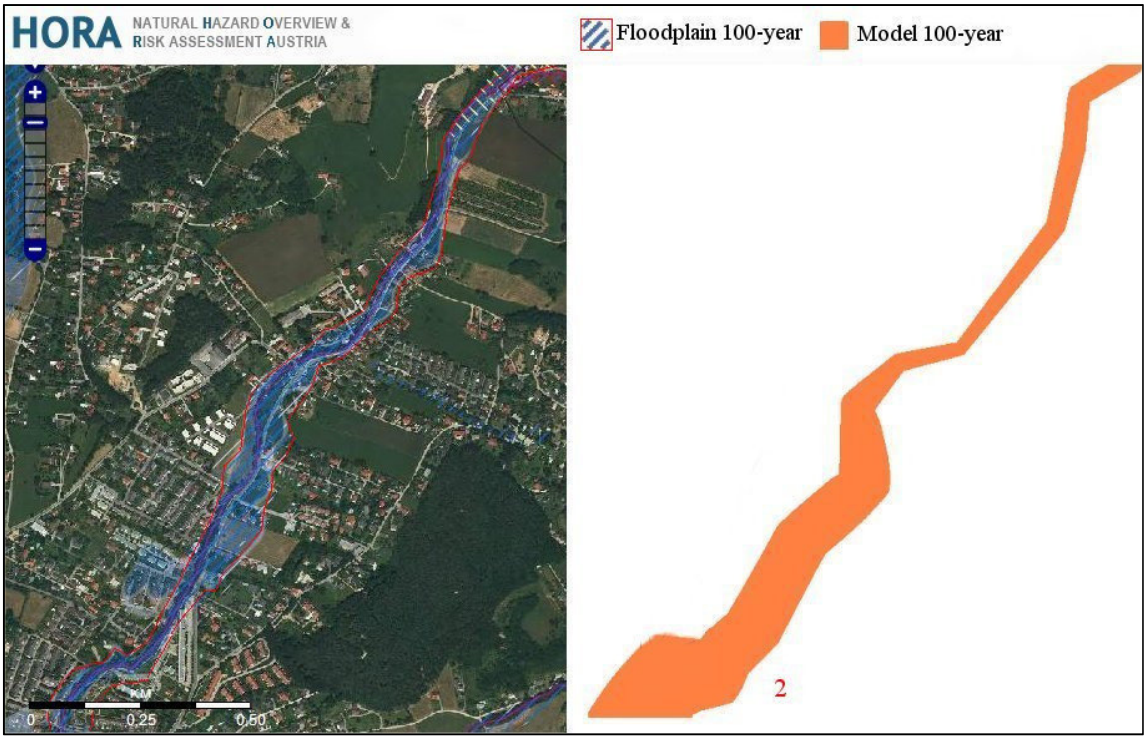


Figure A.2: A comparison between inundation area in Model and HORA (part 2, Fig. 6.14)

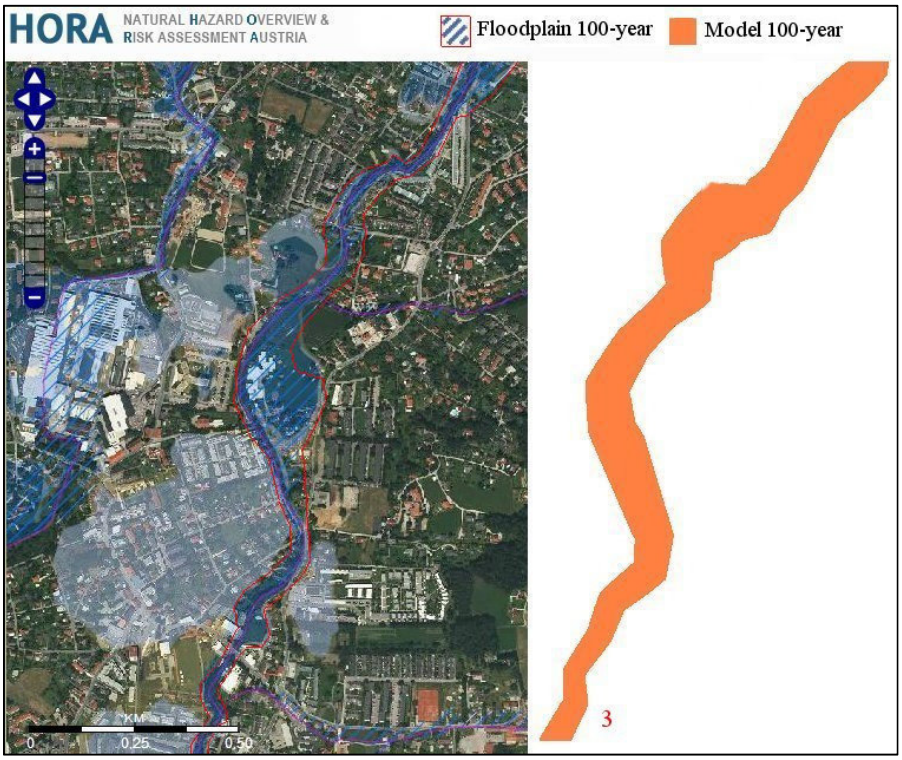


Figure A.3: A comparison between inundation area in Model and HORA (part 3, Fig. 6.14)

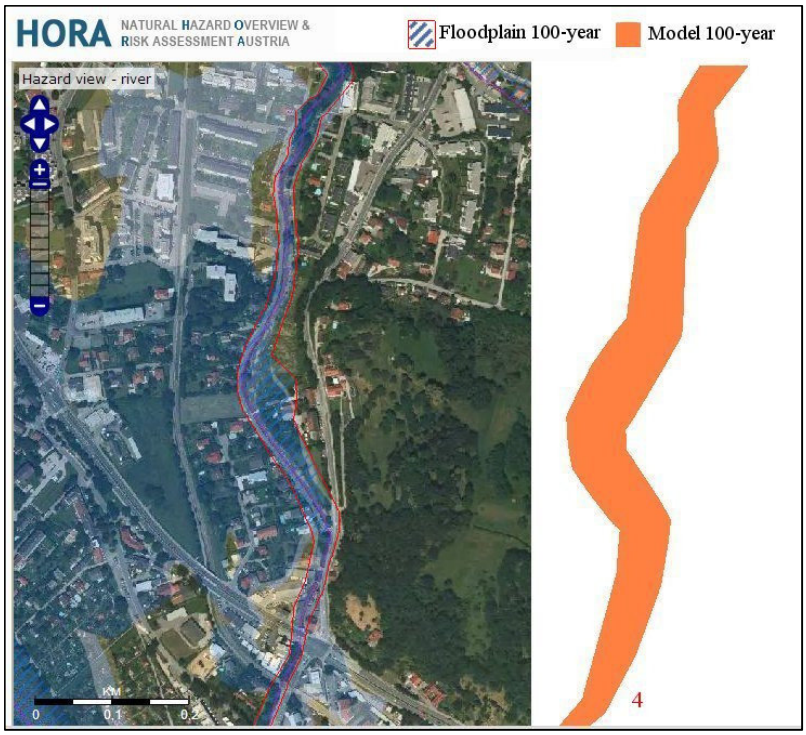


Figure A.4: A comparison between inundation area in Model and HORA (part 4, Fig. 6.14)

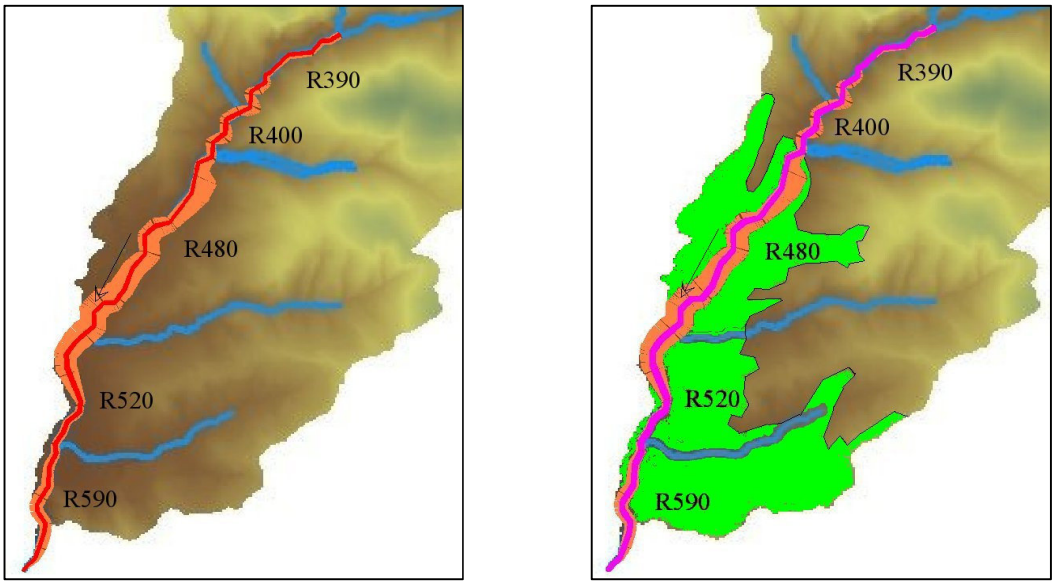


Figure A.5: Position of high flood risk river; left: river before installing levee, right: river after installing levee (green region: urban area)

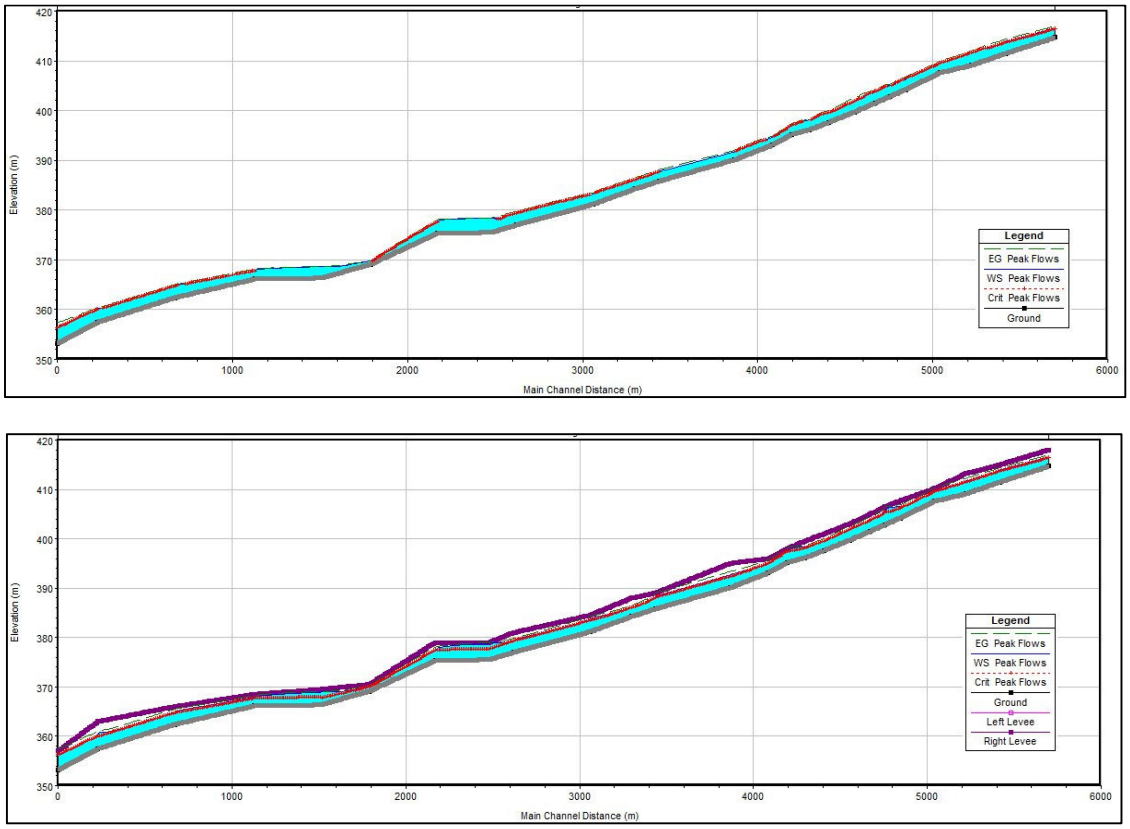


Figure A.6: Longitudinal profile of the river; top: before installing levee, bottom: after installing levee

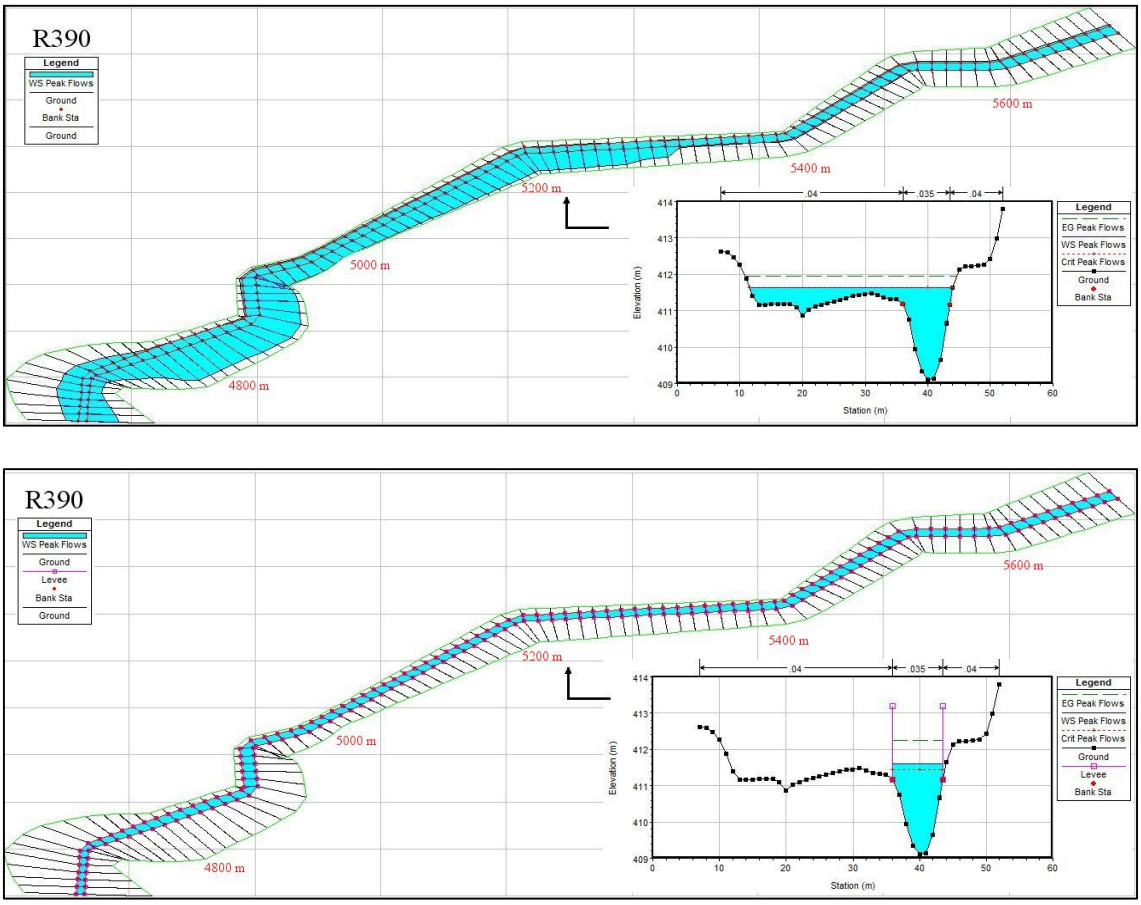


Figure A.7: Flood map for reach R390; top: before installing levee, bottom: after installing levee

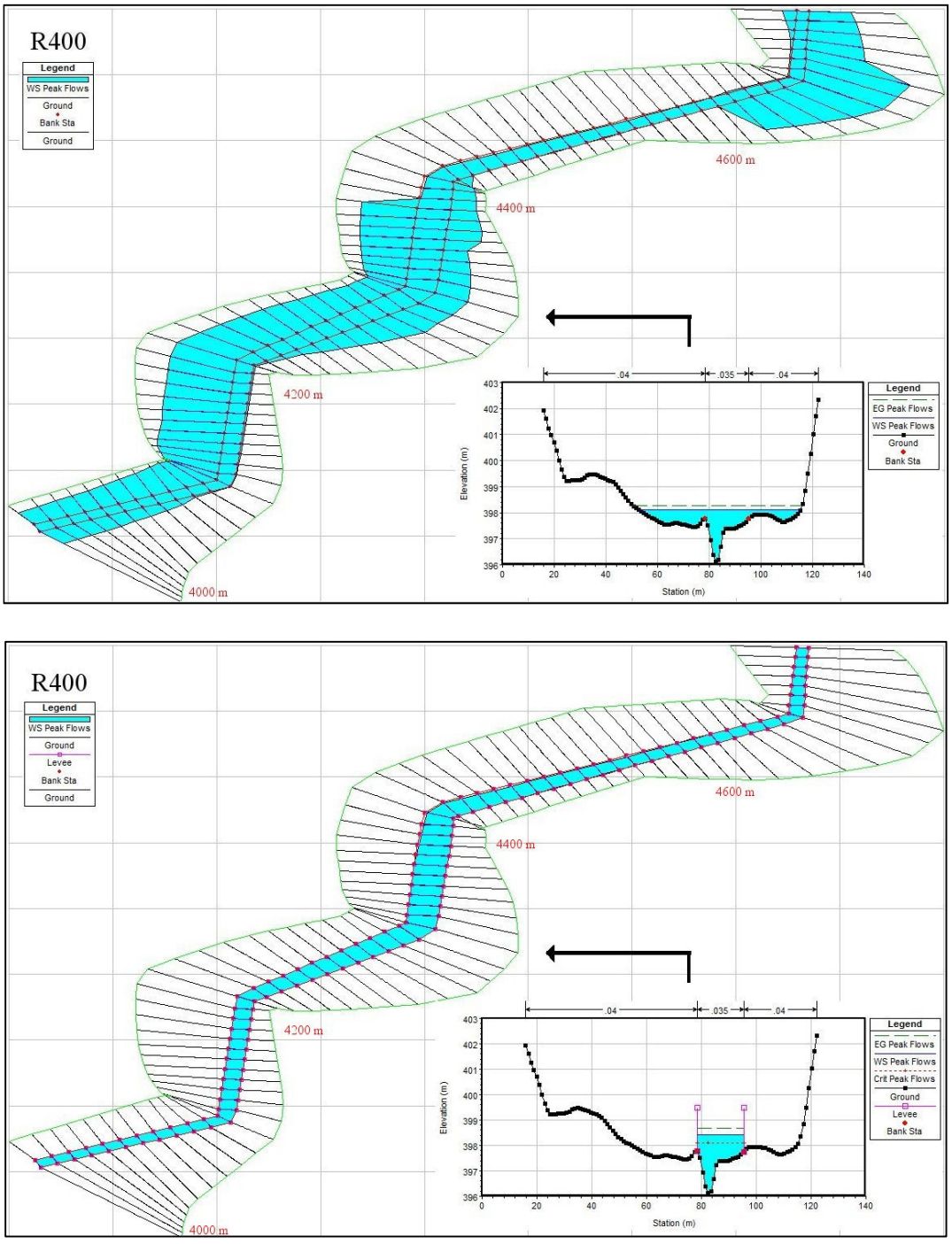


Figure A.8: Flood map for reach R400; top: before installing levee, bottom: after installing levee

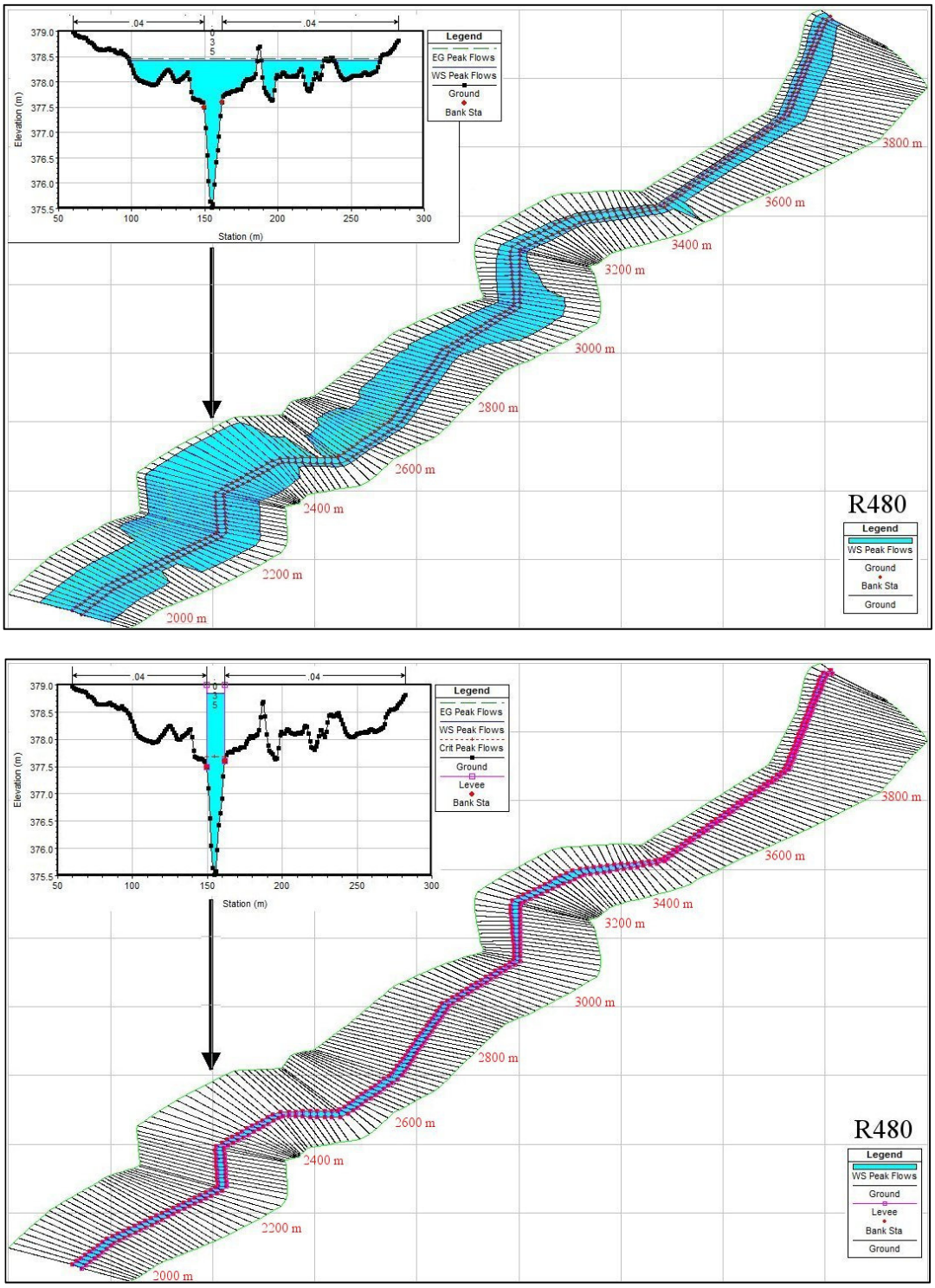


Figure A.9: Flood map for reach R480; top: before installing levee, bottom: after installing levee

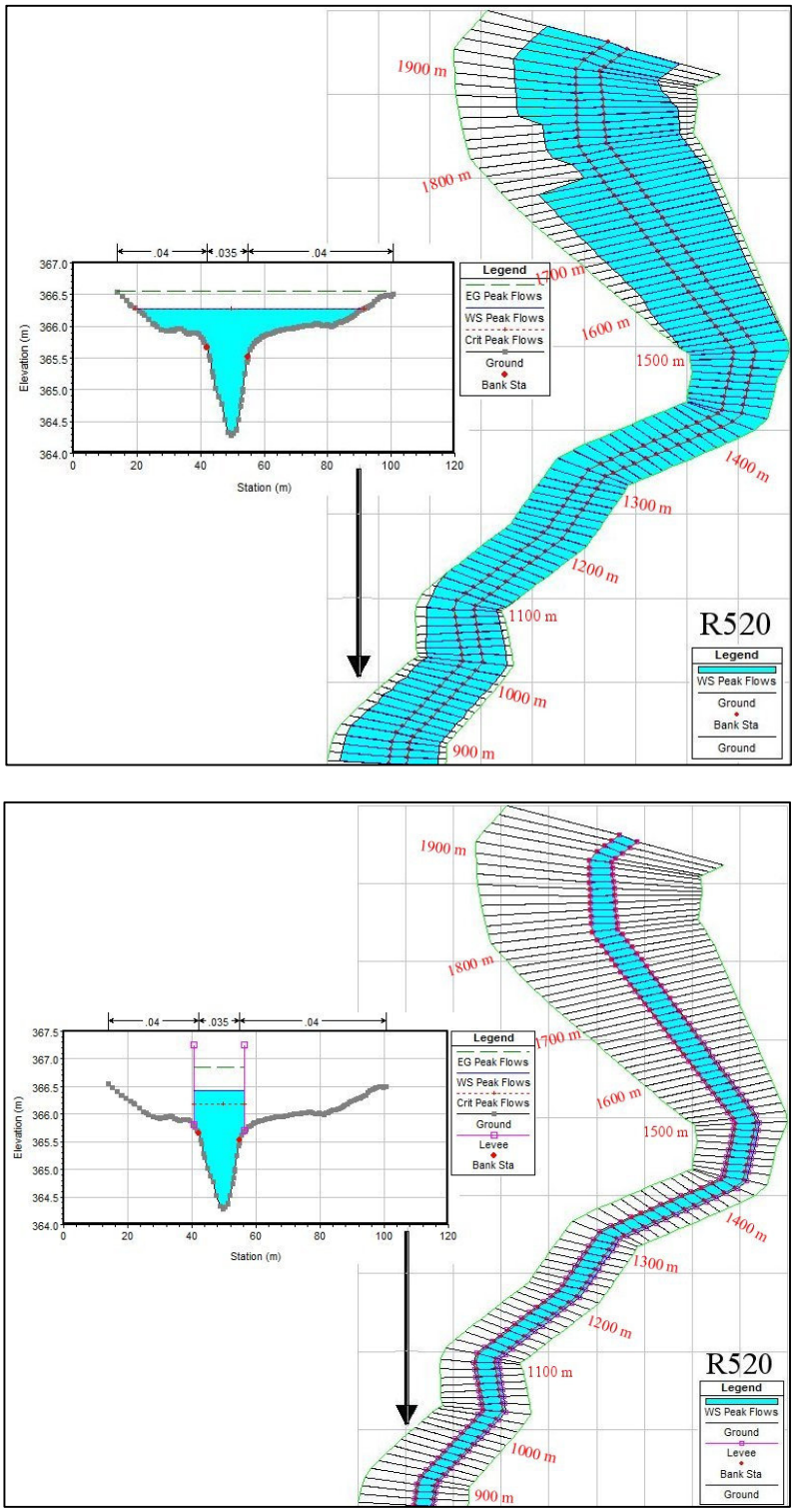


Figure A.10: Flood map for reach R520; top: before installing levee, bottom: after installing levee

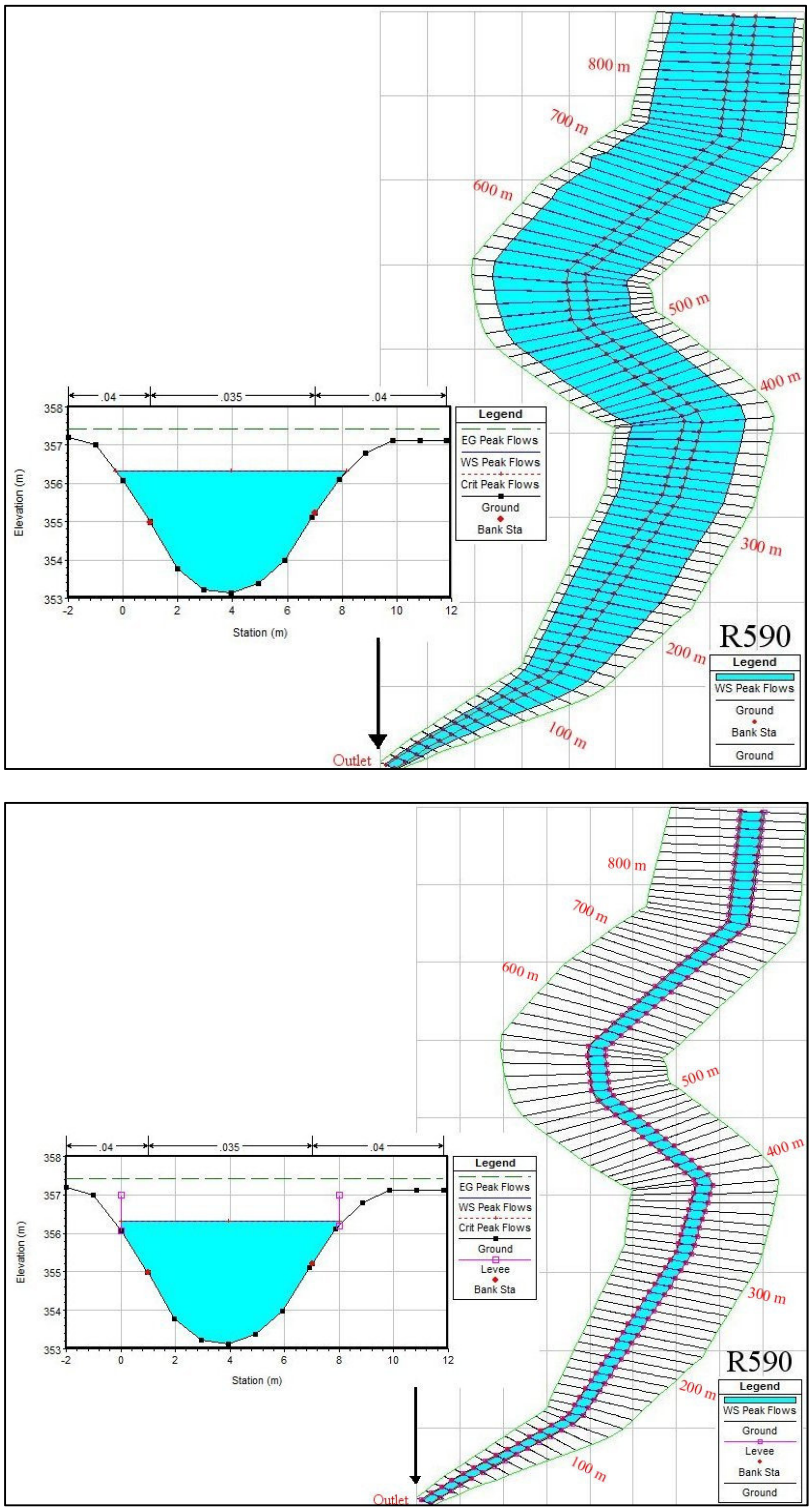


Figure A.11: Flood map for reach R590; top: before installing levee, bottom: after installing levee

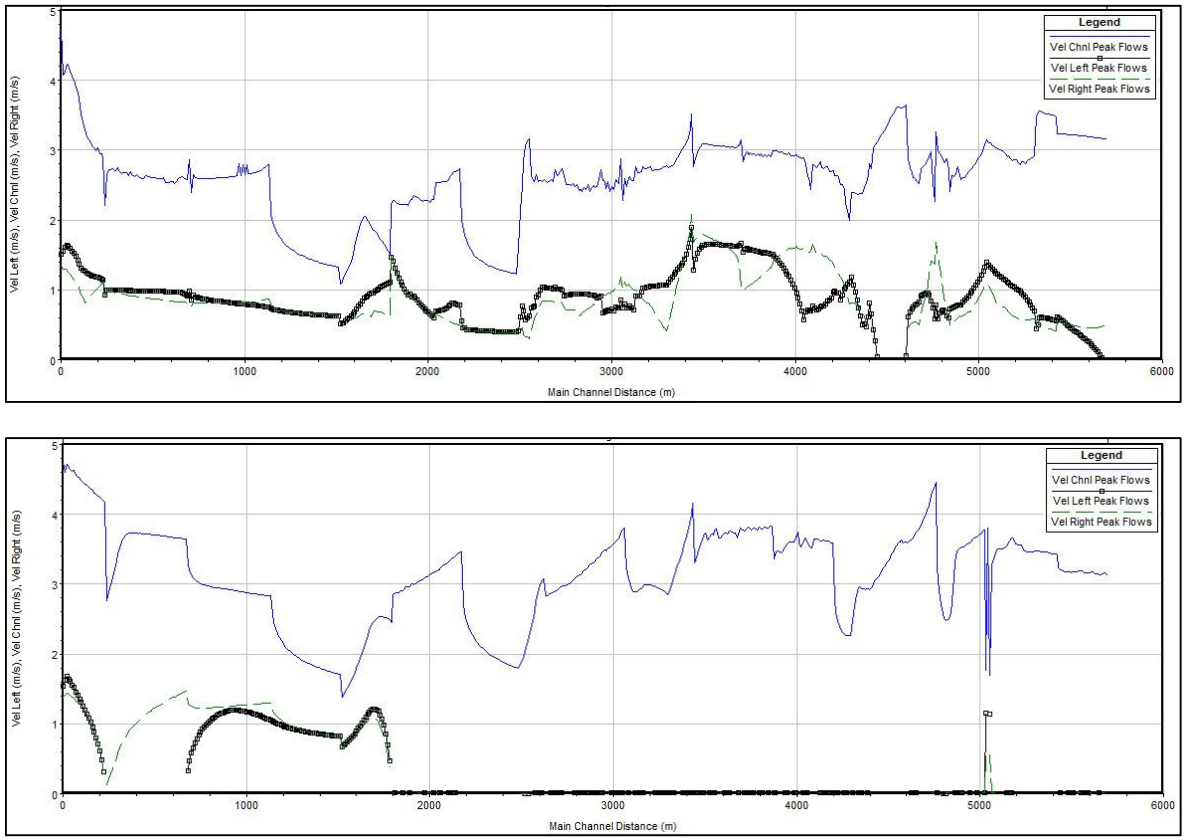


Figure A.12: Velocity variations in the river; top: river without levee, bottom: river with levee

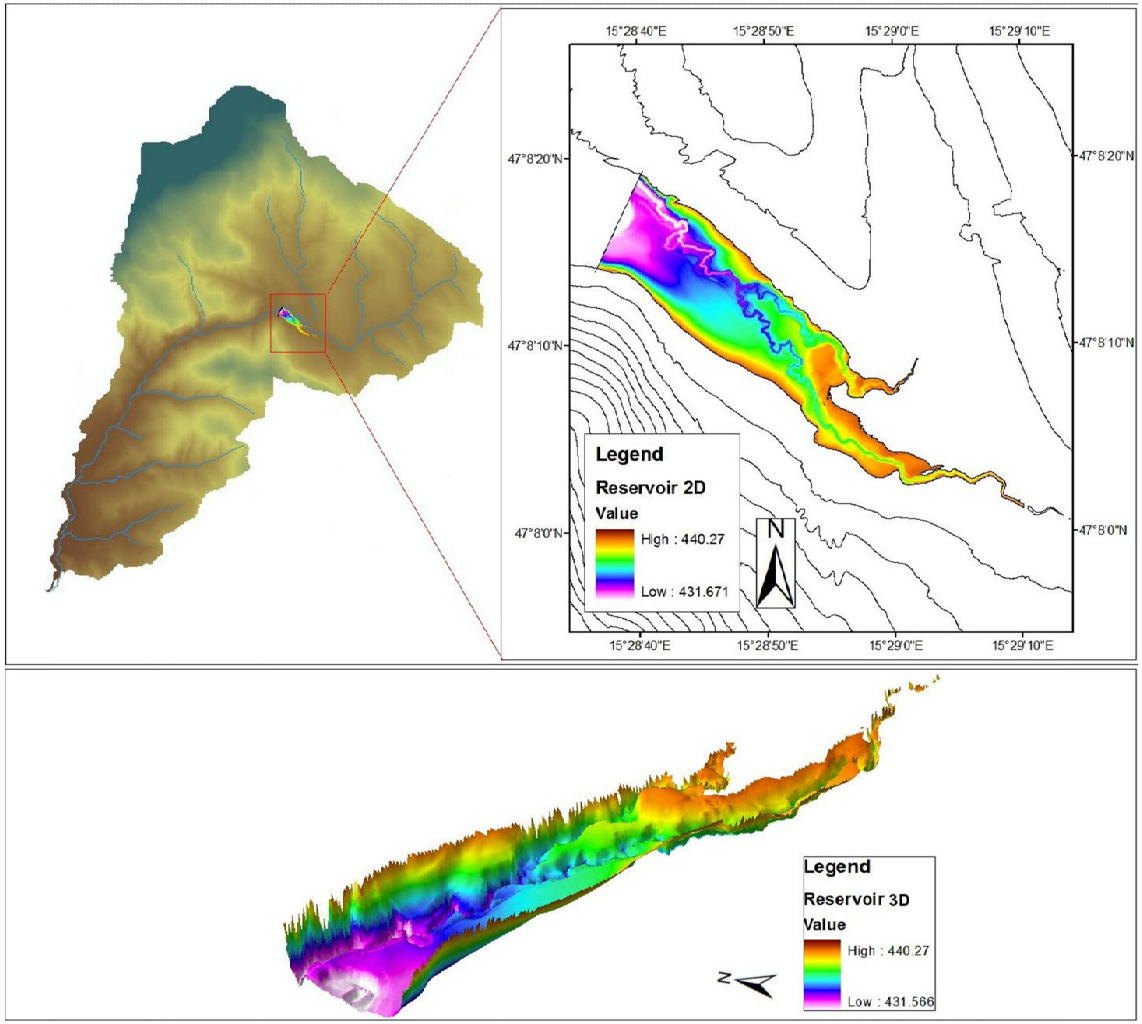


Figure A.13: The position of Weinitzen retention dam in the Schoeckelbach basin (2D and 3D views)

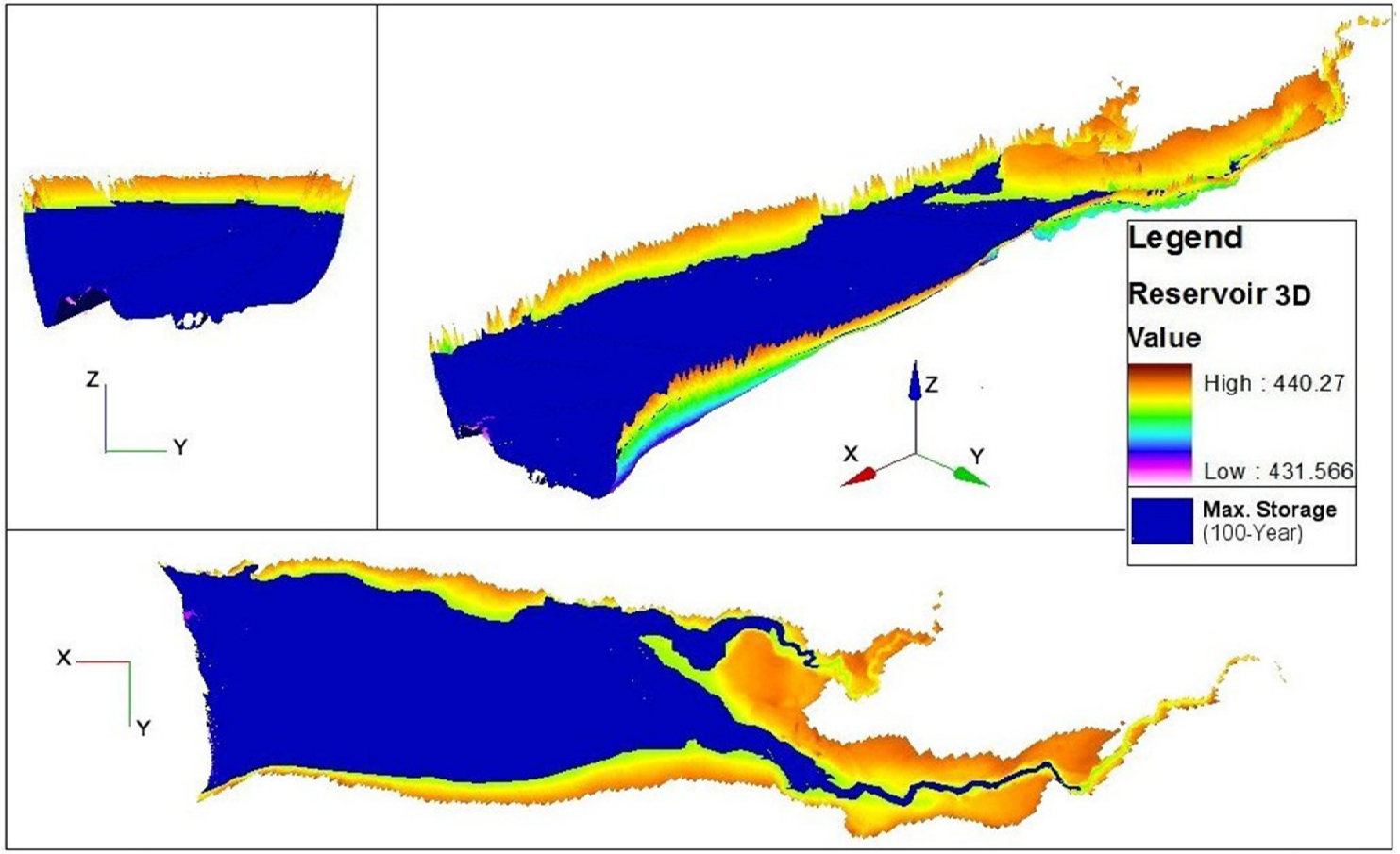


Figure A.14: Maximum storage for 100-year rainfall (2D and 3D views)

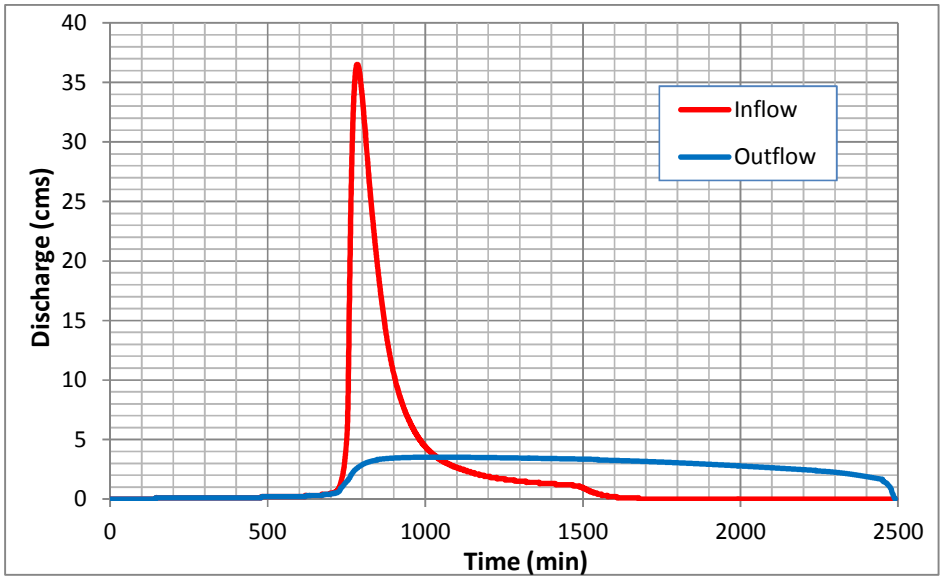


Figure A.15: Dam inflow and outflow, R=0.4 m, volume of storage=206,900 $m^3$

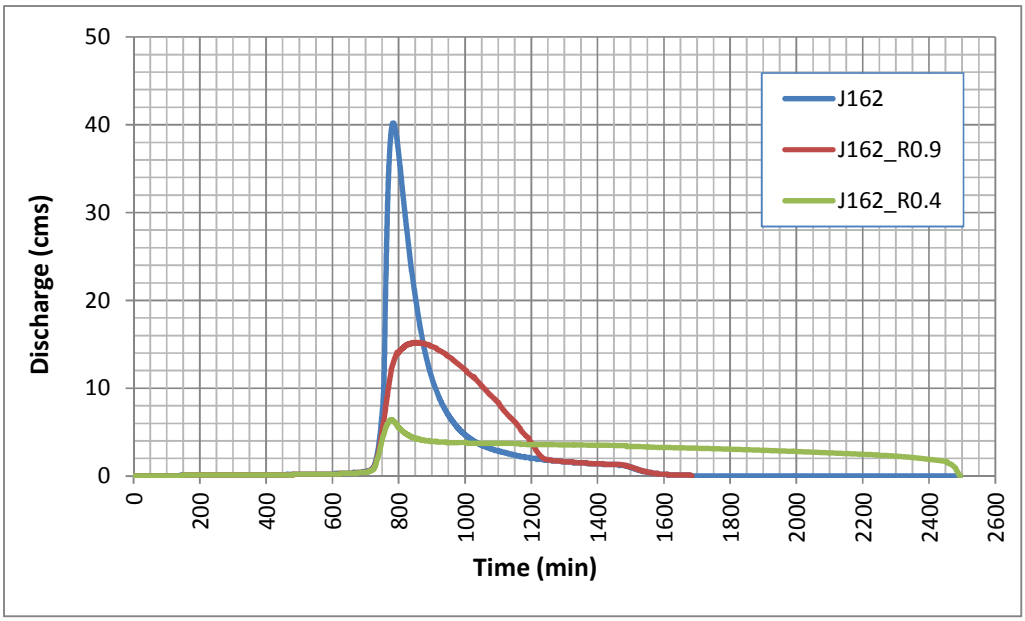


Figure A.16: The influence of the outlet pipe (diameter) on discharges in junction J162 (see Figure 6.7 for the position)

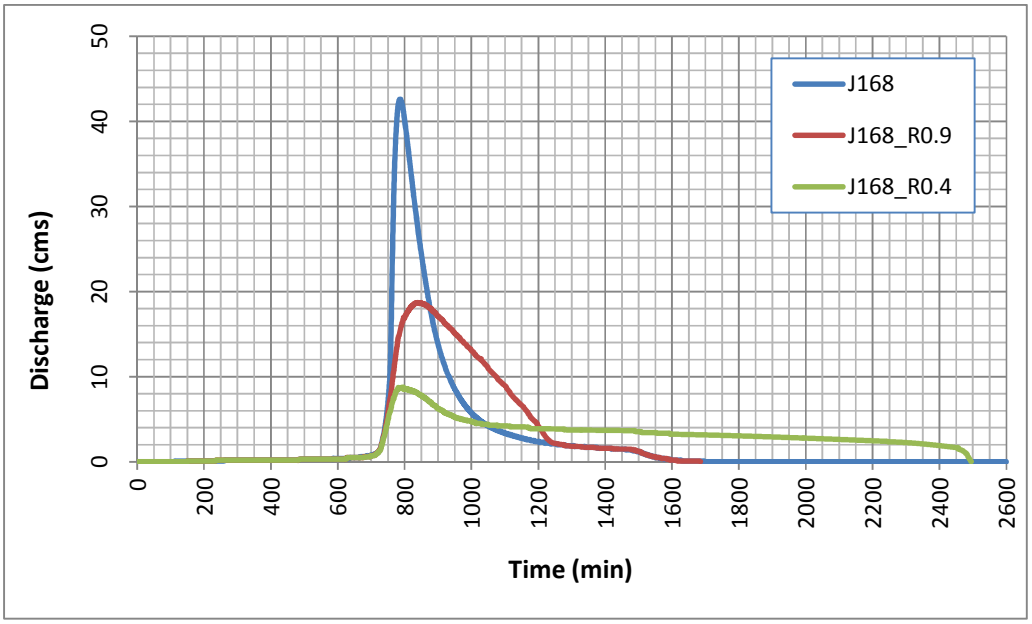


Figure A.17: The influence of the outlet pipe (diameter) on discharges in junction J168 (see Figure 6.7 for the position)

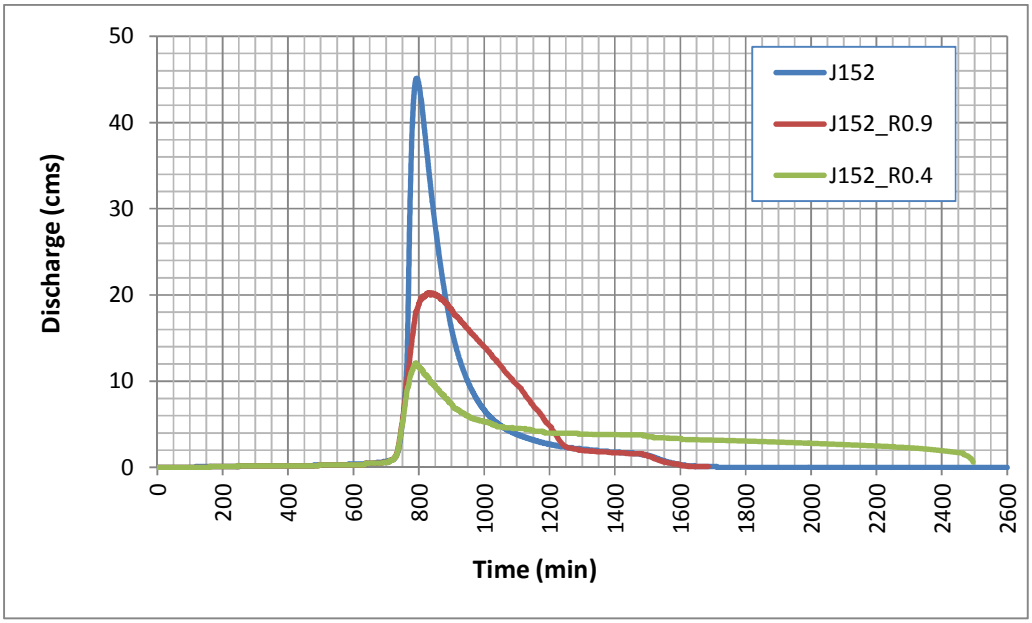


Figure A.18: The influence of the outlet pipe (diameter) on discharges in junction J152 (see Figure 6.7 for the position)

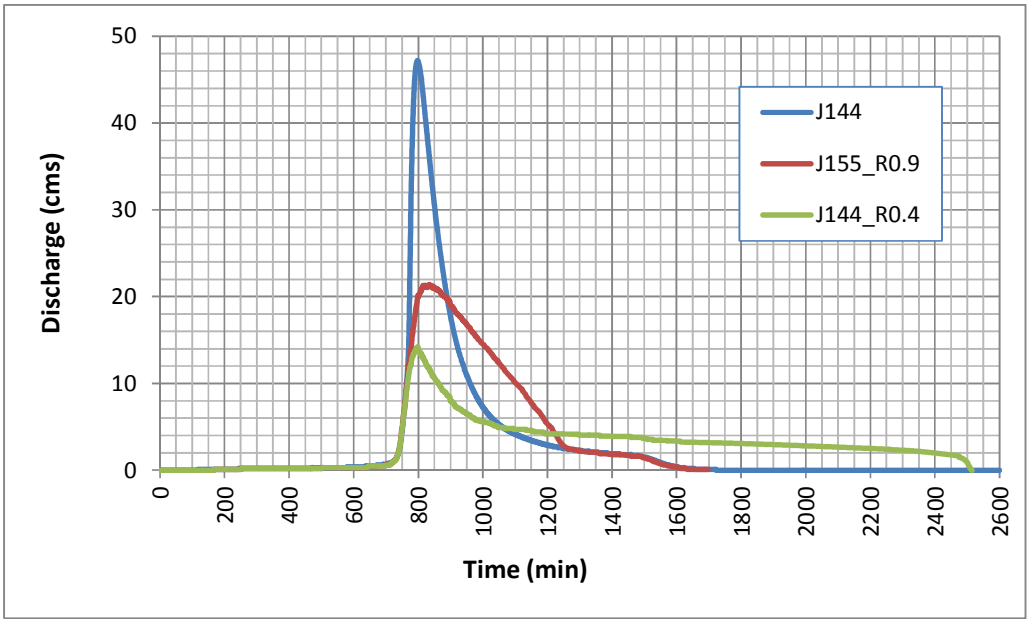


Figure A.19: The influence of the outlet pipe (diameter) on discharges in junction J144 (see Figure 6.7 for the position)

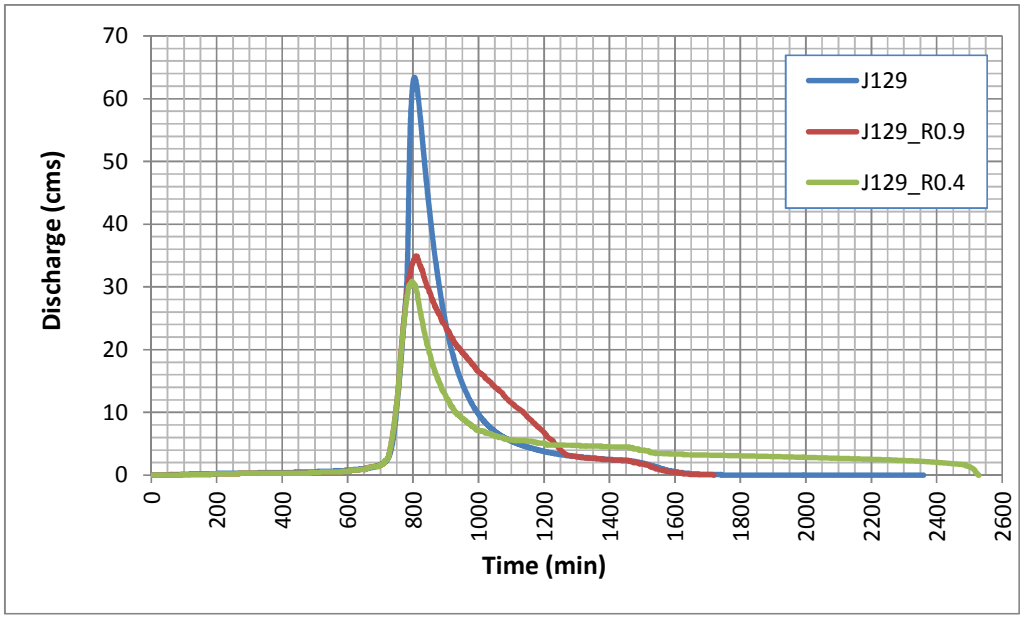


Figure A.20: The influence of the outlet pipe (diameter) on discharges in junction J129 (see Figure 6.7 for the position)

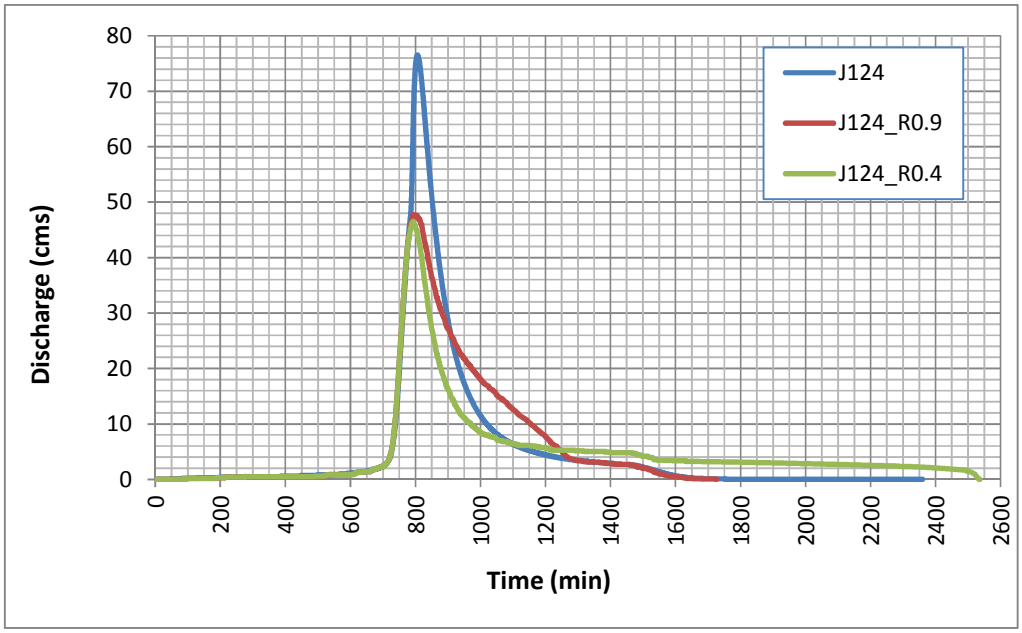


Figure A.21: The influence of the outlet pipe (diameter) on discharges in junction J124 (see Figure 6.7 for the position)

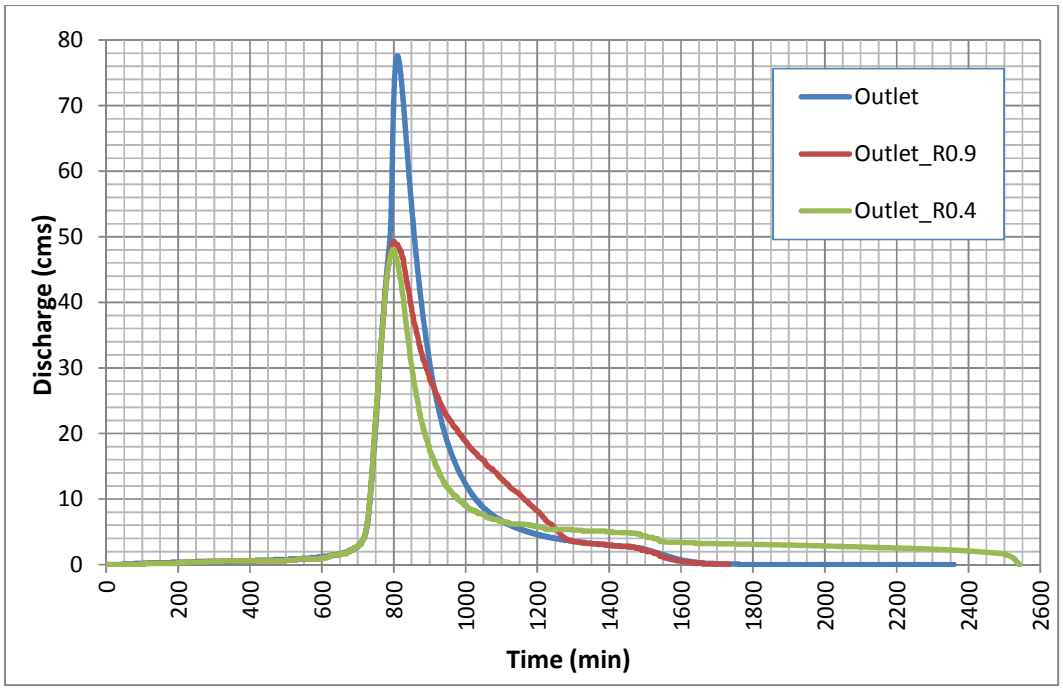


Figure A.22: The influence of the outlet pipe (diameter) on discharges in the outlet of the Schoeckelbach basin (see Figure 6.7 for the position)

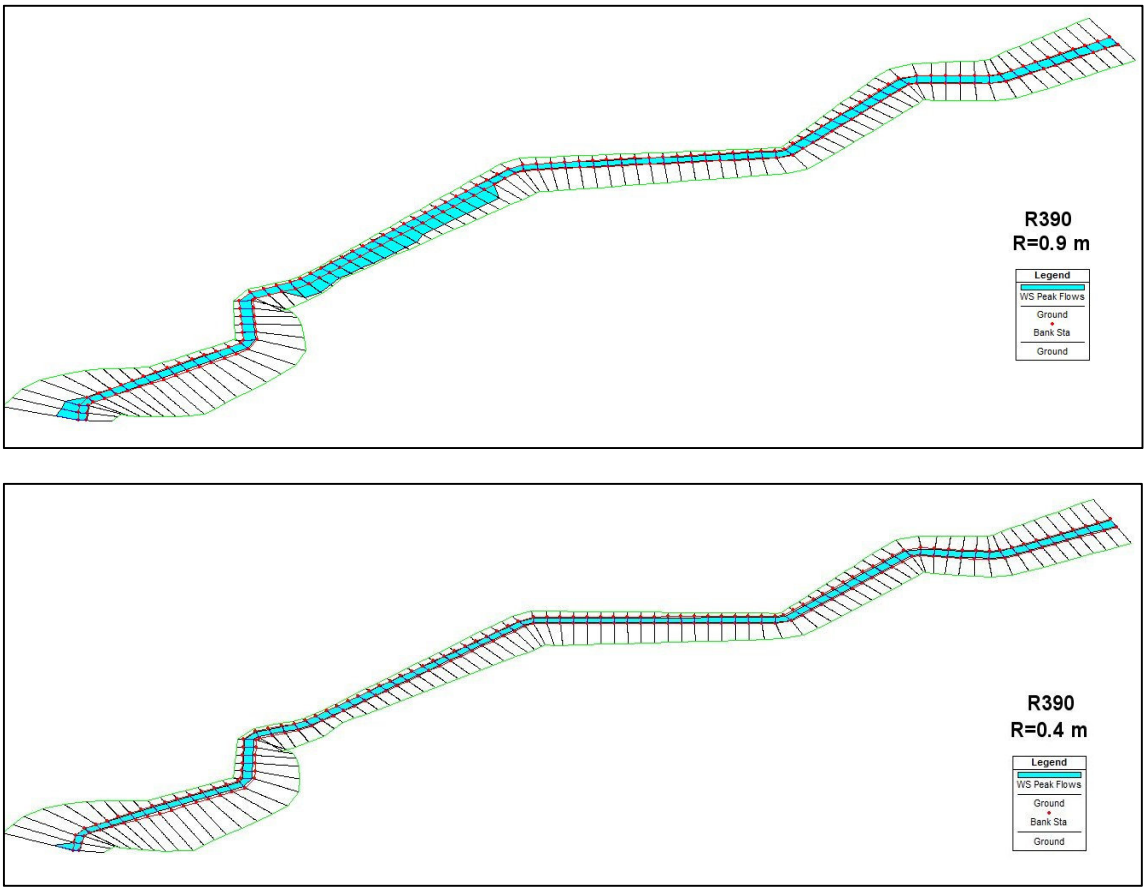


Figure A.23: The influence of the outlet pipe (diameter) on inundation area in the river R390, top: Radius=0.9 m and bottom: Radius=0.4 m (see Figure A.5 for the position)

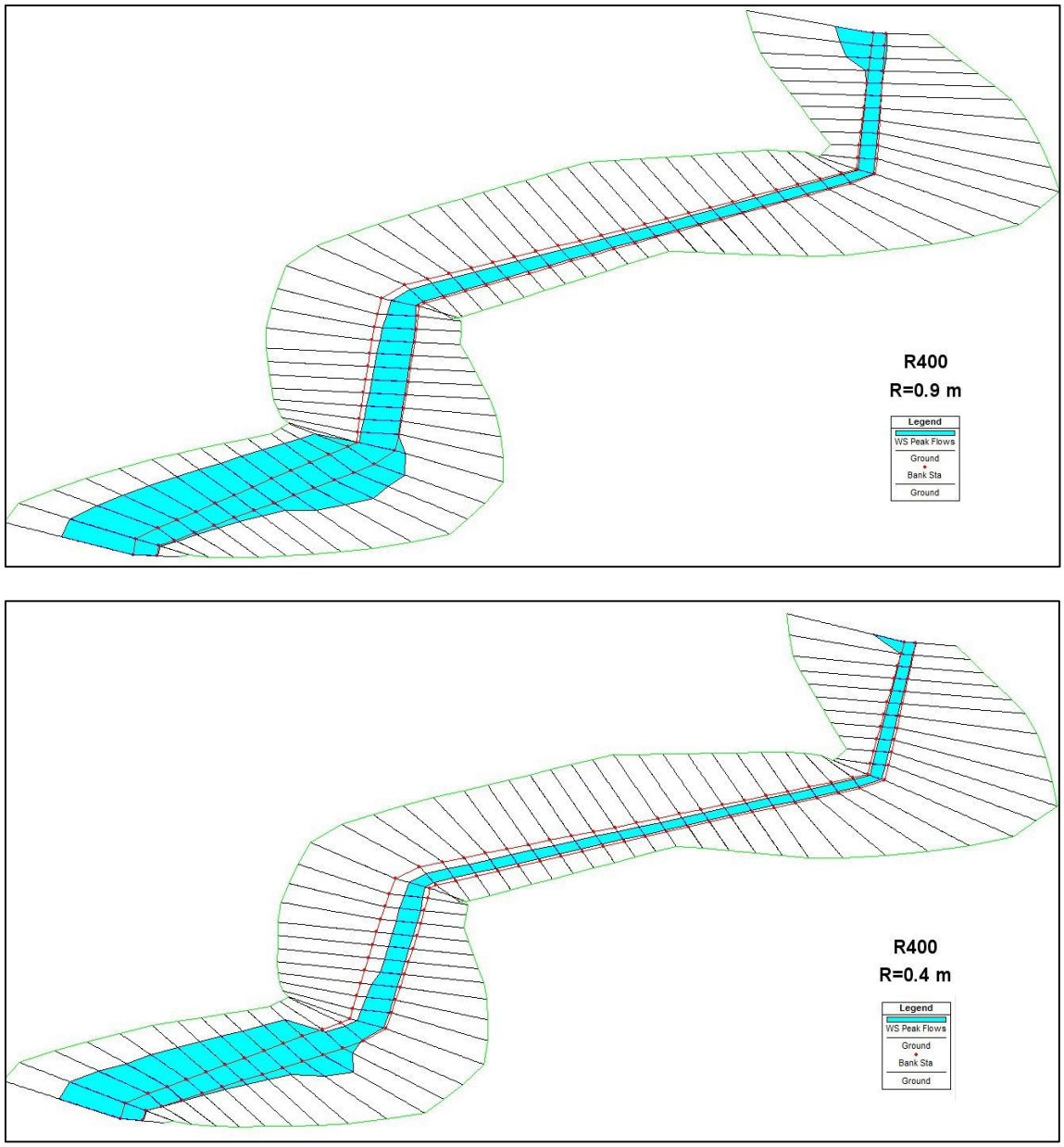


Figure A.24: The influence of the outlet pipe (diameter) on inundation area in the river R400, top: Radius=0.9 m and bottom: Radius=0.4 m (see Figure A.5 for the position)

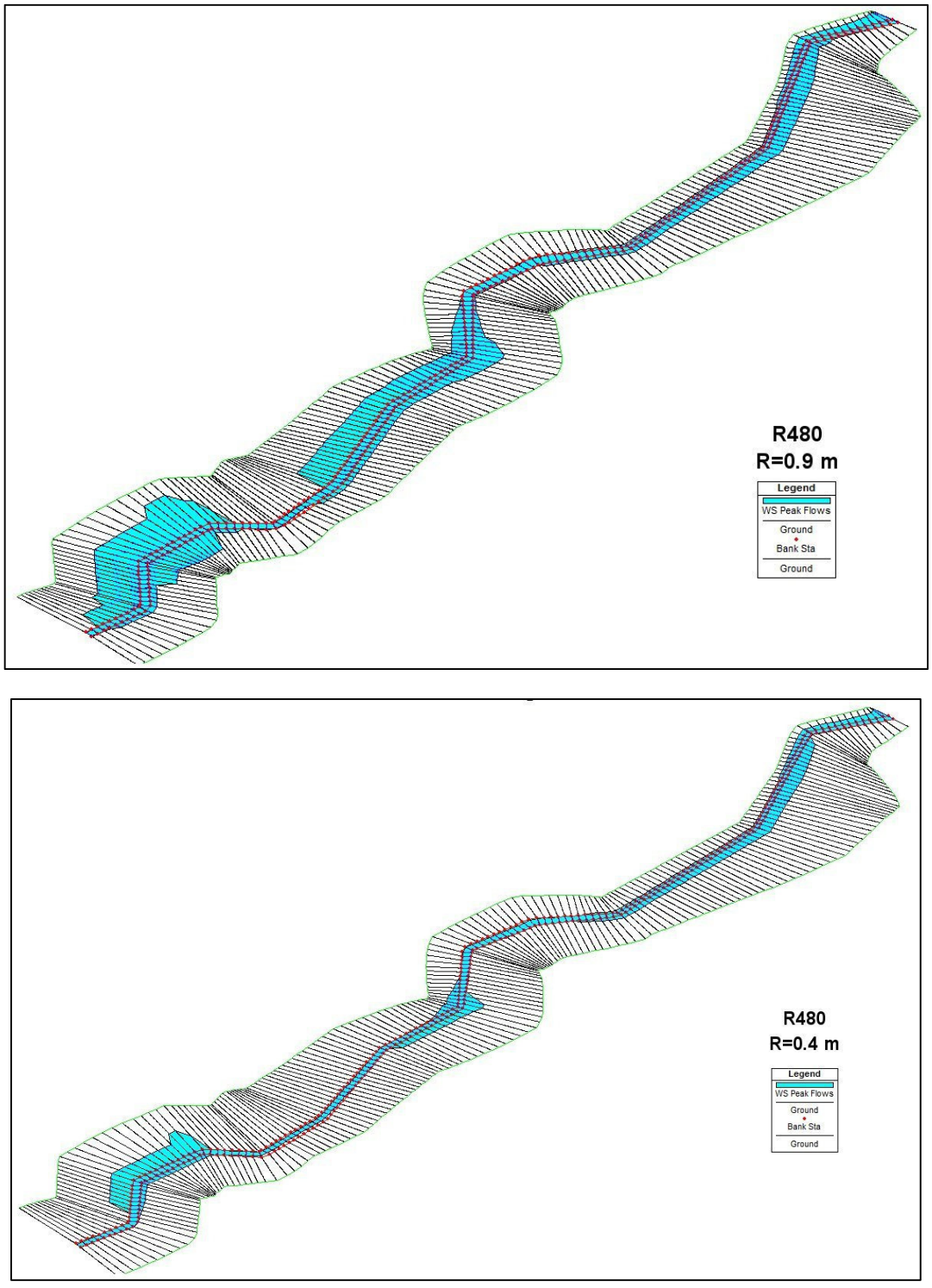


Figure A.25: The influence of the outlet pipe (diameter) on inundation area in the river R480, top: Radius=0.9 m and bottom: Radius=0.4 m (see Figure A.5 for the position)

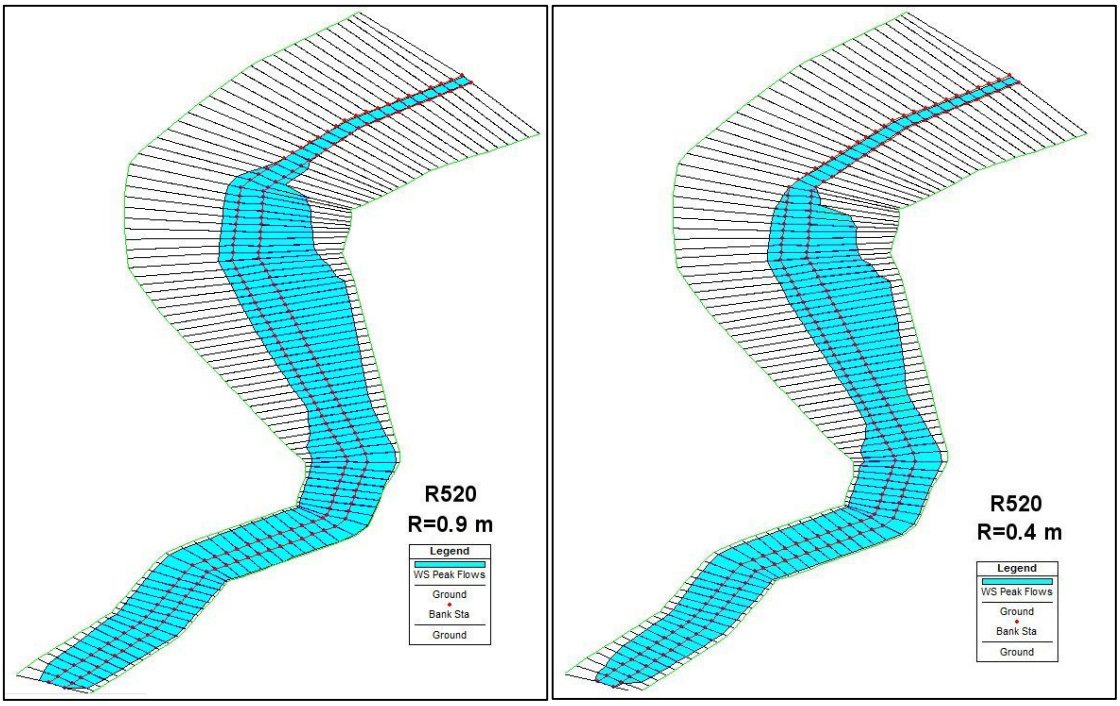


Figure A.26: The influence of the outlet pipe (diameter) on inundation area in the river R520, left: Radius=0.9 m and right: Radius=0.4 m (see Figure A.5 for the position)

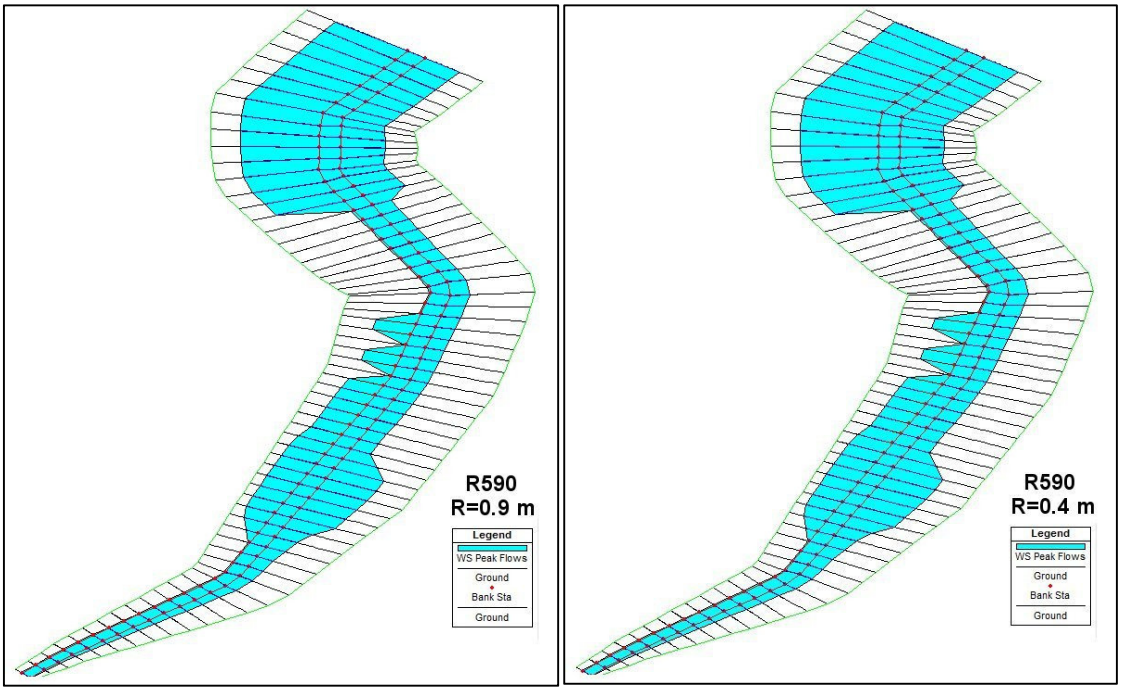


Figure A.27: The influence of the outlet pipe (diameter) on inundation area in the river R590, left: Radius=0.9 m and right: Radius=0.4 m (see Figure A.5 for the position)

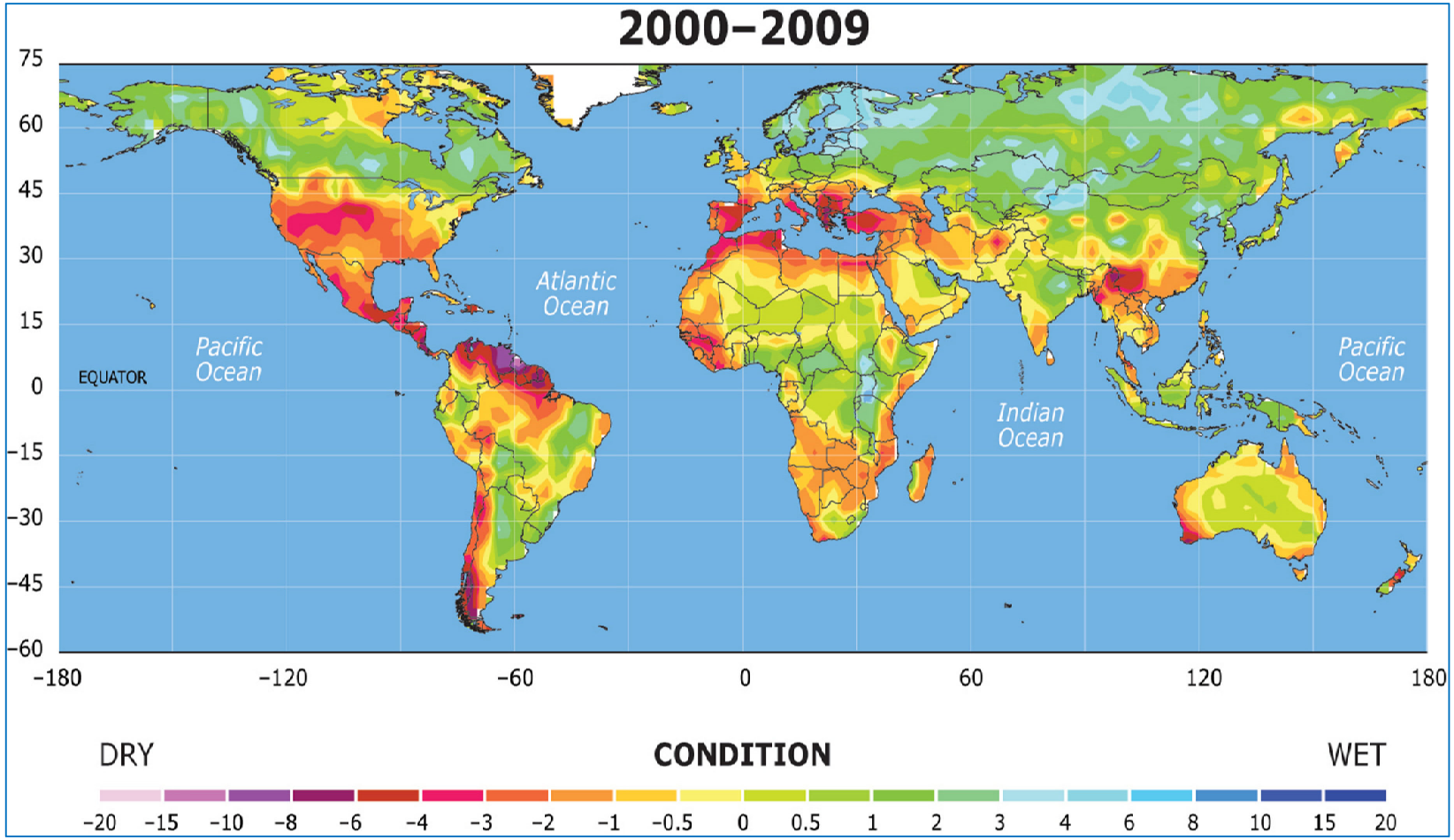


Figure A.28: The global drought changes (2000-2009)

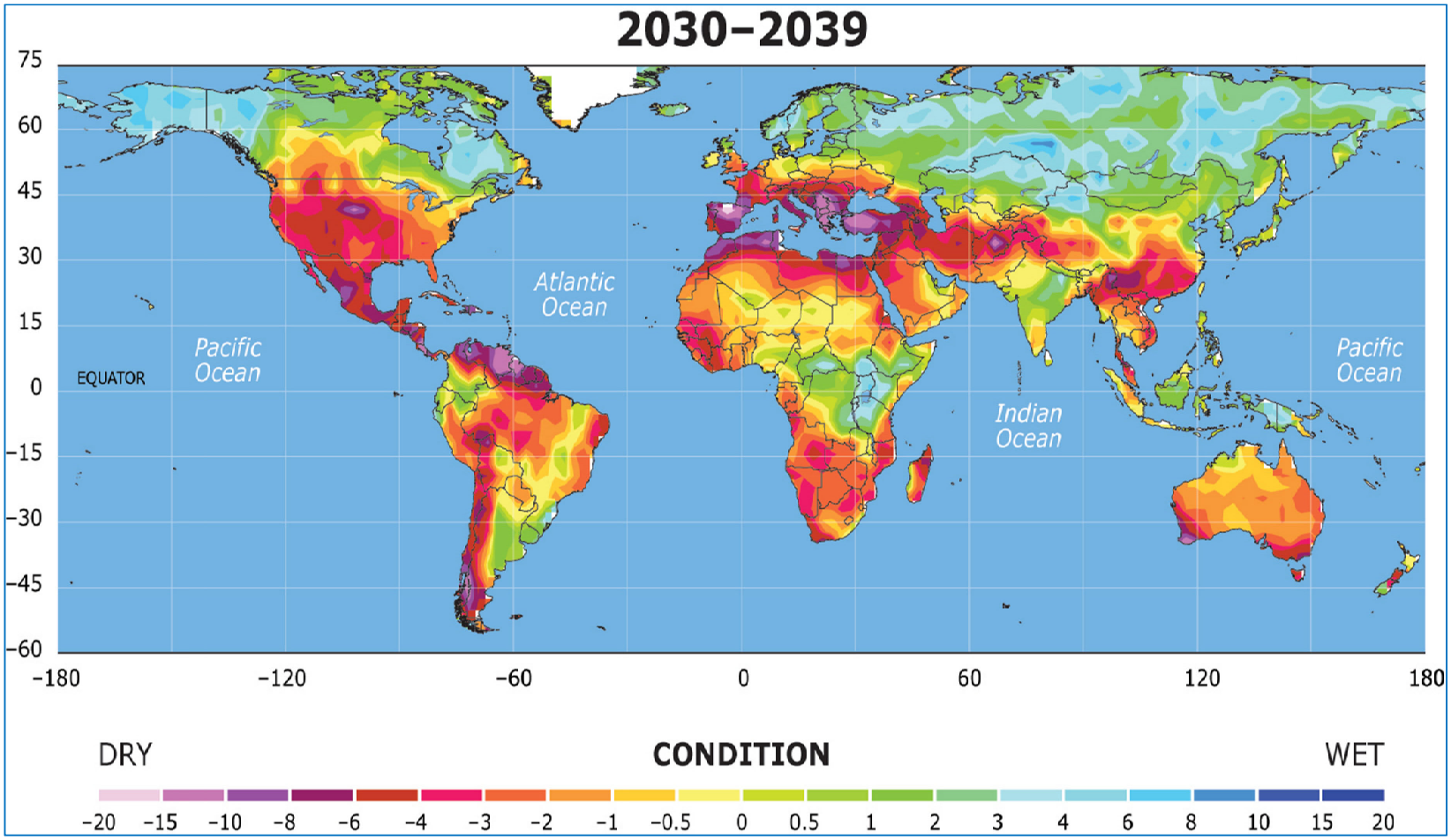


Figure A.29: The global drought changes (2030-2039)

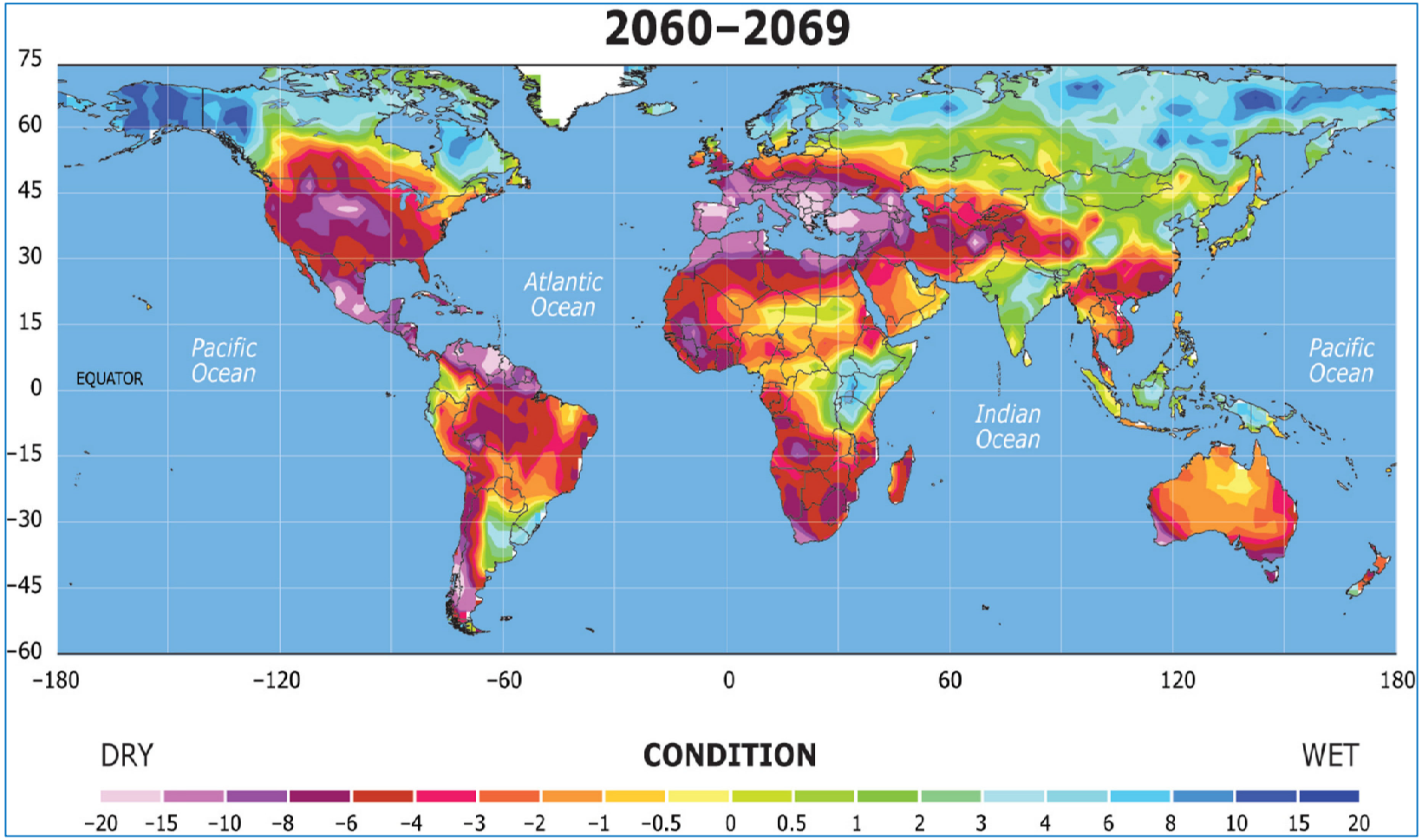


Figure A.30: The global drought changes (2060-2069)

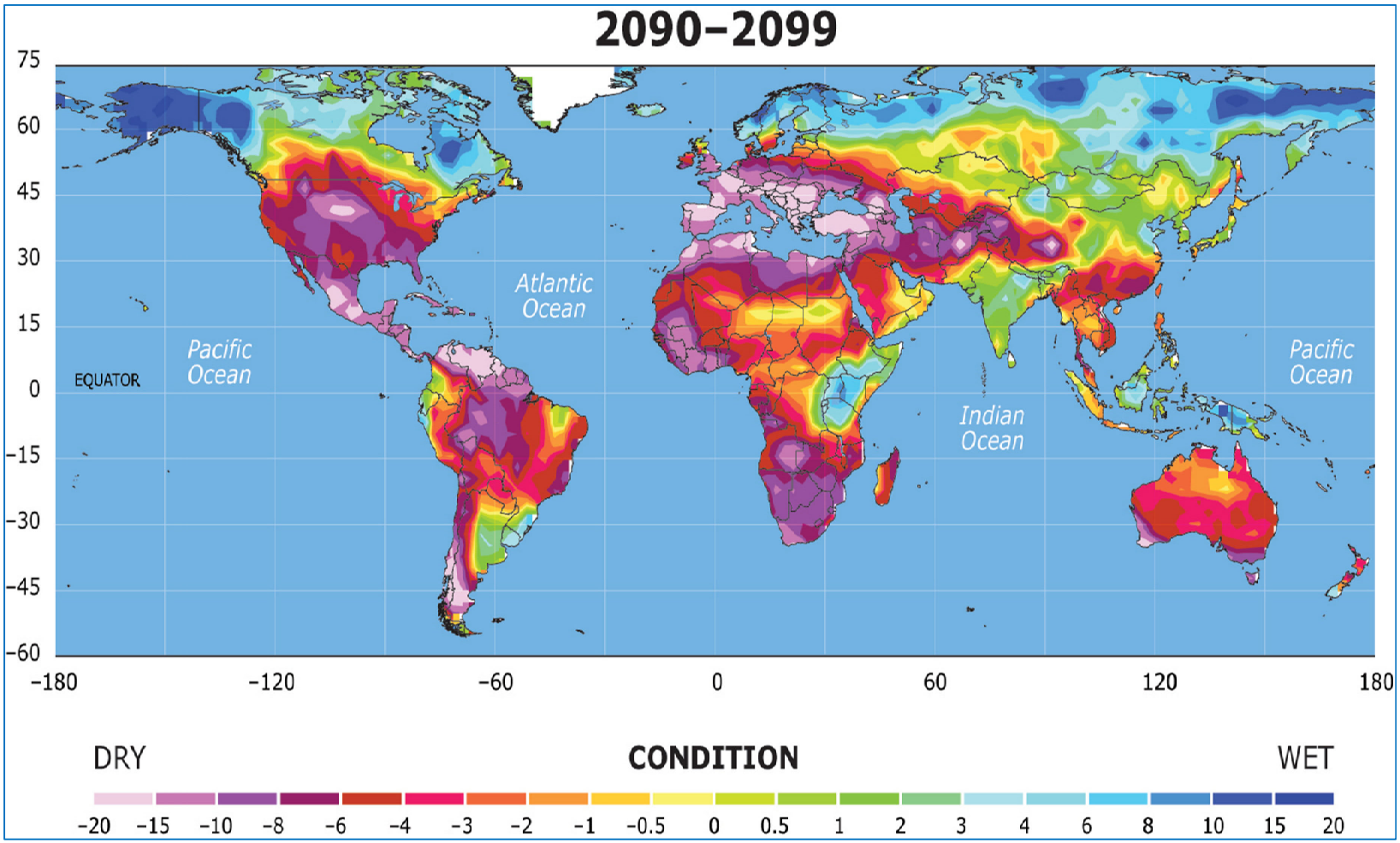


Figure A.31: The global drought changes (2090-2099)

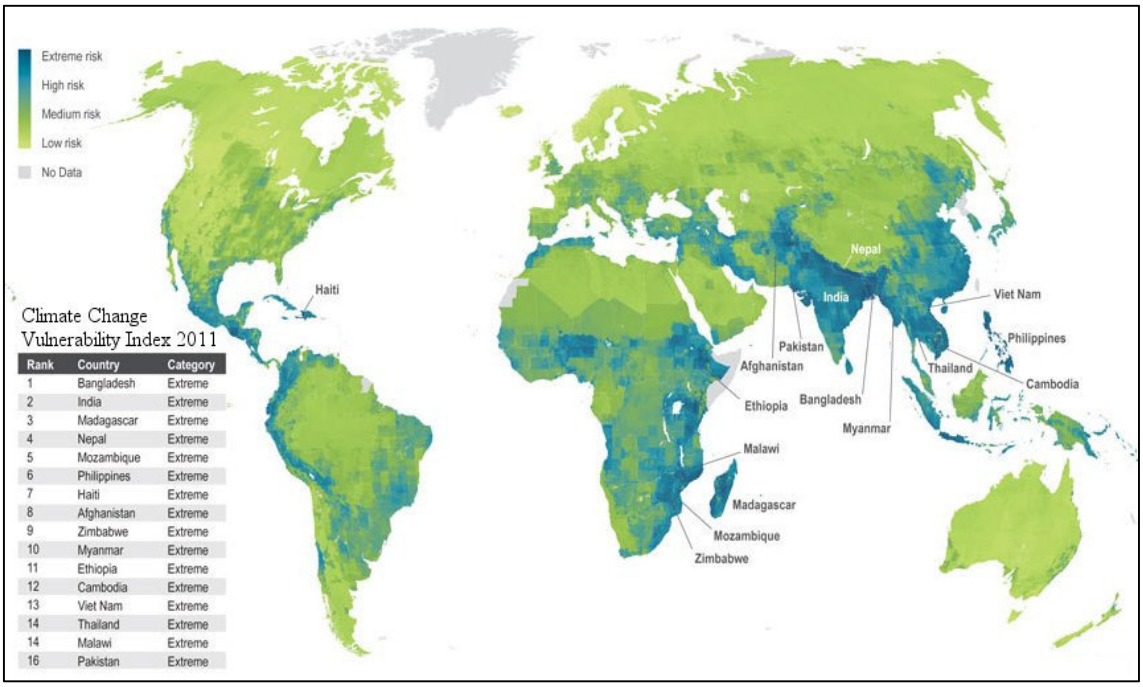


| Rank | Country | Category |
|---|---|---|
| 1 | Bangladesh | Extreme |
| 2 | India | Extreme |
| 3 | Madagascar | Extreme |
| 4 | Nepal | Extreme |
| 5 | Mozambique | Extreme |
| 6 | Philippines | Extreme |
| 7 | Haiti | Extreme |
| 8 | Afghanistan | Extreme |
| 9 | Zimbabwe | Extreme |
| 10 | Myanmar | Extreme |
| 11 | Ethiopia | Extreme |
| 12 | Cambodia | Extreme |
| 13 | Viet Nam | Extreme |
| 14 | Thailand | Extreme |
| 14 | Malawi | Extreme |
| 16 | Pakistan | Extreme |

Figure A.32: Climate change vulnerability index 2011 (www.maplecroft.com)

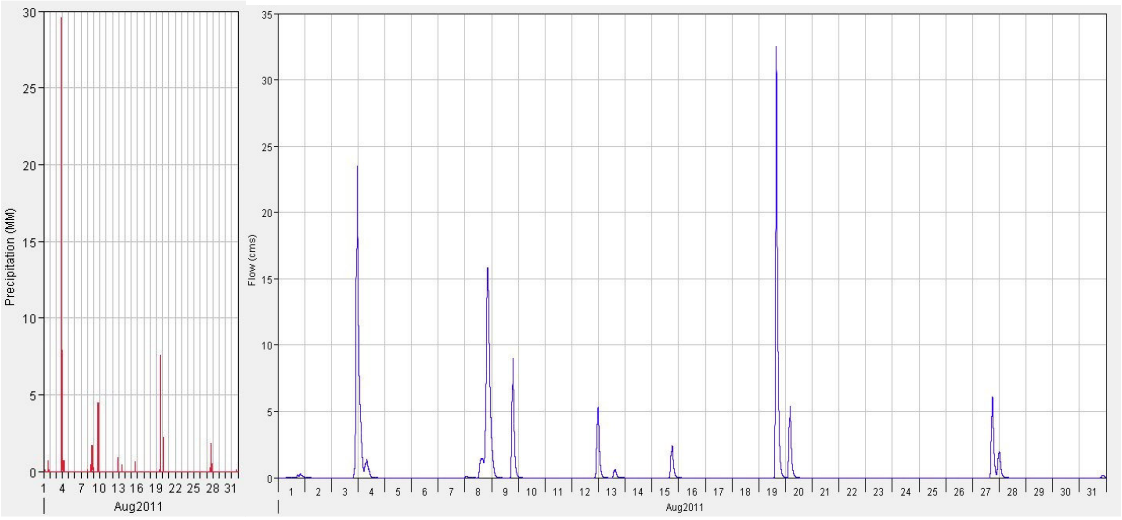


Figure A.33: Continuous simulation (Aug 2011)

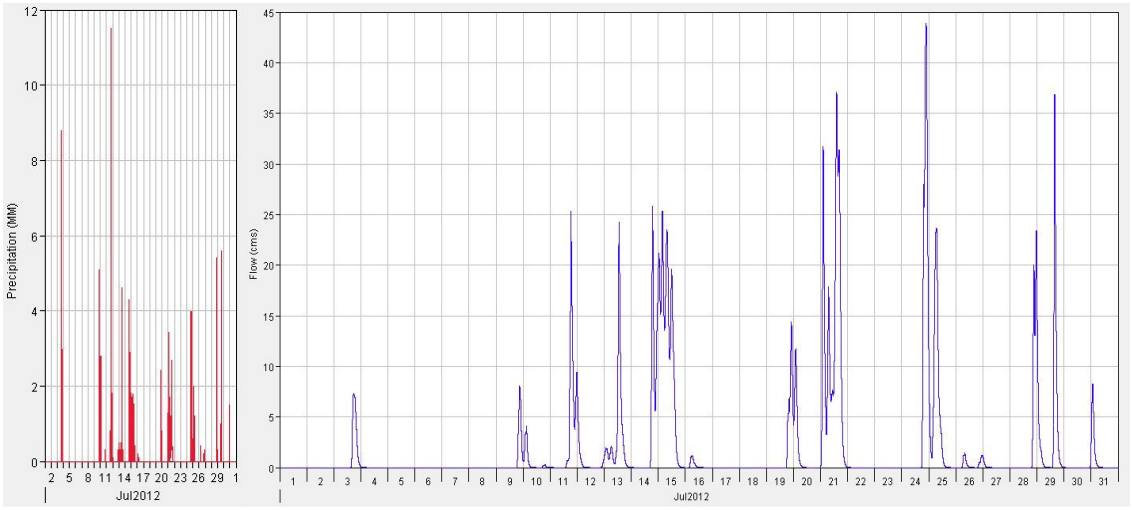


Figure A.34: Continuous simulation (Jul 2012)

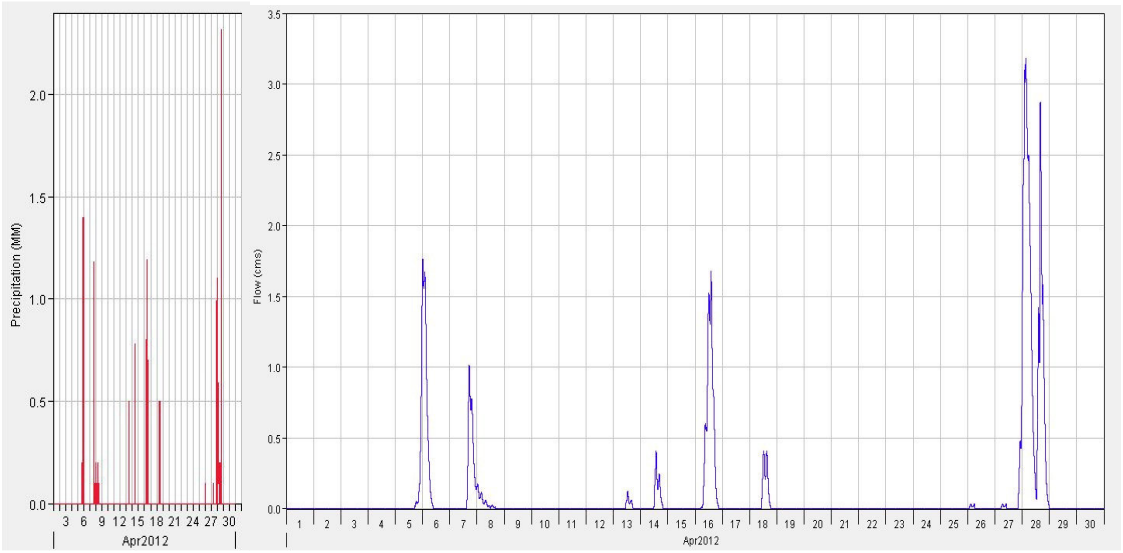


Figure A.35: Continuous simulation (Apr 2012)

# Appendix B

**NOTE:** In this Appendix, some methods which were used in this thesis are presented. These methods can be found in more details in many hydrology textbooks. For more information in this section, each of these methods is cited to a suitable reference which the method can be found there.

## B.1 Time of concentration (Development Process Manual, 2009)

1. For basins with flow path lengths less than 4,000 feet (SCS Upland method):

$$T_c = \frac{2}{3}\sum_{i=1}^{n}\left(\frac{L_i}{36000K_i\sqrt{S_i}}\right) \quad \text{(B-1)}$$

Where:

$T_c$ = Time of concentration in hours

$L_i$ = Length of each unique surface flow conveyance condition in feet

$K_i$ = Conveyance factor (table B.1)

$S_i$ = Slope of the flow path in feet per foot

Table B.1: Conveyance factors (DPM, 2009)

| **K** | **Conveyance condition** |
|---|---|
| 0.7 | Turf, landscaped areas and undisturbed natural areas (sheet flow only). |
| 1 | Bare or disturbed soil areas and paved areas (sheet flow only). |
| 2 | Shallow concentrated flow (paved or unpaved). |
| 3 | Street flow, storm sewers and natural channels, and that portion of sub-basins (without constructed channels) below the upper 2000 feet for sub-basins longer than 2000 feet. |
| 4 | Constructed channels (for example: riprap, soil cement or concrete lined channels). |
| **Remark:** Sheet flow is flow over plane surfaces, with flow depths up to 0.1 feet. Sheet flow applies only to the upper 400 feet (maximum) of a sub-basin. | |

**2.** For basins with flow path lengths greater than 12,000 feet (basin lag equation):

$$T_c = \frac{8}{9} \times 26K_n \left( \frac{L \times L_{ca}}{5280^2 \times \sqrt{5280 \times S}} \right)^{\frac{1}{3}} \quad \text{(B-2)}$$

Where:

$T_c$ = Time of concentration in hours

L = Flow path length in feet

$L_{ca}$ = Distance along L from point of concentration to a point opposite the centroid of the basin in feet

$K_n$ = Basin factor (table B.2)

S = Slope of flow path in feet per foot

Table B.2: Basin factors (DPM, 2009)

| **$K_n$** | **Basin condition** |
|---|---|
| 0.042 | Mountain Brush and Juniper |
| 0.033 | Desert Terrain (Desert Brush) |
| 0.025 | Low Density Urban (Minimum improvements to watershed channels) |
| 0.021 | Medium Density Urban (Flow in streets, storm sewers and improved channels) |
| 0.016 | High Density Urban (Concrete and rip-rap lined channels) |
| **Remark:** $K_n$ in Equation (B-2) is a measure of the hydraulic efficiency of the watershed to convey runoff to the basin outlet. This is analogous to a Manning's roughness coefficient. Selection of $K_n$ should reflect the conditions of the entire watercourse in the basin that convey runoff to the outlet. | |

**3.** For basins with flow path lengths between 4,000 and 12,000 feet (a composite of equations B-1 and B-2):

$$T_c = \frac{2}{3} \times \left( \frac{12000 - L}{72000K\sqrt{S}} + \frac{(L - 400)K_n \left(\frac{L_{ca}}{L}\right)^{\frac{1}{3}}}{552.2 \times S^{0.165}} \right) \quad \text{(B-3)}$$

Where:

$T_c$ = Time of concentration in hours

L = Flow path length in feet

$L_{ca}$ = Distance along L from point of concentration to a point opposite the centroid of the basin in feet

K = Conveyance factor (table B.1)

$K_n$ = Basin factor (table B.2)

S = Slope of flow path in feet per foot

## B.2 Flow routing

### B.2.1 Muskingum method (Raghunath, 2006)

The Muskingum channel routing method is based on two equations. The first is the continuity equation:

$$\frac{(I_1 + I_2)}{2}\Delta t - \frac{(O_1 + O_2)}{2}\Delta t = S_2 - S_1 \quad \text{(B-4)}$$

where:

$I_1$ and $I_2$ are inflow discharges at time 1 and time 2 ($m^3/s$)

$O_1$ and $O_2$ are outflow discharges at time 1 and time 2 ($m^3/s$)

$\Delta t$ = time difference between time 1 and time 2 (sec)

$S_1$ and $S_2$ are values of reach storage at time 1 and time 2 ($m^3$)

The second equation is a relationship of storage, inflow, and outflow of the reach:

$$\mathrm{S} = \mathrm{K}[\mathrm{xI} + (1 - \mathrm{x})\mathrm{O}] \quad \text{(B-5)}$$

K is storage constant which has the dimension of time and x is a dimensionless constant. An approximation for K is the travel time along the reach. The value of x is between 0.0 (maximum attenuation) and 0.5 (minimum attenuation). In natural rivers x is often between 0.1 and 0.3. In order to estimate these coefficients, first a value is assumed for x and 'S vs. [xI + (1 – x) O]' are plotted. If the plot is a stright line then the slope of the line gives K, otherwise another value for x is assumed and the procedure is continued untill the plot become to a stright line. Combining equations (B-4) and (B-5) and simplifying results:

$$\mathrm{O}_2 = \mathrm{C}_1\mathrm{I}_2 + \mathrm{C}_2\mathrm{I}_1 + \mathrm{C}_3\mathrm{I}_1 \quad \text{(B-6)}$$

Where:

$$\mathrm{C}_1 = \frac{0.5\Delta\mathrm{t} - \mathrm{Kx}}{\mathrm{K} - \mathrm{Kx} + 0.5\Delta\mathrm{t}} \quad \text{(B-7)}$$

$$C_2 = \frac{0.5\Delta t + Kx}{K - Kx + 0.5\Delta t} \quad \text{(B-8)}$$

$$C_3 = \frac{K - 0.5\Delta t - Kx}{K - Kx + 0.5\Delta t} \quad \text{(B-9)}$$

And

$$C_1 + C_2 + C_3 = 1 \quad \text{(B-10)}$$

where t is the routing period. The routing period should be less than the travel time for the flood wave alog the reach otherwise the wave crest may pass completely through the reach during the routing period (Raghunath, 2006).

### B.2.2 Muskingum-Cunge method

Cunge (1969) modified the Muskingum method by computing the routing coefficients in a particular way. The equation which is applicable to each $\Delta x_i$ sub-reach for each $\Delta t^j$ time step is:

$$O_{i+1}^{j+1} = C_1 O_i^{j+1} + C_2 O_i^j + C_3 O_{i+1}^j + C_4 \quad \text{(B-11)}$$

$C_4$ accounts for the effect of lateral inflow ($\bar{q}_i$) along the $\Delta x_i$ sub-reach.

$$C_4 = \frac{\bar{q}_i \, \Delta x \, \Delta t}{[2K(1-x) + \Delta t]} \quad \text{(B-12)}$$

Eq. (B-11) is a finite difference form of the classical kinematic wave equation. This equation is able to account for wave attenuation but not for reverse (negative) flows or backwater effects. In this method K and x are computed as follows:

$$K = \frac{\Delta x}{\bar{c}} \quad \text{(B-13)}$$

$$x = 0.5\left[1 - \frac{\bar{Q}}{\bar{c}\,\bar{B}\,S\,\Delta x}\right] \quad \text{(B-14)}$$

Where:

$\bar{c}$ : The kinematic wave celerity

$\bar{Q}$: Discharge

$\bar{B}$: Cross-sectional top width

S: The energy slope

The bar ( $\bar{}$ ) indicates the variable is averaged over $\Delta x$ and $\Delta t$.

### B.2.3 Variable computational time increment

In order to increase numerical efficiency of the routing method, computational time increments are introduced. This method is a finite difference method which depends on time increments. When discharges vary during rainfall event, short time increments are used otherwise larger time increments are applied.

The Muskingum-Cunge routing method is an explicit scheme. In this method only the current space and time increment are important. Also, it is not important to keep $\Delta x$ and $\Delta t$ constant throughout the computational domain.

### B.2.4 Computational space increment

A computational space increment may be equal to the entire routing reach length or to a fraction of that length. If cross section is constant, it is initially selected as the entire each length of the reaches. If the entire length does not meet the accuracy criteria then space increment should be reduced. The accuracy criteria is given by:

$$\Delta x \leq \frac{1}{\alpha}(\Delta x_C + \Delta x_D) \tag{B-15}$$

in which

$$\alpha = 2$$

$$\Delta x_C = c\Delta t$$

$$\Delta x_D = \frac{q}{S} c$$

Where:

$q$: A reference discharge which is generally two thirds of the peak flow above base flow

$c$: A reference celerity which is corresponded to the reference discharge

$\alpha$: An accuracy parameter

$\Delta t$: The minimum time increment.

## B.3 SCS CN method (USDA, 1986)

### B.3.1 Hydrologic soil groups (HSG)

Here soils are classified into four classes A, B, C and D based on the infiltration and other characteristics. Table (B.3) and figure (B.1) explains soil conditions for each hydrologic soil group.

Table B.3: Hydrologic soil groups (HSG) (USDA, 1986)

| **HSG** | **Soil condition** |
|---|---|
| A | Soils which have low runoff potential and high infiltration rates even when thoroughly wetted such as sand, loamy sand or sandy loam. These soils have high rate of water transmission (greater than 0.30 in/hr) |
| B | Soils which have moderate infiltration rates when thoroughly wetted and consist chiefly of moderately deep to deep, moderately well to well drained soils with moderately fine to moderately coarse textures such as silt loam or loam. These soils have a moderate rate of water transmission (0.15- 0.30 in/hr) |
| C | Soils which have low infiltration rates when thoroughly wetted and consist chiefly of soils with a layer that impedes downward movement of water and soils with moderately fine to fine texture such as sandy clay loam. These soils have a low rate of water transmission (0.05-0.15 in/hr) |
| D | Soils which have high runoff potential. They have very low infiltration rates when thoroughly wetted and consist chiefly of clay soils with a high swelling potential, soils with a permanent high water table, soils with a clay pan or clay layer at or near the surface, and shallow soils over nearly impervious material such as clay loam, silty clay loam, sandy clay, silty clay, or clay. These soils have a very low rate of water transmission (0-0.05 in/hr) |

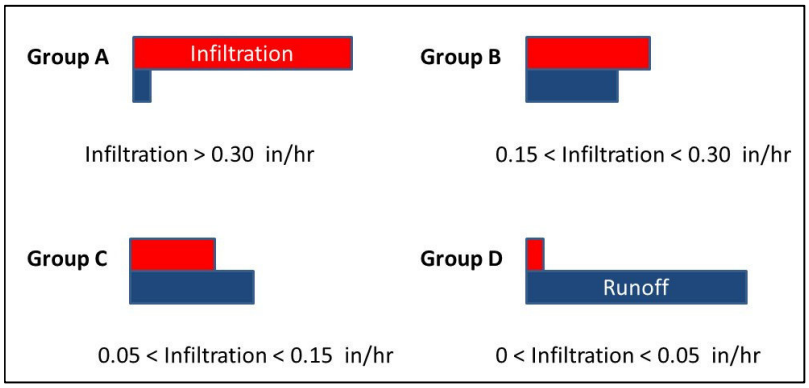


Figure B.1: Infiltration versus runoff rate for each HSG

### B.3.2 Cover type

For determining cover type, it is very common to use "land use" maps.

Table B.4: Land treatment (USDA, 1986)

| **Treatment** | **Land condition** |
|---|---|
| A | Soil un-compacted by human activity with 0 to 10 percent slopes. Native grasses, weeds and shrubs in typical densities with minimal disturbance to grading, ground cover and infiltration capacity. |
| B | Irrigated lawns, parks and golf courses with 0 to 10 percent slopes. Native grasses, weeds and shrubs, and soil un-compacted by human activity with slopes greater than 10 percent and less than 20 percent. |
| C | Soil compacted by human activity. Minimal vegetation. Unpaved parking, roads, trails. Most vacant lots. Gravel or rock on plastic (desert landscaping). Irrigated lawns and parks with slopes greater than 10 percent. Native grasses, weeds and shrubs, and soil un-compacted by human activity with slopes at 20 percent or greater. Native grass, weed and shrub areas with clay or clay loam soils and other soils of very low permeability as classified by SCS Hydrologic Soil Group D. |
| D | Impervious areas, pavement and roofs. |

### B.3.3 Land treatment

This is a modifier to describe the management of cultivated agricultural lands (USDA, 1986). For this reason, four land treatment classifications have been created. Table B.4 describes the land treatment classifications. Three of the land treatment classifications (A, B and C) are for pervious conditions. The fourth classification (D) is for impervious areas.

### B.3.4 SCS curve number method

The SCS runoff equation is (USDA, 1986):

$$Q = \frac{(P - \lambda S)^2}{P - (\lambda - 1)S} \tag{B-16}$$

Where,

$P$ is the total rainfall (in), $Q$ the direct runoff (in), $\lambda$ the regional parameter dependent on geologic and climatic factors ($0.1 \leq \lambda \leq 0.3$). Based on studies of many small watersheds, this parameter ($\lambda$) is often considered as (0.2). The potential maximum retention storage $S$ of watershed is related to a CN, which is a function of land use, land treatments, soil type and antecedent moisture condition of watershed. The CN is dimensionless and its value varies from 30 to 100.The $S$-value in inch can be obtained from CN by using the relationship:

$$S = \frac{25400}{CN} - 254 \tag{B-17}$$

Figure (B.2) illustrates the relation between rainfall, runoff and curve number.

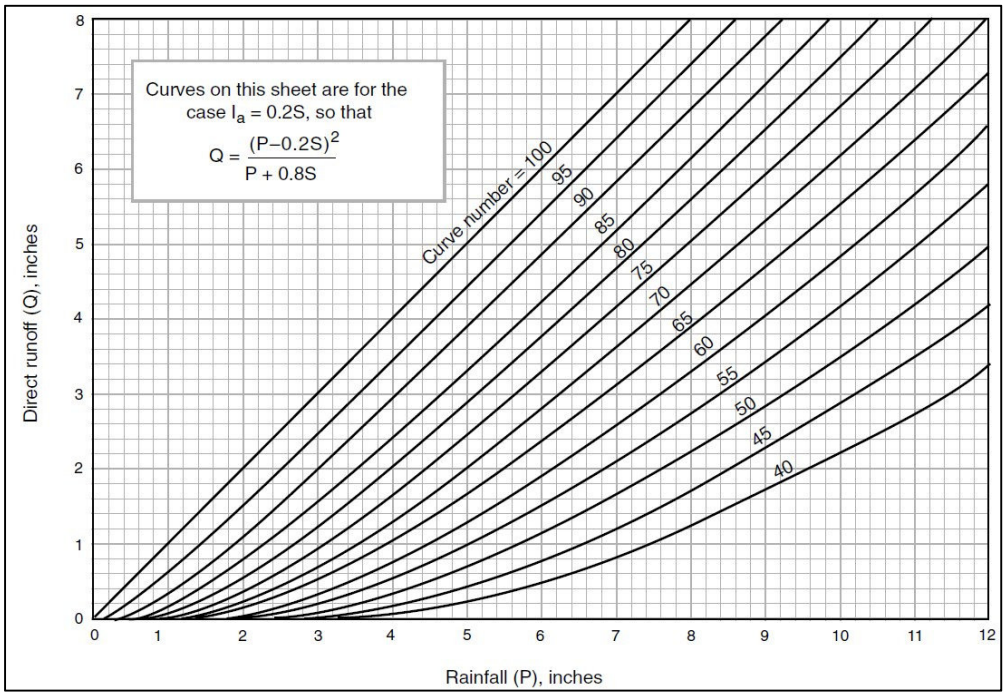


Figure B.2: SCS CN method (USDA, 1986)

### B.3.5 Antecedent Moisture Condition (AMC)

The moisture condition of soil at the begining of the rainfall-runoff event can be considered by AMC. Figure B.3 illustrates that how the infiltration rate can be reduced by the soil moisture condition.

SCS suggested three level of AMC as follows (USDA, 1986):

1. AMC-I: Soils are dry but not to wilting point. Satisfactory cultivation has taken place.
2. AMC-II: Average conditions
3. AMC-III: Sufficient rainfall has occurred within the immediate past five days.

For more information see table (B.5).

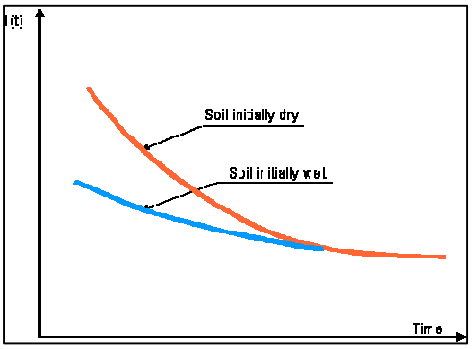


Figure B.3: The infiltration rate in a soil for two conditions: initially wet soil and initially dry soil

Table B.5: Antecedent moisture conditions (UDSA, 1986)

| **AMC Type** | **Total rain in previous 5 days** | |
|---|---|---|
| | **Dormant Season** | **Growing Season** |
| AMC-I | Less than 13 mm | Less than 36 mm |
| AMC-II | 13 to 28 mm | 36 to 53 mm |
| AMC-III | More than 28 mm | More than 53 mm |

The equations of AMC-I and AMC-III are given as (USDA, 1986):

$$CN_I = \frac{CN_{II}}{2.281 - 0.01281 CN_{II}} \tag{B-18}$$

$$CN_{III} = \frac{CN_{II}}{0.427 + 0.00573 CN_{II}} \tag{B-19}$$

Where:

$CN_{II}$ is curve number for hydrologic soil cover under AMC-II conditions and can be obtained from SCS tables.

### B.3.6 Urban impervious area modifications

In computing CN for urban areas, percentage of impervious area should be considered. These areas are often divided into two parts; connected impervious areas and unconnected areas.

- Connected impervious areas: If runoff from an area flows directly into the drainage system then this area is considered as impervious area. Also, if runoff in an area occurs as concentrated shallow flow that runs over a pervious area and then into the drainage system, is considered as impervious area. If all of these condistions are presented for an area but the impervious area percentages or the pervious land use assumptions in SCS table are not applicable, figure (B.4) should be used to compute a composite CN.

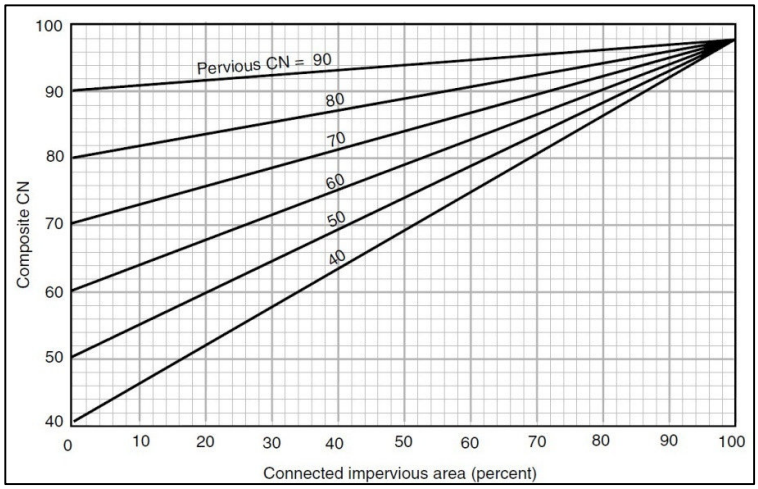


Figure B.4: Composite CN with connected impervious area (USDA, 1986).

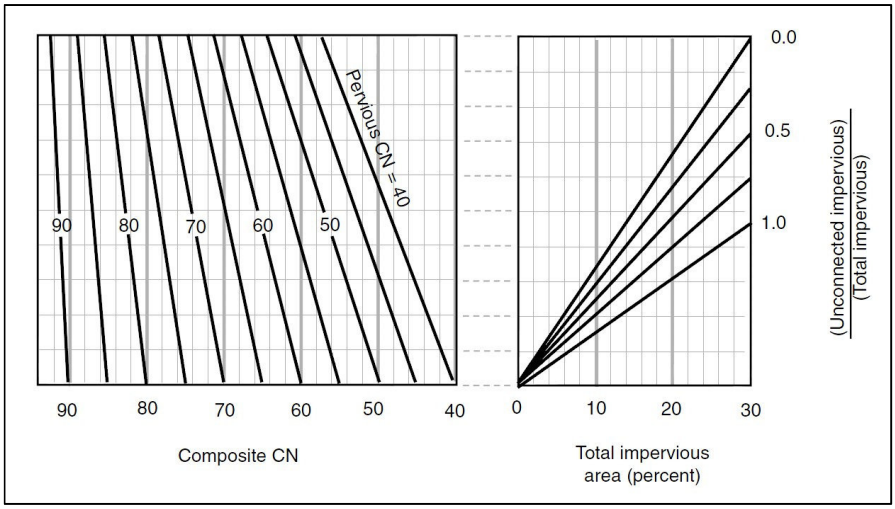


Figure B.5: Composite CN with unconnected impervious areas and total impervious area less than 30% (USDA, 1986)

- Unconnected impervious areas: Runoff from these areas is spread over a pervious area as sheet flow. Based on this condition, for determining CN:
    1. Figure (B.5) should be used if total impervious area is less than 30 percent
    2. Figure (B.4) should be used if the total impervious area is equal to or greater than 30 percent..

## B.4 Emission senarios for climate change (IPCC, 2007)

The Intergovernmental Panel on Climate Change (IPCC) founded by UNEP, has provided some probable scenarios for global warming and carbon dioxide generation rates. The emission scenarios of the IPCC Special Report on Emission Scenarios (SRES) classified as follows (IPCC 2007):

1. "A1 (high): the A1 storyline and scenario family describes a future world of very rapid economic growth, global population that peaks in mid-century and declines thereafter, and the rapid introduction of new and more efficient technologies. Major underlying themes are convergence among regions, capacity building and increased cultural and social interactions, with a substantial reduction in regional differences in per capita income. The A1 scenario family develops into three groups that describe alternative directions of technological change in the energy system. The three A1 groups are distinguished by their technological emphasis: fossil-intensive (A1FI), non-fossil energy sources (A1T) or a balance across all sources (A1B). [Balance is defined as not relying too heavily on one particular energy source, on the assumption that similar improvement rates apply to all energy supply and end use technologies].
2. A2: The A2 storyline and scenario family describes a very heterogeneous world. The underlying theme is self-reliance and preservation of local identities. Fertility patterns across regions converge very slowly, which results in continuously increasing population. Economic development is primarily regionally oriented and per capita economic growth and technological change more fragmented and slower than other storylines.
3. B1: The B1 storyline and scenario family describes a convergent world with the same global population, that peaks in mid-century and declines thereafter, as in the A1 storyline, but with rapid change in economic structures toward a service and information economy, with reductions in material intensity and the introduction of clean and resource-efficient technologies. The emphasis is on global solutions to economic, social and

environmental sustainability, including improved equity, but without additional climate initiatives.

4. B2 (low): The B2 storyline and scenario family describes a world in which the emphasis is on local solutions to economic, social and environmental sustainability. It is a world with continuously increasing global population, at a rate lower than A2, intermediate levels of economic development, and less rapid and more diverse technological change than in the B1 and A1 storylines. While the scenario is also oriented towards environmental protection and social equity, it focuses on local and regional levels.

   An illustrative scenario was chosen for each of the six scenario groups A1B, A1FI, A1T, A2, B1 and B2. All should be considered equally sound."

**References**

Abdul Karim, MD., and Chowdhury, J. U., 1995 "A comparison of four distributions used in flood frequency analysis in Bangladesh" Hydrological Sciences Journal, 40, 1, Feb. 1995.

Ahmad U. N., Shabri A., and Zakaria Z. A., 2011 "Flood Frequency Analysis of Annual maximum Stream Flows using L-Moments and TL-Moments Approach" Applied Mathematical Sciences, Vol. 5, 2011, No. 5, pp. 243-253.

Aldridge, B.N. 1989 "Effects of Vegetation on Floods at Four Arizona Sites" Proceedings of the ASCE 1989 National Conference on Hydraulic Engineering, pp. 392-397.

Aron, G. 1989 "Sensitivity of Storm Runoff Hydrographs to Hyetograph Shape" Proceedings of the International Conference on Channel Flow and Catchment Runoff: Centennial of Manning's Formula and Kuichling's Rational Formula, B.C. Yen (ed.), Charlottesville, VA, pp. 1-9.

Berndtsson, R., and J. Niemczynowicz. 1988 "Spatial and Temporal Scales in Rainfall Analysis - Some Aspects and Future Perspectives" Journal of Hydrology 100: 293-313.

Beven, K.J. 1989 "Changing Ideas in Hydrology - The Case of Physically-Based Models" Journal of Hydrology 105:157-172.

Bradley, A.A., and K.W. Potter. 1990 "Development of Space-Time Rainfall for Hydrological Analysis of Large-Scale Urban Catchments" Proceedings of the AWRA Conference on Urban Hydrology, Denver, CO, in preparation.

Chow V. T., 1964 "Hanbook of Applied Hydrology" McGraw-Hill Publication, PP. 1495, 1964.

Cunge, J.A. 1969 "Food Propagation Computation Method (Muskingum Method)" Journal of Hydraulic Research 7 (2): 205-230.

Dendrou, S.A. 1982 “Overview of Urban Stormwater Models, in Urban Stormwater Hydrology” American Geophysical Union, Water Resources Monograph No. 7, Washington, DC, pp. 219-247.

Development Process Manual (DPM), 2009 ”Vol. II: Design Criteria” Rio Rancho, New Mexico, USA.

Dymond, J. R. & Harmsworth, G. R. 1994 “Towards automated land resource mapping using digital terrain models” ITC Journal 1994-2:129-138.

EasyFit, User’s Manual version 5.5 “Introduction to EasyFit 5.5” Mathwave data analysis and simulation, (www.mathwave.com).

Fread D. L. and Hsu K. S., 1993 “Applicability of two simplifies flood routing methods: Level-Pool and Muskingum-Cunge” ASCE National Hydraulic Engineering Conference, San Francisco, 1993.

Fryer, J. G., Chandler, J.H. & Cooper, M. A. R. 1994 “On the Accuracy of Heighting from Aerial Photographs and Maps: implications to process models” Earth Surface Processes and Landforms 19:577-583.

Gumbel, E. J., 1954 “Statistical theory of extreme values and some practical applications” Applied mathematics series 33. U.S. Dep. of Commerce, National Bureau of Standards.

Goldman, D.M., MA. Marino, and A.D. Feldman. 1990 “Runoff Prediction Uncertainty for Ungauged Agricultural Watersheds” ASCE Journal of Irrigation and Drainage Engineering 116(IR6): 752-768.

Gousie M. B., “Digital Elevation Model Error Detection and Visualization” Department of Mathematics and Computer Science, Wheaton College, Norton, MA 02766, USA.

Greenwood, J. A., Landwehr, J. M., Matalas, N. C., and Wallis, J. R., 1979 “Probability weighted moments: Definition and relation to parameters of

several distributions expressible in inverse form" Water Resources Research, 15 (5), pp. 1049-1054.

Griffis V. W., Stedinger J. R., 2007 "Log-Pearson Type 3 Distribution and Its Application in Flood Frequency Analysis: Distribution Characteristics" Journal of Hydrologic Engineering, ASCE Sep./Oct. 2007, DOI: 10.1061/(ASCE) 1084-0699(2007) 12:5(482).

Haan, C. T. 1988 "Parametric Uncertainty in Hydrologic Modeling" Proceedings of the 1988 ASAE International Symposium, ASAE Publication 07-88, Chicago, IL, pp. 330-346.

Haan C. T., 2002 "Statistical Methods in Hydrology" 2nd edition, Iowa State University Press, USA.

Han, J. (2010) "Streamflow analisis using ArcGIS and Hec-GeoHMS" Texas A&M University, Zachry department of Civil Engineering.

Hec-GeoHMS user's manual (2009) "Hec-GeoHMS Geospatial Hydrologic Modeling Extension version 4.2" US Army Corps of Engineers, Hydrologic Engineering Center, May 2009.

Hec-HMS user's manual (2010) "Hydrologic Modeling System (Hec-HMS) version 3.5" US Army Corps of Engineers, Hydrologic Engineering Center, August 2010.

Herschy R. W. 1995 "Streamflow Measurement" Chapman & Hall, Second Edition.

Hosking, J. R. M., 1990 "L-moment: Analysis and Estimation of Distributions using Linear Combinations of Order Statistics" Journal of Statistic and Soc. B 52, No. 1, pp. 105-124.

Impacts of Climate Change on Austria: Case Studies, Final Report. Institute of Meteorology Department of Water-Atmosphere-Environment BOKU - University of Natural Resources and Applied Life Sciences Vienna, July 2008.

IPCC, 2007: Summary for Policymakers. In: Climate Change 2007: The Physical Science Basis. Contribution of Working Group I to the Fourth Assessment Report of the Intergovernmental Panel on Climate Change [Solomon, S., D. Qin, M. Manning, Z. Chen, M. Marquis, K.B. Averyt, M.Tignor and H.L. Miller (eds.)]. Cambridge University Press, Cambridge, United Kingdom and New York, NY, USA.

James, W. and M.A. Robinson, 1985 "Time and Space Resolution for Continuous, Dynamic Storm and Runoff Model Studies" Proceedings of the ASCE Specialty Conference, Lake Buena Vista, FL, pp. 1160-1165.

Johnston, K., Ver Hoef, J. M., Krivoruchko, K., & Lucas, N. (2003). "ArcGIS 9 Using ArcGIS Geostatistical Analyst" ESRI Corp. USA.

Kafle, T. P., Hazarika, M. K., Karki, S., Sshrestha, R. M., Sharma, R., & Samarakoon, L. (2010). Basin scale rainfall-runoff modeling for flood forecasts. The International Centre for Integrated Mountain Development, ICIMOD.

Kapur, S., Esvaran, H., and Blum, W. E. H., 2011 "Sustainable Land Management, Learning from the Past for the Future" Springer Heidelberg Dordrecht Publication, P. 431.

Keifer, C.J., and H.H. Chu. 1957 "Synthetic Storm Pattern for Drainage Design" ASCE Journal of the Hydraulics Division 83 (HY4): 1332-1 to 1332-25.

Knapp V. H., Durgunoglu A., Ortel T. W., 1991 "A review of rainfall – runoff modeling for stormwater management" US Geological Survey, Illinois District, 1991.

Loaiciga H. A., Leipnik R. B., 1999 "Analysis of Extreme Hydrologic Events with Gumbel Distributions: marginal and additive cases" Stochastic Environmental Research and Risk Assessment, August 1999, Volume 13, issue 4, pp 251-259, Springer publication.

L-RAP, User's Manual, 2011 "L-Moment Statistics" MGS Software LLC, August 2011.

Mahdavi M., 2003 "Applied Hydrology" 2nd edition, Tehran University Press, Iran.

Martins, E. S., and Stedinger, J. R., 2000 "Generalized maximum-likelihood generalized extreme-value quantile estimators for hydrologic data" Water Resources Research, Vol. 36, No. 3, pp. 737-744.

McEnroe, B. M., 2010 "Guidelines for Continuous Simulation of Dtreamflow in Johnson County, Kansas, with Hec-HMS" Department of Civil, Environmental and Architectural Engineering University of Kansas, USA.

Mockus V., 1964 "National Engineering Handbook, Section 4, Hydrology" NEH Notice 4-102. 1964.

Mohammadnejad, R., Zahraie, B., Nasseri, M., and Tootchi A., 2010 "Climate change impact assessment on rainfall-runoff process: Case study of Pishin Reservoir Basin in Iran" School of Civil Engineering. University of Tehran, Tehran-Iran.

Nhat L. M., Tachikawa Y. and Takara K. 2006 "Establishment of Intensity-Duration-Frequency curves for precipitation in the Monsoon area of Vietnam" Annuals of Disaster Prev. Res. Inst. Kyoto Univ. No. 49 B, 2006.

Niemczynowicz, J. 1984 "Can the Rainfall Input Be Modified So That Frequencies of Rainfall-Input and Runoff-Output Will Be Similar?" Water Science and Technology 16: 251-254.

Oksanen J., 2006 "Digital Elevation Model Error in Terrain Analysis" Academic Dissertation in Geography, Faculty of Science, University of Helsinki, November 2006.

Paine, J.N. 1989 "Effects of Hyetograph Shape on Detention Pond Sizing" Proceedings of the International Conference on Channel Flow and Catchment

Runoff: Centennial of Manning's Formula and Kuichling's Rational Formula, B.C. Yen (ed.), Charlottesville, VA, pp. 36-44.

Ponce, V. M., and F.D. Theurer. 1982 "Accuracy Criteria in Diffusion Routing" ASCE Journal of the Hydraulics Division 108 (HY6): 747-757.

Raghunath, H. M. (2006) "Hydrology Principles – Analysis – Design (2nd Edition)" New Age International Publishers, New Delhi, 2006.

Rantz S.E. et al., 1982 "Measurement and computation of stream-flow, Volume 1 Measurement of Stage and Discharge" U.S. Geological Survey Water Supply Paper 2175.

Sackl B., 2009 "Schoeckelbach, n-jaehrliche Hochwasserabfluesse" Ingenieurbuero fuer kulturtechnik und Wasserwirtschaft Wasserbausoftware, Graz, 2009.

Sangal B. P., Biswas A.K., 1970 "The 3-Parameter Lognormal Distribution and Its Application in Hydrology" Water Resources Research, Vol. 6, NO. 2, P. 505, 1970.

Scharffenberg, W., Ely, P., & Daly, S. (2010) "Hydrologic modeling System (Hec-HMS): Physically-based simulation components" 2nd Joint Federal Interagency Conference, Las Vegas, NV, June 27 – June 1, 2010.

Schilling, W. 1984 "Effect of Spatial Rainfall Distribution on Sewer Flows" Water Science and Technology 16:177-188.

Schilling, W. and L. Fuchs. 1986 "Errors in Storm-water Modeling: A Quantitative Assessment" ASCE Journal of the Hydraulics Division 112 (2): 111-123.

Seckin, N., Yurtal, R., Haktanir, T., and Dogan, A., 2010 "Comparison of probability weighted moments and maximum likelihood methods used in flood frequency analysis for Ceyhan river basin" The Arabian Journal for Science and Engineering, Vol. 35, No. 1B, pp. 49-69.

Skøien, J. O., Bloeschl G. and Western A. W., 2003 "Top-kriging Geostatistics on stream networks, Hydrol. Earth Syst. Sci., 10, 277-287.

Snelder M., Kooman E. and Kasse K., 2010 "Land use modeling of Austria with the EuClueScanner" Bachelor thesis, Vrije Universiteit, Amsterdam, 2010.

Tarboton D., "Terrain analysis using Digital Elevation Models in Hydrology" Utah State University.

Third National Climate Report of the Austrian Federal Government Federal Ministry of Agriculture, Forestry, Environment and Water Management Vienna, November 2001.

Todini, E., and J.R. Wallis. 1977 "Using CLS for Daily or Longer Period Rainfall-Runoff Modeling" Mathematical Models for Surface Water Hydrology, John Wiley & Sons, New York, NY, pp. 149-168.

TP-135, 1991 "A Muskingum-Cunge Channel Flow Routing Method for Drainage Networks" US Army Corps of Engineers, Hydrologic Engineering Center, 1991.

Troutman, B.M. 1983 "Runoff Prediction Errors and Bias in Parameter Estimation Induced by Spatial Variability of Precipitation" Water Resources Research 19: 791-810.

USDA, (1986). TR-55: Urban Hydrology for Small Watersheds. US Department of Agriculture, Natural Resources Conservation Service, Conservation Engineering Division, Technical Release 55, June 1986.

Watt, W. E., Lathem, K., Neill, C. R., Richards, T. L., 1989 "Hydrology of floods in Canada" A guide to planning and design. National Research Council Canada, Associate Committee on Hydrology; Ottawa, Ontario, 245 pp.

Wilson, C.B., J.B. Valdes, and I. Rodriguez-Iturbe. 1979 "On the Influence of the Spatial Distribution of Rainfall on Storm Runoff" Water Resources Research 15: 321-328.

Yen, B.C., and V.T. Chow. 1969 "A Laboratory Study of Surface Runoff Due to Moving Rainstorms" Water Resources Research 5 (5): 989-1006.

Yener, M. K., Sorman, A. U., Sorman, A. A., Sensoy, A., & Gezgin, T. (2007). "Modeling studies with Hec-HMS and runoff scenarios in Yuvacik basin" International congress on river basin management, 22-24 March 2007, Antalya, Turkey.

Younkin, L.M., and W.H. Merkel. 1988 "Evaluation of Diffusion Models for Flood Routing" Proceedings of the ASCE 1988 National Conference on Hydraulic Engineering, pp. 674-680.

Yuanfang C., Shengbin X., Zhigui Sh., Pieter V. D., and Sheng-hua GU., 2004 "Study on L-Moment Estimations for Log-Normal Distributions with Historical Flood Data" GIS & Remote Sensing in Hydrology, Water Resources and Environment, Vol. 1, Chen et al. (eds), IAHS Publ. 289.

Yusop, Z., Chan, C. H., & Katimon,A. (2007) "Runoff charactristics and application of Hec-HMS for modeling stormflow hydrograph in an oil palm catchment" Water Science and Technology, Vol. 56 No. 8, pp 41-48.